

Universität
Rostock



Traditio et Innovatio

HelmholtzZentrum münchen

Deutsches Forschungszentrum für Gesundheit und Umwelt

JOINT MASS SPECTROMETRY CENTRE

Investigation of Primary and Secondary Organic Aerosols by Advanced Mass Spectrometric Techniques and Chemometric Approaches

Kumulative Dissertation

zur Erlangung des akademischen Grades

doctor rerum naturalium (Dr. rer. nat.)

der Mathematisch-Naturwissenschaftlichen Fakultät

der Universität Rostock

vorgelegt von

Hendryk Czech

aus Rostock, geboren am 12. Januar 1988 in Rostock

Rostock, September 2017

Gutachter:

1. Gutachter:
Prof. Dr. Ralf Zimmermann
Institut für Chemie, Universität Rostock
2. Gutachter
Prof. Joakim Pagels, PhD
Ergonomics and Aerosol Technology, Lund University, Schweden
3. Gutachter
Prof. Wolfgang F. Rogge, PhD
School of Engineering, University of California, Merced, USA

Datum der Einreichung: 29. September 2017

Datum der Verteidigung: 05. Dezember 2017

Die vorliegende Arbeit entstand in der Zeit von Oktober 2013 bis September 2017 am Lehrstuhl für Analytische Chemie der Universität Rostock im gemeinsamen Massenspektrometrie-Zentrum der Universität Rostock und des Helmholtz Zentrums München.

To measure is to know.

- William Thomson, 1st Baron Kelvin

The classification of facts, the recognition of their sequence and relative significance is the function of science, and the habit of forming a judgment upon these facts unbiased by personal feeling is characteristic of what may be termed the scientific frame of mind.

- Karl Pearson

An approximate answer to the right problem is worth a good deal more than an exact answer to an approximate problem.

- John Tukey

CONTRIBUTIONS TO SCIENTIFIC PUBLICATIONS

First-authorships

The following manuscripts were created with Hendryk Czech as first author and published in peer-reviewed journals. The contribution of Hendryk Czech is described in detail.

Title: On-line analysis of organic emissions from residential wood combustion with single-photon ionisation time-of-flight mass spectrometry (SPI-TOFMS)
Authors: Hendryk Czech, Olli Sippula, Miika Kortelainen, Jarkko Tissari, Christian Radischat, Johannes Passig, Thorsten Streibel, Jorma Jokiniemi and Ralf Zimmermann
Journal: Fuel, 177, 334-342
Year: 2016

Hendryk Czech carried out the on-line SPI-TOFMS analysis at the University of Eastern Finland, calculated the emission factors, performed the statistical data analysis and wrote the manuscript.

Title: Resolving Coffee Roasting-Degree Phases Based on the Analysis of Volatile Compounds in the Roasting Off-Gas by Photoionization Time-of-Flight Mass Spectrometry (PI-TOFMS) and Statistical Data Analysis: Toward a PI-TOFMS Roasting Model
Authors: Hendryk Czech, Claudia Schepler, Sophie Klingbeil, Sven Ehlert, Jessalin Howell and Ralf Zimmermann
Journal: Journal of Agricultural and Food Chemistry, 64(25), 5223-5231
Year: 2016

Hendryk Czech performed the statistical data analysis of the processed PI-TOFMS data and wrote the manuscript.

Title: Time-resolved analysis of primary volatile emissions and secondary aerosol formation potential from a small-scale pellet boiler
Authors: Hendryk Czech, Simone M. Pieber, Olli Sippula, Miika Kortelainen, Heikki Lamberg, Julija Grigonyte, Thorsten Streibel, André S. H. Prévôt, Jorma Jokiniemi and Ralf Zimmermann
Journal: Atmospheric Environment, 158, 236-245
Year: 2017

Hendryk Czech carried out the on-line SPI-TOFMS analysis at the University of Eastern Finland, performed the calculations of emission factors, interpreted all results and wrote the manuscript.

Title: New directions: Beyond sulphur, vanadium and nickel - About source apportionment of ship emissions in emission control areas
Authors: Hendryk Czech, Jürgen Schnelle-Kreis, Thorsten Streibel and Ralf Zimmermann
Journal: Atmospheric Environment, 163, 190-191
Year: 2017

Hendryk Czech performed the search for state of legislation, initiated and wrote the manuscript.

Title: A chemometric investigation of aromatic emission profiles from a marine engine in comparison with residential wood combustion and road traffic: Implications for source apportionment inside and outside sulphur emission control areas
Authors: Hendryk Czech, Benjamin Stengel, Thomas Adam, Martin Sklorz, Thorsten Streibel and Ralf Zimmermann
Journal: Atmospheric Environment, 176, 212-222
Year: 2017

Hendryk Czech carried out the on-line REMPI-TOFMS analysis at the Faculty of Mechanical Engineering and Marine Technology, performed the statistical analysis of the data and wrote the manuscript.

Title: Chemical composition and speciation of particulate organic matter from modern residential small-scale wood combustion appliances
Authors: Hendryk Czech, Toni Miersch, Jürgen Orasche, Gülçin Abbaszade, Olli Sippula, Jarkko Tissari, Bernhard Michalke, Jürgen Schnelle-Kreis, Thorsten Streibel, Jorma Jokiniemi and Ralf Zimmermann
Journal: Science of the Total Environment, 612, 636-648
Year: 2018

Hendryk Czech carried out the particle analysis with TOCA-REMPI-TOFMS, calculated emission factors, interpreted all results and wrote the manuscript.

Title: Direct infusion resonance-enhanced multi-photon ionization mass spectrometry (DI-REMPI-MS) of liquid samples under vacuum conditions
Authors: Claudia Kruth^{||}, Hendryk Czech^{||}, Martin Sklorz, Johannes Passig, Sven Ehlert, Achille Cappiello and Ralf Zimmermann
Journal: Analytical Chemistry
Year: *accepted*

Hendryk Czech evaluated the processed data and wrote the manuscript.

^{||} *These authors contributed equally to the manuscript.*

CO-AUTHORSHIPS

The following manuscripts were created with Hendryk Czech as co-author and published in peer-reviewed journals. The contribution of Hendryk Czech is described in detail.

Title: Characteristics and temporal evolution of particulate emissions from a ship diesel engine

Authors: Laarnie Müller, Gert Jakobi, Hendryk Czech, Benjamin Stengel, Jürgen Orasche, José M. Arteaga-Salas, Erwin Karg, Michael Elsasser, Olli Sippula, Thorsten Streibel, Jay G. Slowik, André S.H. Prévôt, Jorma Jokiniemi, Rom Rabe, Horst Harndorf, Bernhard Michalke, Jürgen Schnelle-Kreis and Ralf Zimmermann,

Journal: Applied Energy, 155, 204-217

Year: 2015

Hendryk Czech carried out the carbon analysis, contributed to the data interpretation and approved the manuscript.

Title: Transformation of logwood combustion emissions in a smog chamber: formation of secondary organic aerosol and changes in the primary organic aerosol upon daytime and nighttime aging

Authors: Petri Tiitta, Ari Leskinen, Liqing Hao, Pasi Yli-Pirilä, Miika Kortelainen, Julija Grigonyte, Jarkko Tissari, Heikki Lamberg, Anni Hartikainen, Kari Kuuspallo, Aki-Matti Kortelainen, Annele Virtanen, Kari E.J. Lehtinen, Mika Komppula, Simone M. Pieber, André S.H. Prévôt, Timothy B. Onasch, Douglas R. Worsnop, Hendryk Czech, Ralf Zimmermann, Jorma Jokiniemi and Olli Sippula

Journal: Atmospheric Chemistry and Physics, 16(20), 13251-13269

Year: 2016

Hendryk Czech contributed to the data interpretation and approved the manuscript.

Title: Aerosol emissions of a ship diesel engine operated with diesel fuel or heavy fuel oil

Authors: Thorsten Streibel, Jürgen Schnelle-Kreis, Hendryk Czech, Horst Harndorf, Gert Jakobi, Jorma Jokiniemi, Erwin Karg, Jutta Lintelmann, Georg Matuschek, Bernhard Michalke, Laarnie Müller, Jürgen Orasche, Johannes Passig, Christian Radischat, Rom Rabe, Ahmed A. Reda, Christopher P. Rüger, Theo Schwemer, Olli Sippula, Benjamin Stengel, Martin Sklorz, Tiina Torvela, Benedikt A. Weggler and Ralf Zimmermann

Journal: Environmental Science and Pollution Research, 24(12), 10976-10991
Special Issue: *Recent Advances in Chemistry and the Environment*

Year: 2017

Hendryk Czech carried out the TOCA-SPI/REMPI-TOFMS analysis of the PM emissions, contributed to the data evaluation, wrote the introduction and all parts related to TOCA-SPI/REMPI-TOFMS, and approved the manuscript.

Rostock, September 2017

Hendryk Czech

ACKNOWLEDGEMENT

This study has been financially supported by the German Research Foundation (DFG) and the Swiss National Science Fund (SNF), which is gratefully acknowledged. Furthermore, I would like to show appreciation to the Helmholtz Virtual Institute of Complex Molecular Systems in Environmental Health (HICE) for its support.

The investigation of complex interactions and relations between combustion, analytical and atmospheric science requires elaborate experiments and interpretation of data from advanced instrumentation. Therefore, many people were involved in this project with scientific, but also with not less important non-scientific contributions, for which I want to express my deep gratitude.

I would like to thank...

...Prof. Ralf Zimmermann for providing me the opportunity to work with advanced analytical instrumentation in interdisciplinary and international projects with the freedom I need to follow my personal scientific interests.

...Dr. Thorsten Streibel for being available at all times for discussion, revisions of manuscripts with valuable feedback, especially for this thesis, and also organisational issues.

...Dr. Martin Sklorz for controversial discussions and comments, his ability to find a solution for any problem and his support at field campaigns and in the laboratory.

...Dr. Johannes Passig, der *wilde Doktor*, for the support a chemist need from a physicist with laser adjustment and mass spectrometer tuning, and Dr. Sven Ehlert for his support in data acquisition and processing.

...Toni Miersch for becoming *Lord of Carbon Analysis*, which enormously eased my labour situation from 2014 on, and enjoyable shared conference participation. *Act hard!*

...Andrea Lehmann for being the good soul of the laboratories.

...Dr. Olli Sippula for being my external aerosol mentor since I started my Master's thesis and his valuable comments on several manuscripts.

...Dr. Simone M. Pieber and Dr. Jürgen Orasche, my *Wooshis*, for the exceptionally successful completion of our project.

...Christopher P. Rürger for being my friend with the same scientific spirit and attitude since we started at University. *Always pushing the limits!*

...Anika Neumann for support with some of the artwork of this thesis in the nick of time.

...my fiancée Dana Grammens for her appreciation for my passion of scientific work, taking much weight off my shoulders and her eternal love and patience for our son Gregor. I also want to apologise to you for all the time I missed with you together.

...Heike and Thorsten Grammens for picking up Gregor every Tuesday from crèche.

ABSTRACT

Deutsch

Primäre und sekundäre Verbrennungsaerosole wurden in verschiedenen Studien der Emissionsquellenzuordnung als Hauptursache für Luftverschmutzung identifiziert. Die chemische Zusammensetzung der Emissionen sowie das Bildungspotenzial von sekundärem Aerosol sind wichtig, um effiziente Maßnahmen zur Emissionsreduktion zu entwickeln und ihre Auswirkungen auf Klima und Gesundheit einschätzen zu können. In jüngster Vergangenheit sind Emissionen von Schiffen und aus der häuslichen Holzverbrennung stärker in das öffentliche Interesse gerückt, welche im DACH-Project „WooShi – WOOd combustion and SHipping“ in Zusammenarbeit der Universität Rostock, dem Helmholtz-Zentrum München und dem Paul Scherrer Institut in Villigen (Schweiz) mit Unterstützung des Helmholtz Virtual Institute for Complex Molecular Systems in Environmental Health (HICE) und der Universität von Ostfinland untersucht wurden.

Der Einsatz neuer Verbrennungstechnologien durch verbesserte Sekundärluftzufuhr oder automatisch arbeitende Verbrennungsöfen, welche auch durch gesetzliche Beschlüsse wie die „Energiewende“ in Deutschland vorangetrieben werden, reduziert Emissionen aus der häuslichen Holzverbrennung beträchtlich. Allerdings ist noch unbekannt, ob die Emissionsprofile erhalten bleiben und in Studien zur Emissionsquellenzuordnung und zur Bestimmung relativer Anteile an der Gesamtbelastung weiterhin verwendet werden können. Des Weiteren ist zu klären, ob die verringerten primären Emissionen auch im direkten Zusammenhang mit einer Verringerung der sekundären Partikelbildung aus der Gasphase stehen.

Obwohl Schiffsemissionen in derselben Größenordnung wie Emissionen aus dem Straßenverkehr eingeschätzt werden, sind sie bis auf die gasförmigen Hauptbestandteile des Abgases (CO_2 , CO , SO_2 und NO_x) und einigen Summenparametern der emittierten Partikel (Partikelmasse, partikulärer organischer und elementarer Kohlenstoff) deutlich weniger in der Literatur beschrieben. 2015 entschied die Internationale Seeschiffahrtsorganisation den Schwefelgehalt im Kraftstoff (FSC) der Schiffe in Schwefelemissionsüberwachungsgebieten (SECAs) auf 0,1% zu begrenzen, was in diesen Gebieten zu einem Wechsel von Schweröl mit einem mittleren FSC von 2,7% zu Diesel-ähnlichen Kraftstoffen wie marinem Gasöl führte.

Mit dem Hintergrund verbesserter Verbrennungstechnologien und neuer Gesetzgebung wurden kohlenstoffhaltige Emissionen aus einem modernen Scheitholzofen, einem Pellet-Heizungskessel und einem marinen Hilfsmotor mit hochentwickelten massenspektrometrischen Methoden untersucht, welche u.a. die Ein-Photon- und resonanzverstärkte Mehrphotonenionisierung kombiniert mit der Flugzeitmassenspektrometrie umfasste. Insbesondere die Zusammensetzung der organischen Emissionen sowie der Einfluss des Kraftstoffs und die sich zeitlich ändernden Verbrennungs- und Motorbedingungen auf die Emissionen wurden mit statistischen Ansätzen versucht zu identifizieren und deren Auswirkungen auf zukünftige Emissionsquellenzuordnungen

abzuschätzen. Zusätzlich zu den primären Emissionen wurden die sekundäre organische Partikelbildung (SOA) in einer Alterungskammer sowie einem Strömungsrohrreaktor simuliert. Die Ergebnisse der Studie ergaben neue charakteristische und statistisch signifikante Markerverbindungen für Schiffsemissionen, welche sowohl innerhalb als auch außerhalb SECAs Gültigkeit besitzen und in der Literatur noch nicht beschrieben wurden, sowie aktualisierte Emissionsprofile verbunden mit verminderter SOA-Bildung für häusliche Holzverbrennung nach dem heutigen Stand der Technik.

English

Primary and secondary aerosols from combustion processes were identified by emission source apportionment as key sources for air pollution. In this context, emission profiles and knowledge about secondary aerosol formation are essential to develop efficient abatement strategies and to assess feedbacks on climate and human health. Recently, emissions from ship traffic and residential wood combustion gained emerging public attention and were subject of this thesis in the framework of the DACH-project “WooShi – WOOD combustion and SHipping” in a collaboration between the University of Rostock, Helmholtz-Zentrum München and Paul Scherrer Institute in Villigen (Switzerland), with support from the Helmholtz Virtual Institute of Complex Molecular Systems in Environmental Health (HICE) and the University of Eastern Finland.

Ongoing advances in wood combustion technology, also driven by legislation such as “*Energiewende*” in Germany, through improved secondary air supply and automatically-fired appliances considerably decreased emissions from residential heating. However, consequences of the emission profile and therefore the identification and quantification of wood combustion in source apportionment are unknown. Furthermore, it is still pending if reduced primary emissions lead to proportional reduction in secondary emissions by gas-to-particle conversion.

Total emissions from ship traffic were estimated to be comparable to emissions from road vehicles, but are poorly described in the literature apart from main gaseous components of the exhaust (CO₂, CO, SO₂ and NO_x) and particle-related quantities (particulate matter, organic carbon, black carbon). In 2015, ship emissions were tackled by the International Maritime Organisation through limiting the fuel sulphur content (FSC) to 0.1% in sulphur emission control areas (SECAs), which caused switching from heavy fuel oil with 2.7% FSC on average to diesel-like fuel, such as marine gas oil.

On account of these changing emissions by improved technologies and new legislation, carbonaceous emissions from a modern masonry heater, a pellet boiler and a marine auxiliary engine were investigated by advanced mass spectrometric techniques, including single-photon and resonance-enhanced multi-photon ionisation time-of-flight mass spectrometry. The focus was put on analysing the complex organic composition as well as the identification of effects of fuel components, temporarily changing burning and engine conditions on the emissions by several chemometric approaches and the relevance for prospective source apportionment. Additionally,

the potential of secondary organic aerosol (SOA) formation was examined in simulation studies using a smog chamber and a potential aerosol mass flow reactor.

The results of this study revealed characteristic and statistically significant organic marker substances for ship emissions inside and outside SECAs, which have not been considered in the literature, and updated emission profiles associated with lower SOA formation for modern residential wood combustion appliances.

TABLE OF CONTENTS

Author contribution to scientific publications

Acknowledgement

Abstract

List of abbreviations

List of figures

List of tables

1	Introduction: atmospheric aerosols.....	1
1.1	<i>Sources and sinks</i>	1
1.2	<i>Chemical composition and classification.....</i>	2
1.2.1	Carbonaceous aerosol	2
1.2.2	Organic aerosol (OA).....	3
1.3	<i>Organic markers in combustion aerosol.....</i>	4
1.3.1	Defining markers and tracers	4
1.3.2	Established organic markers for CA	4
1.3.3	Origin of markers from fuel composition and processing	5
1.4	<i>Atmospheric aerosol transformation.....</i>	7
1.4.1	Atmospheric oxidising agents and products	7
1.4.2	Simulation of atmospheric transformation in batch and flow reactors	8
1.5	<i>Impact of combustion aerosol.....</i>	9
1.5.1	Greenhouse effect and radiative forcing.....	9
1.5.2	Human health	9
2	Focus: wood combustion and shipping (WOOSHI)	10
2.1	<i>Ship traffic and sulphur emission control areas (SECA)</i>	11
2.2	<i>Advanced combustion technology for residential wood combustion.....</i>	12
3	Methodology.....	13
3.1	<i>Aerosol sampling</i>	13
3.2	<i>Ionisation techniques.....</i>	13
3.2.1	General aspects of ionisation	14
3.2.2	Electron Ionisation (EI)	14
3.2.3	Photoionisation (PI)	15
3.2.3.1	Nd:YAG laser as light source for PI.....	15
3.2.3.2	Single-photon ionisation (SPI)	16
3.2.3.3	Resonance-enhanced multi-photon ionisation (REMPI)	17
3.3	<i>Mass analysers.....</i>	17
3.3.1	Time-of-flight mass spectrometer (TOFMS)	17
3.3.2	Quadrupole (QMS)	19
3.4	<i>Instrumentation for aerosol analysis.....</i>	20

3.4.1	On-line PI-TOFMS	20
3.4.2	Thermal-optical carbon analysis (TOCA) and hyphenation to PI-TOFMS	21
3.4.3	In-situ derivatisation thermal desorption gas chromatography mass spectrometry (IDTD-GCMS)	22
3.4.4	Aerosol mass spectrometry (AMS) and soot-particle aerosol mass spectrometry (SP-AMS)	22
3.5	<i>Statistical data analysis</i>	23
3.5.1	One-way Analysis of Variance (ANOVA1) and Kruskal-Wallis test (H-test) with Bonferroni correction for multiple testing	23
3.5.2	Non-negative matrix factorisation (NMF)	24
3.5.3	Principal component analysis (PCA)	25
3.5.4	Projection-on-latent-structures (PLS) regression	26
4	Results and discussion	26
4.1	<i>Primary aerosol emissions from a marine auxiliary engine</i>	26
4.1.1	Chemical composition of carbonaceous particulate emissions	27
4.1.2	Markers in the fraction of aromatic VOCs and IVOCs emissions from SECA-compliant and non-SECA-compliant fuels	28
4.1.3	Prediction model to quantify the contribution of ships in simulated REMPI spectra of mixed anthropogenic emission sources	30
4.1.4	Development of direct infusion REMPI-MS to analyse medium and heavy marine fuels from the liquid phase	31
4.2	<i>Secondary emissions from a marine auxiliary engine</i>	32
4.3	<i>Primary emissions from two modern small-scale wood combustion appliances</i>	33
4.3.1	Time-resolved analysis of volatile emissions	33
4.3.2	Emission factors (EFs) and PAH toxicity equivalents (PAH-TEQ) from 4 h combustion experiments	35
4.3.3	Effect of slow ignition of logwood on EFs and emission patterns	36
4.3.4	Implications for source apportionment of modern wood combustion appliances	37
4.3.5	Statistical concepts from wood combustion for process control: application on coffee roasting	37
4.4	<i>Secondary emissions from modern small-scale wood combustion appliances</i>	38
4.4.1	Ageing of primary emissions from logwood combustion in a smog chamber	38
4.4.2	Ageing of primary emissions from pellet combustion in a PAM flow reactor	39
5	Summary and outlook	40
6	References	42

LIST OF ABBREVIATIONS

ALS...	<i>alternating least-square</i>
AMS...	<i>aerosol mass spectrometer</i>
ANOVA...	<i>analysis of variance</i>
BBOA...	<i>biomass burning aerosol</i>
BC...	<i>black carbon</i>
BrC...	<i>brown carbon</i>
CAFE...	<i>“clean air for Europe”</i>
CCN...	<i>cloud condensation nucleus</i>
CMB...	<i>chemical mass balance</i>
DI-REMPI-MS...	<i>direct infusion REMPI mass spectrometry</i>
DF...	<i>diesel fuel</i>
EC...	<i>elemental carbon</i>
EF...	<i>emission factor</i>
EI...	<i>electron ionisation</i>
ELVOC...	<i>extreme low-volatile organic compound</i>
FID...	<i>flame ionisation detector</i>
FSC...	<i>fuel sulphur content</i>
GC/MS...	<i>gas chromatography mass spectrometry</i>
HACA...	<i>hydrogen abstraction - carbon addition</i>
HFO...	<i>heavy fuel oil</i>
HOA...	<i>hydrocarbon-like organic aerosol</i>
IDTD-GC/MS...	<i>in situ derivatisation thermal desorption GC/MS</i>
IE...	<i>ionisation energy</i>
IR...	<i>infra-red</i>
IVOC...	<i>intermediate-volatile organic compound</i>
LR...	<i>laser reflectance</i>
LT...	<i>laser transmittance</i>
LVOC	<i>low-volatile organic compound</i>
MCP...	<i>micro channel plate</i>
MGO...	<i>marine gas oil</i>
MMH...	<i>modern masonry heater</i>
MSTFA...	<i>N-Methyl-N-(trimethylsilyl)trifluoroacetamide</i>
NMF...	<i>non-negative matrix factorisation</i>

OA...	<i>organic aerosol</i>
OC...	<i>organic carbon</i>
OGC...	<i>organic gaseous carbon</i>
OM...	<i>organic matter</i>
OPO...	<i>optical parametric oscillator</i>
PAH...	<i>polycyclic aromatic hydrocarbon</i>
PB...	<i>pellet boiler</i>
PCA...	<i>principal component analysis</i>
PI...	<i>photoionisation</i>
PICS...	<i>photoionisation cross section</i>
PLS...	<i>projection on latent structures</i>
PAM...	<i>potential aerosol mass</i>
PM...	<i>particulate matter</i>
PMF...	<i>positive matrix factorisation</i>
POA...	<i>primary organic aerosol</i>
QFF...	<i>quartz fibre filter</i>
rBC...	<i>refractory black carbon</i>
RMSE...	<i>root-mean-square error</i>
SECA...	<i>sulphur emission control area</i>
SIA...	<i>secondary inorganic aerosol</i>
SOA...	<i>secondary organic aerosol</i>
SP-AMS	<i>soot-particle aerosol mass spectrometer</i>
SPI...	<i>single-photon ionisation</i>
SVOC...	<i>semi-volatile organic compound</i>
TC...	<i>total carbon</i>
TEQ...	<i>toxicity equivalent</i>
TG...	<i>thermal gravimetry</i>
TOCA...	<i>thermal-optical carbon analysis</i>
TOFMS...	<i>time-of-flight mass spectrometer</i>
UCM...	<i>unresolved complex mixture</i>
ULSD...	<i>ultra-low sulphur diesel</i>
UV...	<i>ultraviolet</i>
VIP...	<i>variable importance in projection</i>
VOC...	<i>volatile organic compounds</i>
VUV...	<i>vacuum- ultraviolet</i>

LIST OF FIGURES

Fig. 1	<i>Sources and sinks of aerosol emissions</i>	1
Fig. 2	<i>Classification of carbonaceous aerosols</i>	2
Fig. 3	<i>Two-dimensional volatility basis set of organic aerosols</i>	4
Fig. 4	<i>Atmospheric conversion of organic aerosol emissions</i>	7
Fig. 5	<i>Interaction between particles and solar radiation</i>	9
Fig. 6	<i>Health impact of ambient PM</i>	10
Fig. 7	<i>Ship tracks over Pacific coast of California</i>	11
Fig. 8	<i>Energy scheme of a 4-level laser</i>	15
Fig. 9	<i>Energy scheme of single-photon ionisation (SPI)</i>	16
Fig. 10	<i>Energy scheme of [1+1] resonance-enhanced multi-photon ionisation (REMPI)</i>	17
Fig. 11	<i>Scheme of a time-of-flight mass spectrometer with Wiley-McLaren ion optic and Reflectron</i>	19
Fig. 12	<i>Scheme of a quadrupole mass spectrometer and channeltron detector</i>	20
Fig. 13	<i>Instrumental setup of on-line photoionisation time-of-flight mass spectrometry (PI-TOFMS)</i>	20
Fig. 14	<i>Instrumental setup of the thermal-optical carbon analyser (TOCA) coupled to photoionisation time-of-flight mass spectrometry (PI-TOFMS)</i>	21
Fig. 15	<i>Instrumental setup of the in-situ derivatisation thermal desorption gas chromatography mass spectrometry (IDTD-GCMS)</i>	22
Fig. 16	<i>Instrumental setup of the Aerodyne aerosol mass spectrometer (AMS)</i>	23
Fig. 17	<i>SPI (left) and REMPI (right) mass spectra of DF and HFO particles</i>	28
Fig. 18	<i>PCA biplots of REMPI spectra from ship and non-ship emissions</i>	29
Fig. 19	<i>Prediction model for the contribution of ship emissions Φ</i>	31
Fig. 20	<i>Instrumental setup of the direct infusion resonance-enhanced multi-photon ionisation mass spectrometry (DI-REMPI-MS) and comparison to thermal gravimetry with evolved gas analysis by REMPI-TOFMS of North Sea crude oil</i>	32
Fig. 21	<i>NMF results of SPI mass spectra from one logwood combustion experiment</i>	34
Fig. 22	<i>Toxicity equivalent (TEQ) of particle-bound PAHs</i>	36
Fig. 23	<i>Application of NMF on SPI mass spectra of coffee roasting off-gas</i>	38

Fig. 24 SOA formation from spruce logwood combustion in a smog chamber. 38

Fig. 25 Van Krevelen diagram of aged and non-aged OA from a pellet boiler..... 39

LIST OF TABLES

Table 1 Organic markers from the incomplete combustion5

1 Introduction: atmospheric aerosols

Aerosols are generally defined as a suspension of liquid or solid particles in a gas, with aerodynamic particle diameters in the range of 10^{-9} – 10^{-4} m, where the lower limit is given by molecules and molecular clusters and the upper limit is determined by rapid sedimentation of large particles or small droplets. Although clouds also comply to the definition, they are usually considered separately [9]. In atmospheric science, the term aerosol actually refers to suspended particles including the condensed matter, which is also called particulate matter (PM). Typical considered fractions of PM appear below the upper limits of $0.1\ \mu\text{m}$ (PM_{0.1}, ultrafine particulate matter), $1\ \mu\text{m}$ (PM₁), $2.5\ \mu\text{m}$ (PM_{2.5}, fine particulate matter) and $10\ \mu\text{m}$ diameter (PM₁₀, coarse particulate matter), but PM of the same aerodynamic diameter can appear in different shape and morphology, dependent on its origin [10].

Although the results of the publications included in this thesis focus on combustion emissions, a brief introduction is given into most important atmospheric (tropospheric) processes to put the emission studies into a broader environmental context.

1.1 Sources and sinks

The sources for atmospheric aerosol can be classically divided into naturally occurring and anthropogenic or primary (directly emitted) and secondary (generated by atmospheric processing of precursors) ones.

The dominant sources of naturally occurring aerosol are sea spray and soil eruptions, but also wildfires and volcanic activity as well as biologically-driven emissions of microorganisms, pollen, plants and plant debris. Anthropogenic aerosol is emitted from land-based, maritime, railroad and air traffic, domestic and large-scale stationary energy generation from the combustion of fossil and non-fossil fuels, industrial production, food cooking and road dust [11]. Regarding mass, natural sources account for the majority of atmospheric aerosol, but the contribution of anthropogenic aerosols to total ambient concentration can substantially increase locally, especially in urban areas, where traffic, industry and energy production are concentrated [12].

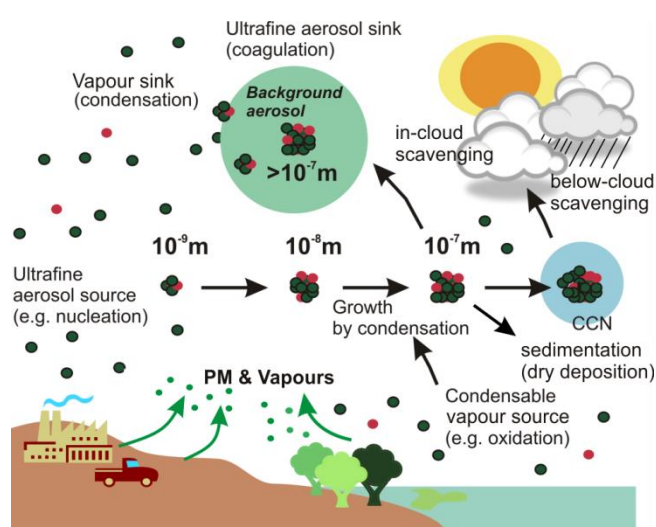


Fig. 1 Overview of primary PM and vapour emissions and their main sinks of dry (sedimentation) and wet deposition (in-cloud and below-cloud scavenging) (adapted from [1]).

The lifetime of an aerosol particle in the atmosphere covers the range from hours to weeks, depending on its properties [13, 14], which may change in atmospheric transformation concerning size, structure and composition, as well as involved deposition mechanisms. Atmospheric aerosols can act as cloud condensation nuclei (CCN) and initiate cloud formation by water uptake. During

precipitation, the aerosol inside clouds fall onto the Earth's surface (*in-cloud scavenging*), but also scavenges other aerosol as well (*below cloud scavenging*), which is the most important aerosol sink and known as "wet deposition" [12]. A sink of lower global relevance is the dry deposition. In particular, small aerosols succumb to Brownian diffusion and impaction on larger aerosols, droplets or other obstacles if they cannot follow the streamlines of the gas flow. On contrast, aerosols of larger size already deposit because of gravitationally sedimentation [15]. Therefore, the meteorological events of rain and wind velocity are key parameters for aerosol deposition and can rapidly and substantially reduce PM concentrations in highly polluted areas [16, 17] (Fig. 1). Typical concentration of PM_{2.5} ranges between 1 $\mu\text{g m}^{-3}$ and 100 $\mu\text{g m}^{-3}$ equivalent to 10^2 to 10^5 particles per cm^3 [9], but peak concentrations in mega cities can even reach concentrations of 400 $\mu\text{g m}^{-3}$ [17, 18].

1.2 Chemical composition and classification

The chemical composition of ambient aerosols can be generally described by an organic and inorganic fraction, whereby the latter one is mainly comprised of sulphate, nitrate, ammonium and chloride [19]. However, the proportions of these fractions can vary considerably at different sites because of diverse emission source contributions and solar radiation available for photochemistry. Nevertheless, further inorganic aerosol constituents, such as alkali and transition metals, can also provide valuable information about the aerosol source in spite of their low concentrations.

1.2.1 Carbonaceous aerosol

The individual studies in this thesis predominantly deal with the fraction of organic aerosol (OA) and aim to identify characteristic emission profiles and possibly new marker substances. Often only carbon as essential element for organic compounds is measured as organic carbon (OC), which can be converted by a source-specific factor to OA (also called organic matter (OM)), thereby accounting for further elements H, O, N and S [20]. An analytical challenge is the separation of OC and elemental carbon (EC), which refers to almost pure graphite-like carbon in soot particles [21], by thermal-optical carbon analysis (TOCA, see also section 3.4.2). In particular, the ratio OC/EC provides useful information about the aerosol origin [22]. Other frequently used terms for carbonaceous PM constituents are black carbon (BC) and brown carbon (BrC), representing together light-absorbing carbon (LAC).

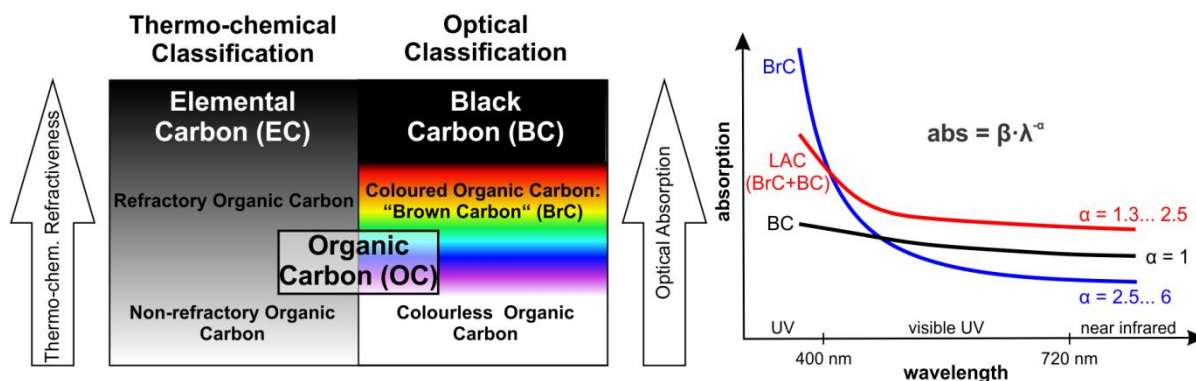


Fig. 2 Classification of carbonaceous aerosol by thermo-chemical or optical properties (left, adapted from [9]) and wavelength dependency of absorption for components of light-absorbing carbon (LAC).

Often BC and EC are used interchangeable, but by definition, BC is determined by optical measurements whereas EC refers to thermal-optical methods. BrC can be simply described as carbon of UV-light-absorbing organic compounds, whose absorption spectrum strongly increases towards shorter wavelengths compared to the more uniformly absorbing BC (Fig. 2). The light attenuation of aerosols by scattering can be fitted by a power law

$$\tau = \beta \cdot \lambda^{-\alpha} \quad (1.1)$$

where τ denotes the aerosol optical depth and λ the wavelength to characterise PM size distribution and concentration by Ångström exponent α and Ångström (turbidity) coefficient β , respectively [23]. If only absorption is considered, α becomes the Ångström absorption exponent, which is close to unity for BC, but can reach values up to 6 for biomass combustion [24]. Apparently, this concept works only for a mixture of several components since single species do not necessarily show a steady decline in absorption towards longer wavelengths, but characteristic absorption bands [25].

1.2.2 Organic aerosol (OA)

Constituents of OA are commonly classified based on combined oxidation state/emission source, volatility range or traditional organic compound classes. The first classification originates from data interpretation of aerosol mass spectra (AMS, see also section 3.4.4.) from ambient air. It comprises of hydrocarbon-like organic aerosol (HOA), biomass burning organic aerosol (BBOA) and oxidised organic aerosol (OOA), which are associated with the sources fossil-fuel combustion, biomass combustion and secondary organic aerosol (SOA) formation [26]. Furthermore, HOA and BBOA are emitted by primary sources and are combined to primary organic aerosol (POA). A physical classification of OA constituents was proposed by the group of Neill M. Donahue based on certain volatility bins from saturation vapour pressures and consequential gas-particle partitioning [27]. The gas-particle partitioning coefficient ζ for a compound i is defined as

$$\xi_i = \left(1 + \frac{C_i^*}{C_{OA}}\right)^{-1} \quad (1.2)$$

where C_i^* denotes the effective saturation concentration ($C_i^* = \gamma \cdot C_i$, with γ being the activity coefficient) of a single compound and C_{OA} defines the total mass concentration of organic aerosol.

$$C_{OA} = \sum_i C_i \xi_i \quad (1.3)$$

Later on, this one-dimensional volatility basis set was extended to a second dimension by incorporation of the oxygen content (by oxygen to carbon ratio O:C) of the OA. [28]. On that account, five volatility fractions of OA called volatile (VOC), intermediate-volatile (IVOC), semi-volatile (SVOC), low-volatile (LVOC) and extreme low-volatile organic compounds (ELVOC) were defined, linked to the average carbon oxidation state and combined with OA fractions from AMS mass spectra to LV- and SV-OOA (Fig. 3 [29]). Traditionally ELVOC was included in LVOC and IVOC was split between SVOC and VOC. However, in the studies of this thesis these new definitions are applied, which sum the total organic components of the gas phase to organic vapours.

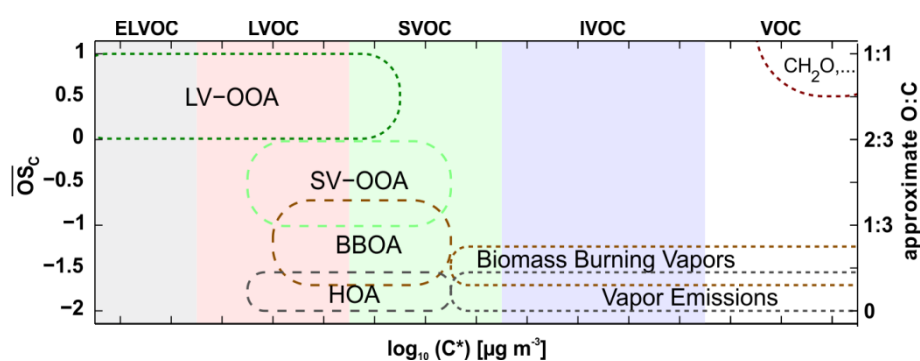


Fig. 3 Two-dimensional volatility basis set of saturation concentration C^* and average carbon oxidation state \overline{OS}_C derived from molecular ratio oxygen to carbon (O:C) [4], adapted from [29].

1.3 Organic markers in combustion aerosol

1.3.1 Defining markers and tracers

An earlier approach on the molecular level goes back to the work of Bernd R. T. Simoneit and co-workers, who stuck to the classical chemical compound classes and examined OAs of several primary emission sources down to the molecular level [30-34]. This type of classification does not involve the total OA composition anymore as can be seen from the still substantial amount of “unresolved complex mixture” (UCM) in their publications, but aims to figure out the most important components for discrimination between sources. However, for a view of source specific OA constituents on a molecular level, it is necessary to introduce the term “marker” and “tracer” in atmospheric science.

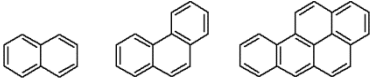
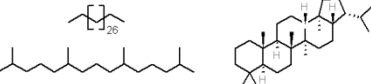
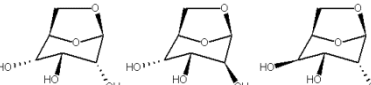
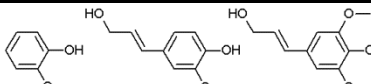
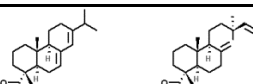
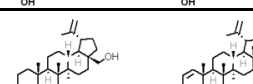
“By definition, an atmospheric *tracer* is ‘an entity which preserves its identity as it moves with the air from a known source, where the tracer is created or otherwise introduced into the atmosphere, to a known sink where it is destroyed or removed from the atmosphere’” [35]. In contrast, *markers* refer to compounds which are uniquely emitted by a specific source. Consequently, tracers cannot be found in OA because sinks of organic compounds on particles are manifold, which counteract the requirement of preservation [35]. Both tracers and markers can be utilised to calculate the contribution of single emission sources receptor models, such as positive matrix factorisation or chemical mass balance.

1.3.2 Established organic markers for CA

In the following table (Table 1), frequently used compound classes and markers for emission source apportionment are introduced. Although some compounds and whole classes are not restricted to a specific source, such as polycyclic aromatic hydrocarbons (PAH) and alkanes, they have been proven useful in diagnostic ratios (DR). DR refers to a ratio of two compounds giving an upper or lower limit, which is not breached by a certain type of emission. Therefore, this approach may allow rapid identification of dominating emission sources. For example, the ratio of anthracene to phenanthrene exceeds 0.1 for OA formed by pyrosynthesis in combustion while for petrogenic origins (unburned fuel) 0.1 denotes an upper limit [36]. However, this concept has been also criticised since compounds involved in a DR often haven different degradation kinetics in the

atmosphere and bias the results [37]. Especially for markers in the particle phase, kinetics of heterogeneous reaction are distinctly affected by the particle composition [38].

Table 1 Organic markers from the incomplete combustion of fossil and biomass fuels

Compound class	Example	Structure	Origin
Polycyclic Aromatic Hydrocarbons	naphthalene phenanthrene benz[a]pyrene		- any combustion emissions - formed by HACA, aromatisation of precursors or cleavage of
Alkanes	pristane triacontane hopane		- fossil fuels - plant wax
Anhydrous Sugars	levoglucosan mannosan galactosan		- combustion of cellulose and hemicellulose
Phenolic Species	guaiacol coniferyl alcohol sinapyl alcohol		- combustion of lignin from coniferous and deciduous wood
Resinoic Acids	abietic acid pimaric acid		- combustion of coniferous wood
Phytosterols	betulin glochidone		- combustion of specific wood types

In the more volatile fraction of organic emissions (organic vapours) from combustion, less potential molecular markers have been found compared to the particle phase. So far, only acetonitrile was accepted as marker for biomass burning, but has been proven to be less suitable for residential wood combustion in urban areas [39]. However, compounds without marker status in all volatility ranges, including VOCs [40], can be principally involved in emission source apportionment when taking the entire emission pattern into consideration by multivariate statistics or chemical mass balances.

1.3.3 Origin of markers from fuel composition and processing

Emission patterns can be explained by combustion conditions, such as temperature, as well as fuel properties and composition. The combustion process can be broadly divided in two categories: combustion of liquid and gaseous fuels in internal combustion engines and solid fuel combustion, such as biomass combustion in stoves.

Generally, for fuel combustion in engines, the fuel is premixed with air or directly injected and ignited by sparks (spark-ignition engine) or self-ignition (diesel engine). Regardless the possible variations for combustion engines and conditions, temperatures about 1500°C to 2000°C are achieved inside the combustion chamber [41], thus the main elements of common fuels, C and H, are efficiently converted into CO₂ and H₂O. However, trace concentrations (compared to the main combustion products) of organics from VOCs to ELVOCs and soot particles can be detected, which either survive the combustion process as unburned fuel or are formed during the combustion. The general reason for this phenomenon is a deficit in oxygen availability, which can also locally appear in diesel

engines despite their categorical operation on excess oxygen ($\lambda > 1$). For engine-based combustion at high temperatures, the formation of organic compounds by pyrosynthesis [42] affects the emission pattern substantially. As previously mentioned, PAHs are found in almost every combustion process. At temperatures above 500°C, C-H and C-C bonds break and free radicals are formed, which combine to acetylene. By further condensation aromatic ring structures start to grow and form initially PAH, which are thermodynamically stable and resistant to thermal degradation, and finally soot. This mechanism is formally known as Hydrogen-Abstraction-Carbon-Addition (HACA) [43]. Since the fuel-air mixture is exposed to high temperatures, but relatively short residence times inside the combustion chamber, not only thermodynamic products, but also kinetic reaction products are formed in noticeable yields. Again considering the isomers phenanthrene and anthracene, the first one denotes the thermodynamically more stable compound due to more intact aromatic rings in all resonance structures. Anthracene is hardly detected in the fuels, but formed during combustion, which allows the separation of the emission source by DR.

In contrast to engine emissions, the combustion of biomass, including wood, occurs at lower temperatures below approximately 1000°C [44, 45], so HACA plays a minor role for organic emissions. On that account, the emissions are dominated by the fuel rather than pyrosynthesis.

Generally, the composition of wood and woody biomass can be almost completely described by the polymers lignin and the carbohydrates cellulose and hemicelluloses. While cellulose is solely comprised of alpha-1,4-condensed glucose units, other monosaccharides, such as mannosan or galactosan, can be constituents of hemicelluloses. Lignin consists of different phenolic species and is responsible for the variable degree of lignification of plants. Low temperature combustion, i.e. smouldering, breaks the chemical bonds between these monomers with low efficiency for further combustion to CO₂ and H₂O. For the carbohydrates, these monomers are anhydrous sugars, such as levoglucosan, which has been established since its introduction as a universal marker for biomass combustion in general [46]. Lignin thermally decomposes in phenolic species, whereby the substituents of the aromatic ring allow differentiation between angiosperms, gymnosperms and gramineae, which is approximately equivalent to hardwood, softwood and grasses [30]. The higher the combustion temperature, the lower is the yield of these characteristic (woody) biomass combustion markers because of ongoing thermal degradation, e.g. from levoglucosan to furans or lignin monomers to low-substituted phenols [47-49]. Apart from the three biopolymers, miscellaneous organic constituents of wood can be phytosterols or resins. The molecular composition of these classes can even provide the origin of the CA to the point of wood species. They belong to the class of LVOCs and are usually emitted by evaporation during an early stage of the combustion [8]. Many of them decompose before evaporation by releasing H₂, H₂O (elimination) or CO₂ (decarboxylation), forming alteration products. Nevertheless, similar information can be obtained from those species due to conservation of the fundamental molecular structure.

1.4 Atmospheric aerosol transformation

1.4.1 Atmospheric oxidising agents and products

As pointed out in section 1.3.1., organic emissions released to the atmosphere do not remain stable, but undergo chemical reactions (“ageing”) with atmospheric oxidising agents OH radicals, O₃ and NO₃ radicals [50-52]. During daytime, OH radicals are produced by photolysis of O₃ at wavelengths below 355 nm and subsequent reaction of the formed O(¹D) with water vapour [50]. Tropospheric O₃ involved in the ageing process results from the photolysis of NO₂ by UV light or oxidation of VOC by OH radicals with several partial reactions, which involves the photolysis of NO₂ as well and lead to near-ground O₃ formation [53, 54]. However, NO₂ is also oxidised by OH radicals to HNO₃, which is a sink for NO₂. At night, O(¹D) is not generated from photolysis, so O₃ undertake the oxidation of NO₂, but to nitrate radicals. All of the three atmospheric oxidising agents are naturally in equilibrium to each other in complex reaction cycles, which further involves CO, NO and HO₂ as well [53]. However, OH radicals, O₃ and nitrate radicals are regarded as the key drivers for atmospheric conversion of organic emissions. The main difference between OH and NO₃ radicals compared to O₃ refers to the structural requirements of the reaction partner. While OH and NO₃ radicals are able to react with constituents of VOC and OA emissions, O₃ requires a double bond to attack and form the primary ozonide [55]. Consequently, ozone is not directly involved in the degradation of saturated organic compounds, such as alkanes and halocarbons [56], but affect the oxidation product distribution [57].

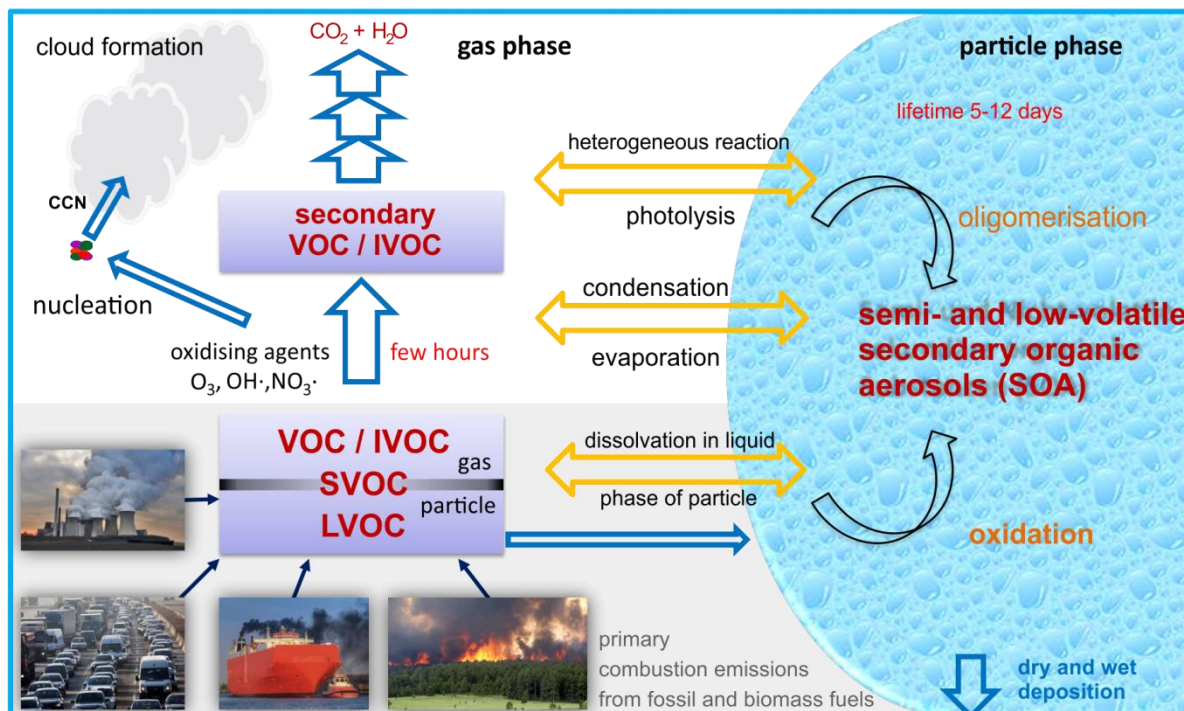


Fig. 4 Atmospheric conversion of primary combustion aerosol by gas-particle partitioning, homogeneous and heterogeneous oxidation.

OA constituents over the full volatility range undergo atmospheric oxidation. If bond cleavage is avoided, the addition of functional groups is associated with a decrease in volatility, which leads to

nucleation or condensation on existing particles by molecular interactions. Additional generated mass by gas-to-particle conversion in a homogeneous reaction refers to secondary organic aerosol (SOA) or secondary inorganic aerosol (SIA), such as the oxidation of NH_3 and NO_x to nitrate [58]. In contrast, gained particle mass by oxidation of particle constituents in a heterogeneous reaction strongly depends on the particle composition [59, 60] and is referred to aged primary organic aerosol (aged-POA) [61]. However, further homogeneous reactions take place in the liquid phase of a particle between its constituents, forming not only highly oxidised, but also high-molecular weight compounds. Typical compound classes of SOA and aged-POA cover carbonyls, acids as well as organic nitrates and sulphates depending on the oxidising agents involved [62, 63] and also contribute to the fraction of BrC [64]. Since SOA and aged-POA have higher functionality and polarity than their precursors, they are hygroscopic and act as more effective cloud condensation nuclei (CCN) [65].

1.4.2 Simulation of atmospheric transformation in batch and flow reactors

The atmospheric fate of organic emissions can be studied in two different types of reactor. The first is called “smog chamber” and basically consists of a Teflon bag and UV-lamps around to simulate the influence of solar radiation. After the chamber was filled with a realistically-diluted emission, the ageing of the aerosol can be monitored in real-time, either at daytime with UV-lamps switched on or night-time with external feed of O_3 . However, since the volume of many smog chambers is not large enough to neglect losses of particles at the wall, this effect has to be corrected by a non-reactive particle emission constituent, such as BC. A limitation of this approach is the minimum ratio of VOCs to NO_x to start the ageing process. Relatively high amounts of NO_x consume atmospheric oxidising agents, disturb their equilibria [53] and therefore suppress SOA formation. Furthermore, a low ratio of primary VOCs to OA requires high sensitivity for measuring changes in particle mass. To overcome these issues and to enable the SOA formation at unfavourable conditions, a second instrumental approach was developed.

The smog chamber may be regarded as a batch reactor, the second instrument for simulating ageing, called Potential Aerosol Mass (PAM), refers to plug flow reactors [66-68]. It consists of a single glass cylinder which is also equipped with UV-lamps to start photochemistry from an external feed of O_3 . The resulting OH generation can be controlled by adjusting the humidity of the aerosol. In contrast to the smog chamber, the PAM flow reactor is capable to age aerosol concentrations higher than in ambient air, but expose the aerosol to higher concentrations of OH radicals. Therefore, a maximum enhancement ratio of OA, i.e. the potential aerosol mass can be determined. Depending on the UV-lamp intensity, the short residence time inside the PAM flow reactor of approximately one minute is regarded as equal to atmospheric ageing of days with daily OH exposure of $1.5 \cdot 10^6$ molecules cm^{-3} h [69]. On the one hand, it has been criticised that this type of ageing is very artificial and questionable to compare with real atmospheric process, but on the other hand it offers a possibility to study the atmospheric fate of emission sources with unfavourable properties for smog chamber experiments [70].

1.5 Impact of combustion aerosol

1.5.1 Greenhouse effect and radiative forcing

Primary emissions from combustion contain several organic and inorganic greenhouse gases, which absorb infrared (IR) solar radiation leading to a net warming effect on climate. CO_2 , CH_4 , N_2O and fluorinated gases including hydro- and perfluorohydrocarbons as well as SF_6 are regarded as key greenhouse gases emitted by human activity, while the first three ones are emitted by several combustion processes [71]. In contrast, for the determination of the net effect of atmospheric particles on radiative forcing and consequently on climate, more processes and particles properties have to be considered. Particles directly interact with incident solar radiation through reflection, diffraction, refraction, absorption and re-radiation (Fig. 5). Depending on the ratio between particle size d and light wavelength λ , the scattering can be physically described by the laws of geometrical optics ($d \gg \lambda$), Mie scattering ($d \approx \lambda$) or Rayleigh scattering ($d \ll \lambda$) [72]. In addition to d and λ , the chemical composition of the particles and therefore the absorption properties affect interactions with light. Colourless particles cover a higher degree of reflection, thus scattering solar radiation back to space and causing negative feedback on global warming. In contrast, BC has been identified as substantially light-absorbing constituent of atmospheric particles and counteracts the negative feedback [73]. The ratio of absorption to reflection, referred to the term albedo, is high for BC particles, which turns BC into the most important anthropogenic emission after CO_2 [74].

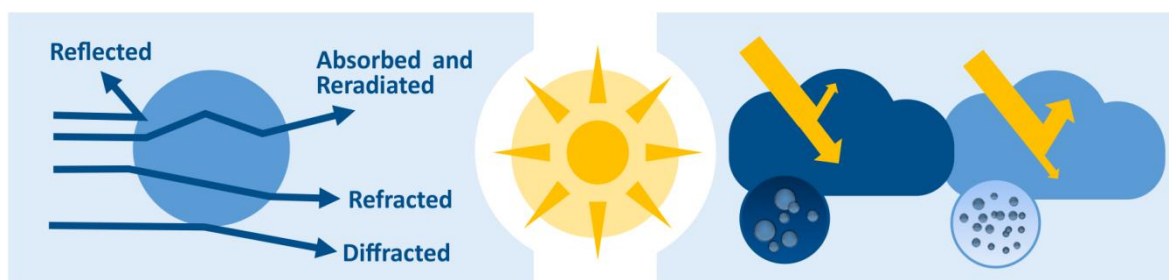


Fig. 5 Light-particle interaction of a single particle (left) and scattering of solar radiation by clouds dependent on droplet size and composition (right).

Moreover, also the fraction of BrC (see section 1.2.1.) covers a positive radiative forcing by absorption [75], which represents approximately 25% of the total downward UV attenuation [21]. However, particles also indirectly affect radiative forcing by acting as CCN. The ability to initiate cloud formation also depends on the chemical composition of the particle and thus its hygroscopicity. On the one hand, clouds reflect incident solar radiation and prevent absorption, dependent on the droplet size and composition. On the other hand they also diminish the energy radiation emitted from Earth [76]. In total, the feedback of clouds on global warming is regarded as to be negative [77].

1.5.2 Human health

The second motivation for the investigation of combustion aerosols is the severe impact on human health. Inorganic gaseous emissions CO and NO_x as well as many VOCs, such as 1,3-butadiene, benzene and naphthalene, are known for their deleterious effect on human health through inhalative

uptake [78, 79]. Bad air quality by high levels of PM are often caused by activity from traffic, industry and residential heating, especially in urban areas and megacities [18, 80, 81], and can lead to several fatal diseases [82]. Two of the most well-known examples for bad air quality are “London Smog” in the year 1952 [83] and the “Harvard Six Cities Study”, which firstly exhibited an inverse relation between products of incomplete combustion in urban air and life expectancy [84]. In the programme “*The Clean Air for Europe*” [85], a map was created for Europe showing the reduction in life expectancy because of PM, [86-89] which highlights the described situation in built-up and industry areas, e.g. northern Italy and the Ruhr region in Germany (Fig 6). However, it must be noted that PM is not generally harmful to human health, but may be dependent on its physical properties (size, shape, surface and morphology) and chemical composition. An obvious example is the fairly high concentration of sea salt aerosol in climatic health-resorts at coast. If PM is inhaled, it enters the respiratory tract, but penetrates it to different depths. Therefore, not the total inhaled PM reaches the alveolar region of the lung, which carries out the gas exchange between air and blood. Generally, PM in the size ranges between $2.5\ \mu\text{m}$ and $1\ \mu\text{m}$ as well as below $100\ \text{nm}$ efficiently deposit in the respiratory tract [90], which explains the classification given in section 1. While the deposition of particles in the micrometre range takes already place in the pharynx and larynx, PM_{0.1} most effectively deposits in the alveoli. Especially PM emissions from combustion aerosols cover this size range and contain several chemical species, such as PAH and metals, which can enter the human body and are known for their acute and long-term toxicity [91, 92].

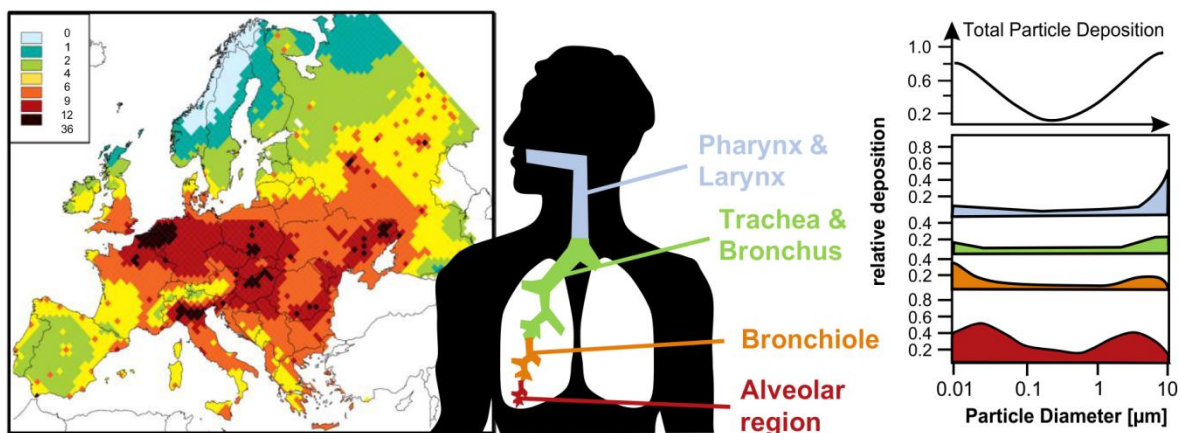


Fig. 6 Reduction of life expectancy in Europe caused by exposure of ambient PM (left, taken from [85]) and size dependence of PM deposition in human airways (centre). Especially ultrafine PM with aerodynamic diameter below $100\ \text{nm}$ reaches the alveolar region (right, adapted from [90]) in which the gas exchange takes place.

2 Focus: wood combustion and shipping (WOOSHI)

The experiments were designed for the DACH-project WOOSHI (“Wood combustion and shipping”) funded by German Research Foundation (DFG) and Swiss National Science Fund (SNF). Collaborators of the project are located at University of Rostock, Helmholtz-Zentrum München and Paul-Scherrer Institute in Villigen, Switzerland. Additionally, some of the experiments were carried

out together with the Helmholtz Virtual Institute of complex molecular systems in environmental health (HICE).

Although wood combustion and ship emission are very different in many senses, they gained more public attention for their effect on air quality and climate. Furthermore, both emission sources are changing due to new legislation and improved combustion technology.

2.1 Ship traffic and sulphur emission control areas (SECA)

During the oil crises of the 70s and the associated increase of the oil price, the usage of marine fuels shifted from middle distillates of the crude oil refinery, such as marine diesel oil (MDO) or marine gas oil (MGO), towards cheaper heavy fuel oils (HFO), also called residual fuel oil. The latter refers to the vacuum residue of the crude oil refinery blended by lighter refinery products, such as kerosene, to meet a certain maximum viscosity. Those HFOs are rich in sulphur and heavy metals which end up as significant constituents in emitted PM_{2.5} after combustion. Especially for harbour cities or highly frequented ship traffic routes, HFO-derived PM_{2.5} has been identified as an important perpetrator of increased mortality by cardiopulmonary diseases and lung cancer on global down to local scale [93, 94].

In order to tackle air pollution by ship traffic, the Marine Environmental Protection Committee of the International Maritime Organisation decided to restrict the marine fuel-sulphur content (FSC) in international waters from 3.5% to 0.5% (from 2020 on) and from 1% to 0.1% in sulphur emission control areas (SECA, from 2015 on), which comprises coastal regions of Europe and North America, respectively. Therefore, the consumption of marine fuels in SECAs returned to predominantly marine distillates since exhaust after-treatment such as sulphur scrubbers are not economic at low oil prices [95]. Although MGO or MDO are subjected to the same FSC limitation as HFO, they have intrinsically lower FSCs because sulphur is concentrated in the heavier fraction of the fuel [96].

Generally, the number of studies investigating primary ship emissions is remarkably low compared to other emission source, such as land-based traffic or wood combustion, and mainly focus on cumulative parameters (e.g. PM, BC, OC), main gaseous combustion products (CO₂, CO, NO_x, SO_x) and inorganic particle constituents [97-100]). Thus, emission factors for ships are demanded for the calculation of global emission inventories. Especially the composition of organic emissions on a molecular level was investigated only in few studies before this project had been started in 2013 [101-103]. For source apportionment studies, some of the emitted species have been proved useful for the identification of ship emissions in ambient air, such as the ratio of V to Ni and high concentrations of SO₂ and sulphate, but unfortunately they are restricted to ingredients of HFO

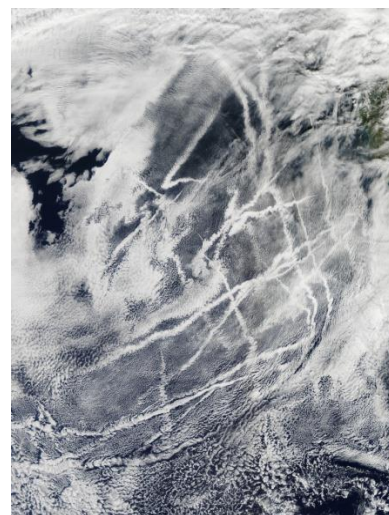


Fig. 7 Satellite image of Pacific Ocean and Californian coast illustrating cloud formation on frequented ship routes. Primary and secondary sulphate from HFO combustion act efficiently as cloud condensation nuclei (CCN)[5].

and likely work less efficiently or even not at all. Studies of ambient air measurements predicted and confirmed a reduction in PM after the introduction of SECAs [104, 105]. However, despite “cleaner” fuels an *in vitro* study by Oeder et al. (2015) [106] demonstrated that also emissions from a marine engine even operating on ultra low-sulphur diesel (ULSD, 10 ppm FSC), i.e. marine fuel with lowest available FSC. induces effects on human lung cells concerning energy metabolism, protein synthesis, and chromatin modification.

In contrast to biological responses, an opposite trend was found for the effect of ship emissions on climate. Despite the high emissions of greenhouse gases, the net effect of HFO combustion on radiative forcing is negative, i.e. HFO combustion emissions cool the climate. This finding can be explained, but also weakened by including atmospheric chemistry and physics. Outstanding high anthropogenic emissions of SO₂ have only an atmospheric half-life between 4 and 28 days below 10 km altitude with respect to oxidation by OH radicals [107]. The resulting sulphates nucleate to hygroscopic particles and contribute to cloud formation, which is commonly regarded as cooling effect due to enhanced back-scattering of solar radiation to space. Clouds along the main ship routes are known as “ship tracks” [108] and are even visible on satellite images (Fig. 7). Therefore, despite general reduced emissions by distillate marine fuels which are limited in FSC and consequently SO₂ emissions as well, a total warming effect was obtained in simulation studies [104]. However, climate effects of HFO and distillate marine fuels converge to each other on longer time-scales towards warming because of shorter atmospheric half-lives for PM compared to CO₂ and tropospheric O₃ [109, 110]).

Considering the high relevance and complexity of this aerosol emission type, three further questions need to be answered:

- (1) What is the molecular composition of organic ship emissions and are emission factors relevant for global emission inventories?
- (2) How does the emission profile change from HFO to MGO combustion and which compounds can be used to track MGO combustion in marine engines?
- (3) Is SOA formed from primary ship emissions and, if yes, what are its components?

On that account, primary emissions from a marine engine, located at the *Faculty of Mechanical Engineering and Marine Technology* of the University of Rostock, operating on HFO, MGO and ULSD under various engine conditions were studied.

2.2 Advanced combustion technology for residential wood combustion

In many countries of Europe as well as in North America, the residential combustion of biomass, in particular wood, as a renewable energy source is encouraged by legislation, such as “Energiewende” in Germany to decrease the dependence on fossil fuels and contribution to global warming due to a favourable carbon footprint. Installations of small-scale wood combustion appliances have been subsidised and can be classified into batchwise-fired logwood stoves and continuously-/automatically-fired pellet burners and boilers. Especially the logwood stoves have

been characterised as high emission sources for various pollutants, including BC, several metals, particle-bound and volatile organic compounds. Automatically-fired appliances often have lower emissions by one order of magnitude [8, 111, 112]. In regions with substantial residential wood burning, decreased air quality was observed related to high PM levels [113-115]. In several studies, wood smoke was proven to cause severe biological effects in exposure experiments with cells, animals and humans [116-119]).

To tackle this issue, combustion technologies of small-scale wood combustion appliances are continuously developed to decrease emissions of various pollutants and increase energy conversion. One strategy to reduce emissions is the implementation of air staging technology in secondary air supply [120], which became an established technique for modern wood combustion appliances [121]. In air staging, a secondary combustion zone is generated and supplied with secondary air through many channels. Hence, VOC and PM emissions are substantially reduced for both logwood stoves and pellet boilers [122, 123], but two questions remain unclear:

- (1) Does the emission profile (“fingerprint”), i.e. the relations between pollutant concentrations, remain stable and can be identified in emission source apportionment studies?
- (2) Does the reduction in primary emissions also accompany lower secondary particle formation?

On that account, the emission profiles of organic vapours and PM_{2.5} from a modern wood stove and pellet boiler as well as their secondary aerosol formation potential were investigated in a measurement campaign at the *Fine Particle and Aerosol Technology* laboratories of the University of Eastern Finland.

3 Methodology

3.1 Aerosol sampling

First, the combustion aerosol, e.g. from the tailpipe or chimney, passed a temperature-insulated pre-cyclone to remove coarse particles with an aerodynamic diameter larger than 2.5 µm at a temperature of approximately 300 °C to minimise losses. Subsequently, a porous tube ejector system (Venacontra, DAS, Finland) [124] diluted the emissions by a factor from 10 to 40 upon simultaneous cooling to room temperature for particle collection on quartz fibre filters (QFF). The dilution ratio was monitored by CO₂ measurements in the raw exhaust and after dilution, which was adjusted by critical orifices. On-line photoionisation mass spectrometry for gas phase analysis sampled directly from the raw exhaust while particles were removed by a cylindrical glass fibre filter. Stepwise heating of the sampling line from glass fibre filter at 220°C to 250°C in front of the ion source avoid condensation.

3.2 Ionisation techniques

For mass spectrometric analysis of a sample, atoms or molecules are converted into ions, separated according to the mass-to-charge ratio m/z and detected by secondary electron multipliers. Different

ionisation techniques are available, which are classed as either soft or hard by means of generating predominantly molecular ions or fragment ions. In the following, the most common hard ionisation technique electron ionisation and two laser-based soft photoionisation techniques are introduced.

3.2.1 General aspects of ionisation

The generated ions from molecules, atoms or clusters can carry positive or negative charges, but this section considers only positive ionisation, which is preceded by electron removal from an analyte. For this purpose, a minimum energy has to be supplied to the analyte which is known as ionisation energy (IE). More precisely, the IE is defined as the energy necessary to convert an analyte in its electronic and vibrational ground state to an analyte ion, which is also in its ground state (adiabatic IE), by ejection of an electron. Principally, electrons can be removed from σ -bonds, π -bonds and lone pairs of electrons, while the latter ones are the most favoured.

The ionisation process is allowed to be described only with consideration of the electrons without the nucleus due to the Born-Oppenheimer approximation and Franck-Condon principle. Electronic transitions occur at much faster time-scales than nuclei require reaching equilibrium positions. Hence, it is assumed that the bond length remain constant during ionisation. The probability of a (vertical) transition leading to ion formation is highest for the maximum interference of the electronic wave functions of ground state and ionised state, i.e. transitions with similar nucleus distances r for both states, while the probability distribution of possible transitions are expressed by Franck-Condon factors. Regardless Franck-Condon factors, the larger the difference between r_0 and r_1 of a transition is, the higher is the probability that the dissociation barrier is exceeded, which finally lead to fragmentation.

3.2.2 Electron Ionisation (EI)

Electron ionisation (EI) represents the most commonly used approach for ionisation in organic mass spectrometry, especially for gas chromatography mass spectrometry (GCMS) applications, in which the analytes are already vaporised for ionisation. However, because of the higher relevance of photoionisation for the presented studies, EI is rather superficially considered in the following paragraphs.

The underlying principle of EI is the interaction of high energy electrons with valence electrons of the analytes. First, electrons are emitted from a heated tungsten filament and subsequently accelerated by a voltage of 70 V. Thus, they obtain a kinetic energy of 70 eV, which is far above the typical IEs from 7 to 15 eV of organic compounds. In the ion source, accelerated electrons orthogonally hit the molecular beam from the inlet or interface of the GC and generate ions. Due to a large transfer of excess energy on the analyte, EI causes not only molecular, but many fragment ions, which classifies EI as hard ionisation technique. Primarily generated molecular ions are in excited vibrational and rotational states, which may cause several bond cleavages through relaxation [125]. The fragmentation is advantage and disadvantage at the same time: On the one hand, induced fragmentation gives structural information about the analyte and can be further exploited for identification or multivariate calibration for quantification. Due to the plateau of ionisation cross section in the range of 60-80 eV, EI at 70 eV offers highest ionisation efficiency and reproducible

mass spectra [126], which allows the comparisons of mass spectra acquired at different instruments and databases. On the other hand, many of the fragments are not specific to a compound class and in particular ineffective for the identification of analytes from a homologue series when the molecular ion is absent, especially in the analysis of complex mixtures. Moreover, EI includes the ionisation of the main air components as well as typical GC carrier gases (He, H₂ and N₂), which limits trace analysis through extension of the dynamic range of a mass analyser to higher concentration. On these accounts, soft and more selective ionisation techniques, such as photoionisation techniques, are demanded and introduced in the following section.

3.2.3 Photoionisation (PI)

In contrast to EI, photoionisation (PI) belongs to the class of soft ionisation techniques because the (total) photon energy is close to the typical IEs of analytes, so that the abundance of molecular ions greatly exceeds the fragmentation. For the ionisation, light sources are required which either provide photons with sufficient energy to cross the ionisation energy of an analyte or sufficient density to induce multi-photon processes. Moreover, it can be distinguished between continuously emitting light sources, which are usually characterised by lower power densities, and pulsed light sources. From a technical point of view, lasers and lamps have been successfully applied as light sources for photoionisation. In the following, the Nd:YAG laser is introduced, which have been used in this study for single-photon (SPI) and resonance-enhanced multi-photon ionisation (REMPI).

3.2.3.1 Nd:YAG laser as light source for PI

Laser stands for *light amplification by stimulated emission of radiation* and provides coherent and intensive light with low divergence and small band width. In particular, Nd:YAG laser refers to 4-level solid state lasers, which are widely applied in natural science, medicine and technique [127]. Electrons of the laser medium, consisting of an yttrium aluminium garnet host lattice, in which Y³⁺ is partially replaced by Nd³⁺, are excited from ground state (E₁) to higher electronic and vibrational states (E₄) by radiation from a xenon-filled flash-lamp (optical pumping).

Those vibrational states have usually short lifetimes, so that electrons promptly reach the lower energy state E₃, accompanied by fluorescence or non-radiative transitions. For Nd:YAG lasers, the lifetime of E₃ substantially exceeds E₄, so the electron population is accumulated in E₃. If the excited state of lower energy E₂ also has a lower lifetime, a permanent population inversion required for the stimulated emission is generated (Fig. 8).

The high intensities are achieved by continuous repetition of the process (laser oscillation) inside the Perot-Fabry resonator, which is basically comprised of a mirror for full reflection and semi-transparent mirror with the laser medium in between. Emitted photons are reflected by the mirrors and meanwhile hit the laser medium, inducing electron excitation and the emission of additional

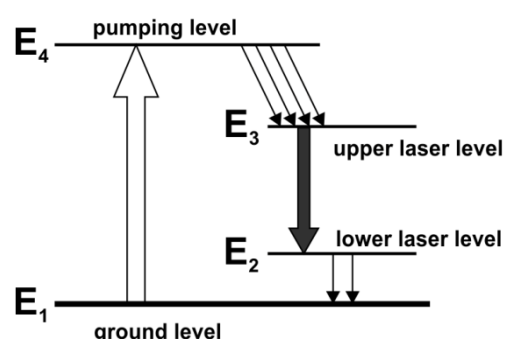


Fig. 8 Energy scheme of a 4-level laser, such as Nd:YAG lasers. The dark grey arrow shows emitted fundamental laser radiation with the photon energy $E_3 - E_2$.

photon, which is called the stimulated emission. The semi-transparent mirror enables to partly use the generated radiation for applications. However, only photons of parallel motion to the resonator axis can contribute to light amplification. Hence, the laser beam leaving the resonator exhibits low divergence and small band width of a wavelength equal to the energy difference between E_3 and E_2 , which is 1,064 nm for an Nd:YAG laser and referred to the fundamental radiation [128].

Despite the highest power of 7 W at 1,064 nm of the applied Nd:YAG laser, the photon energy is equivalent only to 1.17 eV, which is far beyond the appropriateness for ionisation. Therefore, the high laser intensity is exploited in anisotropic crystals or isotropic gases for frequency multiplication, i.e. shortening of the wavelength to generate photons of higher energy. High radiation intensities negate the linear relation between polarisation response P and the strength of the electric field E of the valence electrons, and also induce inharmonic oscillations. If the linear relation between P and E

$$P = \alpha \cdot E \quad (3.1)$$

with α as susceptibility for the anisotropic medium, is developed in a series expansion

$$P = \alpha \cdot E + \beta \cdot E^2 + \gamma \cdot E^3 + \dots \quad (3.2)$$

terms of higher order can exceed the first term, which still describe the linear relation. In case of anisotropic crystals, photon frequencies can be doubled (second harmonic generation, SHG) or even matched to provide photons of 266 nm (fourth harmonic generation, FHG, 4.66 eV photon energy) for REMPI or 355 nm (third harmonic generation, THG, 3.51 eV photon energy) [129]. The latter wavelength is further tripled (THG2) by passing a cell filled with xenon to provide 118 nm for SPI. Due to self-absorption of solid anisotropic media, frequency multiplication below 190 nm is restricted to gases. In a simpler concept of energy conservation, two or three photons are combined to one photon with the energy of the two or three initial photons. However, the conversion yield for those processes decreases strongly towards shorter wavelengths, with 30 % efficiency for SHG and 0.01 % for THG2 [130].

3.2.3.2 Single-photon ionisation (SPI)

In single-photon ionisation (SPI), the ionisation of a molecule or atom is carried out by absorption of only one photon of energy greater than the ionisation energy (Fig. 9). The deployed wavelength of 118 nm is equivalent to photon energy of 10.49 eV. Considering typical ionisation energies for organic molecules between 7 and 12 eV, the majority of compounds, but also some inorganic compounds, such as H_2S and NO , are principally accessible. In contrast, main components of air (N_2 , O_2 , H_2O , Ar , CO_2), but also frequently used GC carrier gases (He and H_2 , cannot be ionised because of too high ionisation energies. Moreover, mainly molecular ions can be expected due to small differences between photon and ionisation energy, leading to small excess energy and low potential for fragmentation [131]. However, fragmentation and also the probability for successful ionisation of a

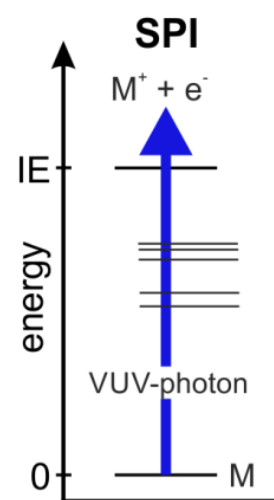


Fig. 9 In SPI, the absorption of one VUV-photon causes the ionisation.

molecule (in the following referred as photoionisation cross sections, PICS) depend on the functionality and compound class, but also on the wavelength. A PICS range of approximately one order of magnitude has been reported between single aromatic and aliphatic hydrocarbons at 118 nm [132].

3.2.3.3 Resonance-enhanced multi-photon ionisation (REMPI)

In contrast to the universal ionisation technique SPI, resonance-enhanced multi-photon ionisation (REMPI) is regarded as a selective ionisation technique for aromatic compounds if performed with UV-photons, which are often provided by the FHG of an Nd:YAG laser (266 nm), KrF excimer laser (248 nm) or ArF excimer laser (193 nm). In the first step, an UV-photon is absorbed by a molecule, which becomes excited to an intermediate state. If the lifetime of this intermediate state is long enough, a second photon can be absorbed that the energy of the two photons can exceed the ionisation energy (Fig. 10). From this scheme it can be seen that the selectivity of REMPI is controllable by several parameters, such as photon wavelength(s), pulse duration and light intensity, and linked with UV-spectroscopy. Thus, the selectivity for aromatics does not hold in general, but for 266 nm and laser intensities between 10^6 and 10^8 W cm⁻². Generally, REMPI processes are labelled by $[m+n]$, where m photons excite the analyte and n photons lead to ionisation. Thus, the applied REMPI technique refers to the simplest case of $[1+1]$ -REMPI although higher processes are also possible [133].

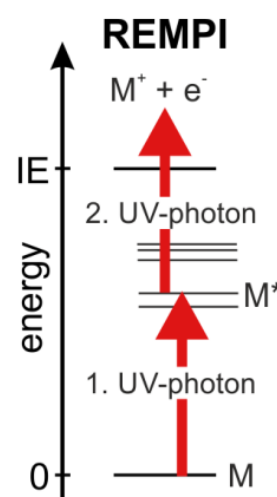


Fig. 10 In REMPI, the absorption the first UV-photon excites the analyte while the second UV-photon causes the ionisation.

3.3 Mass analysers

3.3.1 Time-of-flight mass spectrometer (TOFMS)

In a TOFMS, ions which have been generated at a defined point of time are accelerated by an applied high voltage U . Subsequently, the ions pass through a free drift tube of the distance s and hit the detector. In case of single-charged ions, the drift time t depends on the mass m because under the same kinetic energy, i.e. the same acceleration voltage, heavier ions need longer t for the drift path s .

Independent from the ionisation technique, the electric charge q of an ion with the mass m is equal with the number z of elementary charges e :

$$q = z \cdot e \quad (3.3)$$

The energy of the electric field E_{el} caused by the acceleration voltage U can be expressed as

$$E_{el} = q \cdot U = z \cdot e \cdot U \quad (3.4)$$

while E_{el} is converted into kinetic energy E_{kin} of the ions:

$$E_{el} = E_{kin} = \frac{1}{2} \cdot m \cdot v^2 \quad (3.5)$$

Suppose that the generated ions are at rest, the ion velocity can be described as

$$v = \sqrt{\frac{2 \cdot e \cdot z \cdot U}{m}} \quad (3.6)$$

By substitution of $v = s \cdot t^{-1}$ and a constant drift path s , the equation is reconverted to demonstrate the proportional relation between the drift time t and square root of m/z , which is considered for the mass calibration of the instrument:

$$t = \frac{s}{\sqrt{2 \cdot e \cdot U}} \cdot \sqrt{\frac{m}{z}} \quad (3.7)$$

Furthermore, it can be seen that due to the direct proportional relation between the drift path s and the flight time t , longer drift paths s enables to maximise difference in arrival times Δt between two ions and consequently the mass resolution of the instrument. Therefore, isobaric compounds, i.e. compounds with the same nominal mass, but different sum formula, can be separated. However, the theoretical Δt between two ions is not reached, i.e. the mass resolution is affected by basically three reasons [125]:

(1) Independent from the ionisation technique, the ionisation volume (e.g. the laser spot) is not infinitesimal, so generated ions differ in starting points for acceleration to the drift path and consequently in energy due to different distances to the acceleration electrodes (extractor and repeller). Ions with starting points closer to the repeller undergo higher acceleration voltage, so they will overtake ions with higher distance to the repeller. The associated velocity distribution broadening of ions increases with time and renders the advantage of longer flight paths less effective. However, at a certain spot in the drift path these ions have a minimum of difference in distance (space focus) in which the detector should be located, but in such a setup the spatial focus would appear too close to the ion source and would result in insufficient mass separation.

(2) The generated ions cover an isotropic velocity distribution, which is caused by the kinetic energy of the neutral molecules or atoms and space-charge effects. Thus, an ion can initially move diametrically to the electric extraction field before its sense of direction is changed towards the detector that it requires a so-called “turn-around-time”.

(3) Ions are generated during a non-infinitesimal period of time that some ions are earlier accelerated than others.

By implementation of a two-stage ion extraction invented by Wiley and McLaren [134], the spatial focus of the ions can be shifted to higher applicable drift paths through adjusting the first and second extraction voltage according to the Wiley-McLaren criterion

$$s = 2x_1 \cdot \sqrt[2]{k^3} \left(\frac{1-x_2}{(k+\sqrt{k}) \cdot x_1} \right) \quad (3.8)$$

with s is the flight path, x_1 is the distances between first extractor and ionisation zone, x_2 is the distances between first and second extractor, and k is the ratio of the first and second acceleration

voltages for a space focus equal to the flight path s . Therefore, the space focus compensates the energy uncertainty for an optimal k for the fixed drift path s .

A second improvement on the mass resolution was achieved by the application of a two-stage Reflectron, which was developed by Boris A. Mamyrin [135]. The Reflectron consists of two consecutive electric fields, which firstly decelerate and a subsequently accelerate the ions in the opposite direction. Ions of higher kinetic energy penetrate deeper into the Reflectron than

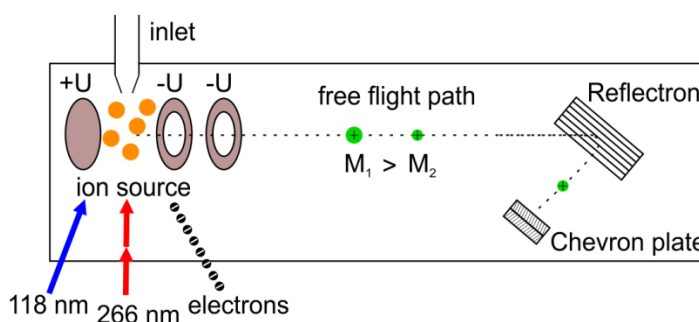


Fig. 11 Scheme of a time-of-flight mass spectrometer with Wiley-McLaren ion optic and Reflectron.

ions of lower energy. Thus, the broadening of the ion package after the Wiley-McLaren space focus can be corrected with additional doubling of the drift path, which allowed during the time of the invention already mass resolutions $> 10,000$. However, the overall mass resolution of a TOFMS with both Wiley-McLaren ion optic and Reflectron is limited by the Liouville theorem, which states that the volume of a closed system in phase space is constant. Consequently, a complete correction of the spatial and energy uncertainty cannot be achieved at the same time, but can be approached by applying preferably high voltages.

In order to enhance the quality of the spectra, the ions were extracted by pulsed extractor and repeller voltages with a delay of 100 ns between laser shot and extraction. Thereby, electrons which were simultaneously generated to the (positive) ions were allowed to leave the ion source due to their order of magnitude higher velocity (Born-Oppenheimer approximation). In a continuous electric extraction field, electron would be accelerated in the direction of the repeller electrode and cause additional fragment ions, which reduces the advantages of molecular ion yields in soft photoionisation, but also the reproducibility of EI spectra.

In TOFMS, ions of different m/z arrive with high frequency at the detector, thus it has to comply with fast responsiveness. The micro channel plate (MCP) refers to a commonly used detector which is composed of many parallel-connected secondary electron multipliers with a channel diameter between 10 and 25 μm . Each channel is capable to generate secondary electrons from impinging ions at the channel wall, which are amplified and induce a measurable voltage drop. To prevent that ions pass the channels without collision, they are tilted a few degrees away from orthogonal impact angle. Often two or three standard MCPs were combined to a *chevron plate* or *z-stack*, which achieve amplifications up to 10^6 and 10^8 , respectively, using voltages in the kilovolt range [125].

3.3.2 Quadrupole (QMS)

Quadrupole are known as compact, cheap, robust and the most frequently used mass analysers in mass spectrometry [128]. It consists of four parallel cylindrical rods, which are linked and arranged in a square. One pair of two opposing rods is linked with the positive pin of an adjustable direct current supply while the remaining pair is linked with the negative pin. Additionally, alternating voltages,

which are phase-shifted by 180°C , are applied between each pair of rods. Thus, an alternating positive and negative electrical field is generated relative to the centreline, which forces cations to the centreline (positive field) or to the rods (negative fields), and enables to filter single m/z or to scan a full mass spectrum in the sub-second range. Usually, ions are detected by secondary electron multiplier (SEM), or more precisely by channel electron multipliers (CEM), which amplifies impinging ions as a single channel of an MCP described in section 3.3.1.1. Compared to TOFMS, quadrupole operate substantially slower, but are regarded as more robust. For the analysis of few single compounds, the quadrupole is preferred, whereas for rapid analysis of ions with several m/z or monitoring of fast dynamic processes, TOFMS offers better performance.

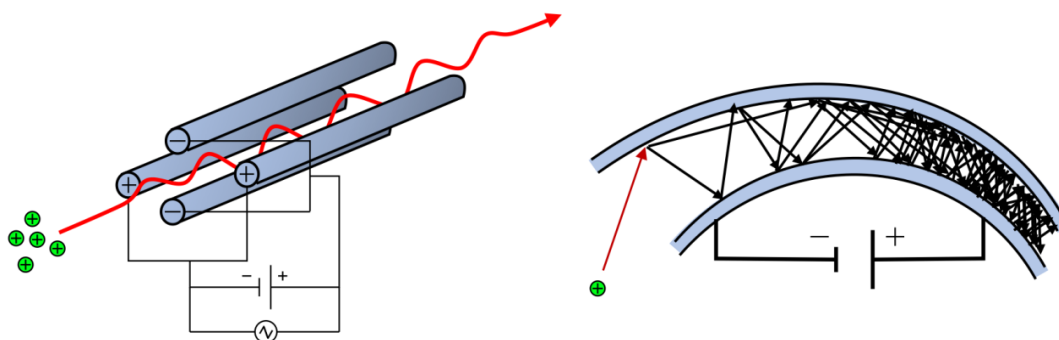


Fig. 12 Disposal of electrodes in a quadrupole mass spectrometer and possible ion flight path (left) and channeltron detector for secondary electron multiplication.

3.4 Instrumentation for aerosol analysis

3.4.1 On-line PI-TOFMS

Two identical TOFMSs (*compact time-of-flight II*, Firma Stefan Kaesdorf, Geräte für Forschung und Industrie, Germany) were equipped with Nd:YAG lasers (*Spitlight400*, Innolas, Germany; *Big Sky Ultra*, Quantel, France) for on-line monitoring of organic vapours, which includes the VOCs, IVOCs and the gas-phase of SVOCs, and few volatile inorganic compounds using SPI and REMPI in parallel [136, 137]. On-line instrumentation is especially demanded for the investigation of dynamic processes, e.g. batchwise wood combustion, but can also yield in low limit of detections (LOD), which decreases with the square root of the number of averaged mass spectra.

The TOFMSs were connected to the raw or diluted exhaust of an emission source by heated transfer lines at minimum 220°C and a support flow of

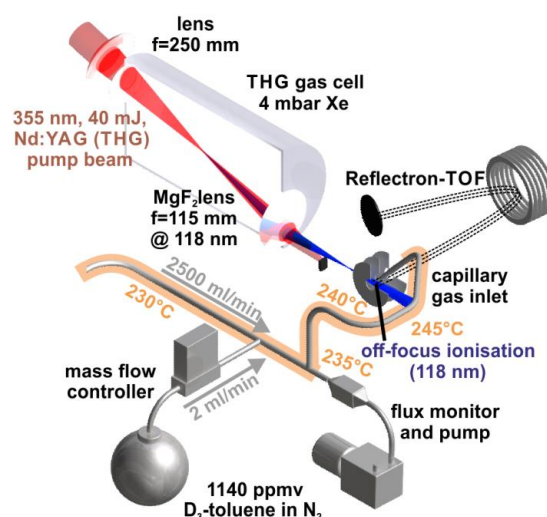


Fig. 13 Instrumental setup of on-line photoionisation time-of-flight mass spectrometry (PI-TOFMS, shown for SPI) for the analysis of organic vapours in real-time. The addition of isotope-labelled toluene to the raw exhaust enables semi-quantification of selected analytes.

2.5 l min⁻¹. After removal of particles by a glass fibre filter, the remaining organic vapours were mixed with an internal standard of triply deuterium-labelled toluene (D₃-toluene, m/z = 95; *toluene methyl-D3*, 98% purity, Cambridge Isotope Laboratories, Inc.) for a final concentration between 100 and 1000 ppb and subsequent ionisation and detection. With the knowledge of PICS relative to toluene, semi-quantification was possible.

For the investigation of the composition of coffee roasting off-gas, a second TOFMS (custom-made, Firma Stefan Kaesdorf, Geräte für Forschung und Industrie, Germany) was equipped with an Nd:YAG laser (*Continuum Surelite III*, Santa Clara, USA) and optical parametric oscillator (OPO, GWU Lasertechnik, Erfstadt, Germany) to perform SPI at 118 nm and REMPI at 227 nm, 248 nm and 266 nm.

3.4.2 Thermal-optical carbon analysis (TOCA) and hyphenation to PI-TOFMS

Thermal/optical carbon analysis (TOCA, DRI Model 2001a) coupled to photon ionisation time-of-flight mass spectrometry (PI-TOFMS) refers to an untargeted technique and enables to quantify organic (OC) and elemental carbon (EC), but also to investigate the molecular composition of the thermal sub-fractions related to OC. The TOCA consists of an oven surrounding a quartz cross, laser diodes of seven wavelengths, detectors for laser reflectance and transmittance, an MnO_x catalysts (*oxygenator*), a Ni catalyst adsorbed on silica (*methanator*) and a flame ionisation detector (FID). A punch of 0.5 cm² from the QFF sample is placed into the oven by a push rod and heated in He according to the *ImproveA* protocol, defining four thermal subfractions of OC (OC1 – OC4) [138]. During thermal analysis of the sample, material from the filter evolves and becomes oxidised inside the oxygenator at 900°C. Subsequently, the formed CO₂ is mixed with H₂ and converted to CH₄ inside the methanator unit at 420°C. Finally, the carbon is quantified by an FID, which is known for

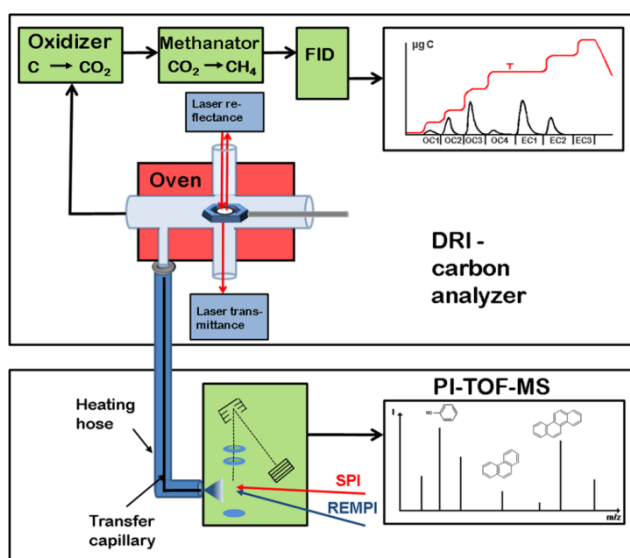


Fig. 14 Instrumental setup of the thermal-optical carbon analyser (TOCA) coupled to photoionisation time-of-flight mass spectrometry (PI-TOFMS). Besides organic carbon (OC) and elemental carbon (EC), the evaporation of single analytes over four OC fractions can be monitored.

its carbon sensitive and selective detection. After OC4 (580°C), the atmosphere is changed to 2% O₂ in He to oxidise EC from the filter to CO₂, which is analogously quantified. However, thermally unstable or low-volatile organic compounds decompose before evaporation and may form pyrolytic organic carbon (OC_{pyr}), which cannot be distinguished from original EC on the filter. Therefore, the initial laser transmittance (LT, for low loaded QFFs) and laser reflectance (LR, for heavy loaded QFFs) of the filter sample are measured at 635 nm and continuously monitored during the entire analysis. When OC_{pyr} is formed, LT and LR decrease compared to their initial values since additional OC_{pyr} additionally absorbs 635 nm light. In EC1, LR and LT re-increase due to

simultaneous oxidation of OC_{pyr} and true EC. After LR and LT have reached their initial level, the quantified carbon belongs to OC_{pyr} , whereas further quantified carbon accounts for true EC.

Approximately 8 % of the total flow enters the TOFMS through a deactivated transfer capillary (inner diameter of 320 μm), which is connected to the carbon analyser oven by a modified quartz cross stepwise heated from 230 $^{\circ}\text{C}$ to 245 $^{\circ}\text{C}$ to prevent condensation [139, 140]. Evolving compounds entering the ion source are ionised and analysed by PI-TOFMS as described in section 3.2.3. and 3.3.1. Thus, a molecular fingerprint of the four subfractions from OC1 to OC4 can be obtained.

3.4.3 In-situ derivatisation thermal desorption gas chromatography mass spectrometry (IDTD-GCMS)

The in-situ derivatisation thermal desorption gas chromatography mass spectrometry (IDTD-GC/MS) consists of a conventional GC oven (*Agilent 6890 gas chromatograph*, Agilent, USA) with a EI-TOFMS (*Pegasus III TOFMS*, LECO, USA), but advanced sample injection system, which enables to simultaneously investigate polar and non-polar constituents of PM from filter samples [6]. Polar compounds may have too low volatility for GC analysis or may decompose during the GC run, which can be overcome by derivatisation of hydroxyl and carboxyl groups. Polar compound classes of interest include anhydrous sugars, aliphatic alcohols, phenolic species, fatty acids and resin acids. For the analysis, a filter aliquot damped by N-methyl-N-(trimethylsilyl)trifluoroacetamide (MSTFA) is placed in the injector, which constantly heated to 300 $^{\circ}\text{C}$ to accelerate the reaction rate and shorten the analysis time. He as carrier gas, which is mixed with additional MSTFA, passes the injector to desorb PM constituents and ensure complete derivatisation. Other non-polar analytes, such as PAHs, are not affected by the derivatisation. The resulting silyl ether (from alcohols) and esters (from carboxylic acids) can be easily identified by EI fragments of m/z 73, corresponding to trimethylsilyl group, as well the characteristic isotopic distribution of Si.

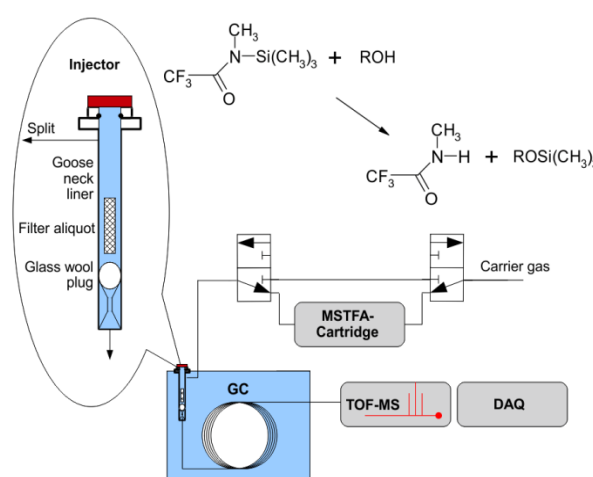


Fig. 15 Instrumental setup of the in-situ derivatisation thermal desorption gas chromatography mass spectrometry (IDTD-GCMS) with addition of derivatisation agent (MSTFA) and highlighted construction of the injector (taken from [6]).

3.4.4 Aerosol mass spectrometry (AMS) and soot-particle aerosol mass spectrometry (SP-AMS)

The aerosol mass spectrometer (AMS) was first introduced in 2000 [141] and enables the on-line investigation of the bulk composition of submicron particles in the aerodynamic diameter range of 75 nm to 650 nm. It basically consists of three main sections, starting with the aerosol sampling unit (including aerosol inlet and aerodynamic lens), through which particles are sampled under atmospheric pressure, transferred to vacuum conditions and focused to generate a particle beam. In

the particle sizing unit, a mechanical spinning chopper wheel allow only small portions of particles to pass. From the flight time of the particle packages to the particle composition detection unit, a size distribution is obtained, which can be refined for chemical species. After the flight path, particles hit the porous tungsten vaporiser of 600°C in a pressure of 10^{-5} Pa, so non-refractory particle components are volatilised, subsequently ionised by EI, separated and detected by a mass spectrometer [142], in this study a high resolution TOFMS (HR-TOF-AMS, Aerodyne Research Inc., USA). The total content of particle-bound organics derived from AMS are called organic matter (OM), which is quantified together with nitrate, ammonium, sulphate and chloride by a fragmentation table together with particle properties including elemental ratios (O:C, H:C), ratio of organic matter to

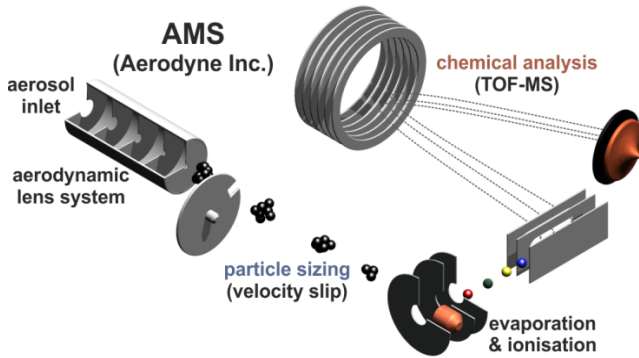


Fig. 16 Instrumental setup of the Aerodyne aerosol mass spectrometer (AMS) comprising of aerosol inlet with aerodynamic lens system, particle flight path, thermal vaporiser, filament for EI and time-of-flight mass spectrometer.

organic carbon (OM/OC), and mean carbon oxidation state (\overline{OS}_C) [143].

In addition to the AMS, the soot-particle aerosol mass spectrometer (SP-HR-TOFAMS, Aerodyne Research Inc., USA) is equipped with laser vaporiser (Nd:YAG laser, 1064 nm) to partially volatilise refractory components of the particles. With only the laser vaporiser on, the SP-AMS is selective for near infra-red light-absorbing particles, such as refractory black carbon (rBC) and metal nanoparticles, which are ionised by EI as described in the previous paragraph [144].

3.5 Statistical data analysis

3.5.1 One-way Analysis of Variance (ANOVA1) and Kruskal-Wallis test (H-test) with Bonferroni correction for multiple testing

The one-way Analysis of Variance (ANOVA1) refers to the generalisation of the Student's t-test for k instead of only two groups. Basically, ANOVA1 compares the variances of a variable within the k groups with the variances between the groups by calculating the sum of squares (SS)

$$SS_b = \sum_{j=1}^k n_j \cdot (\bar{y}_j - \bar{y})^2 \quad (3.9)$$

$$SS_w = \sum_{j=1}^k \sum_{i=1}^{n_j} (y_{i,j} - \bar{y}_j)^2 \quad (3.10)$$

for n_j observations in each of the k groups where \bar{y} denotes the mean of the total distribution and \bar{y}_j refers to the mean of the j th group. Subsequently, an F-test is performed by calculating the ratio of SS_b and SS_w corrected by the degrees of freedom $df_b = k-1$ and $df_w = k \cdot (n_j-1)$:

$$F = \frac{\frac{1}{df_b} \cdot SS_b}{\frac{1}{df_w} \cdot SS_w} \quad (3.11)$$

Finally, the obtained F-value is compared to the critical values from the F-distribution (F_{crit}) at common significance level α of 0.05, which represents probability of 5% for a random error (Type I error). The assumption, i.e. null hypothesis H_0 , for ANOVA is that the group means are equal, which is tested against the alternative hypothesis H_1 of unequal means. If the calculated F exceeds F_{crit} , the null hypothesis is rejected, so there is a *significant* difference between the group means. However, it cannot be determined which two or more group means are different. If t-tests are performed for each possible combination c of the k groups, α would increase exponentially because the probability p of making a Type I error is

$$p = 1 - (1 - \alpha)^c \quad (3.12)$$

since for each new test there implies a new probability of Type I error. For the example of 5 groups and thus 10 possible combinations, p increases to 0.401 for all group comparison although each comparison has only a Type I error of 0.05. This phenomenon is called α -error accumulation.

To identify different group means, there are several possibilities to adjust α for appropriate multiple testing (posthoc analysis), which are regarded as liberal or conservative in terms of rejecting H_0 . Conservative posthoc tests are not recommended for high numbers of k , but in all studies presented here, the k did not exceed 11, so the conservative Bonferroni posthoc correction was applied. The α adjustment was performed according to the equation

$$\alpha_{adj} = \frac{\alpha_{single}}{c} \quad (3.13)$$

where α_{adj} is the new significance level and α_{single} the significance level for a single comparison of two groups [145].

Technically speaking, ANOVA1 is only allowed to be carried out if normal distribution and variance homogeneity is given between the distributions of the k groups. However, it has been shown that ANOVA performs generally robust with not-normally distributed data [146]. In contrast, different variances of the groups substantially affect the results of ANOVA. In this case, the non-parametric Kruskal-Wallis test (H-test) [147] was performed, which does not make any assumption about the distribution. First, the metrically scaled variable is transferred to an ordinal scale by replacing the exact values by their ranks. For no ties (i.e. no equal values), the test statistic H is calculated according to

$$H = \frac{12}{N(N+1)} \sum_{j=1}^k \frac{R_j^2}{n_j} - 3(N+1) \quad (3.14)$$

where N denotes the total number of observations in all groups k , n_j is the number of observations in one group and R_j refers to the sum of the ranks in the j th group. The H value is compared to critical values (H_{crit}), which follow a χ^2 -distribution, under the same H_0 and α follow by posthoc analysis equal to ANOVA.

3.5.2 Non-negative matrix factorisation (NMF)

Non-negative matrix factorisation (NMF) was applied to examine the temporal evolution of variables (i.e. m/z, compound classes) and to pool them into classes. Generally, NMF partitions iteratively a

non-negative m -by- t matrix M into an m -by- k matrix W (hereinafter referred to as factor loadings) and a k -by- t matrix H (hereinafter referred to as scores). The variable k refers to the rank of the NMF solution but can be practically regarded as the number of processes to identify and has to be predefined [148]. In this context, the matrix dimension m stands for m/z and t for the total time. In the presented studies, the rank of the NMF solution was preset based on previous knowledge about the investigated processes or the physical reasonability of the result.

Factor loadings W and scores H are computed by an alternating least-squares (ALS) algorithm to minimise the cost function

$$f(W, H)_k = \|M - WH\|_F^2 \quad (3.15)$$

where $\|X\|_F^2$ computes the Frobenius-norm of a non-negative matrix X . Consequently, the product of W and H is an approximation of the original data matrix M . Because the iteration starts with random initial values W_0 and H_0 for W and H , the NMF may lead to different solutions when repeated if the algorithm converges in a local minima for $f(W, H)_k$. To improve reproducibility of NMF, initial values for W_0 and H_0 are optimised by a multiplicative update algorithm [149] which is slower, but more sensitive for initial value optimisation [148], before running the ALS algorithm [150]. The temporal evolution of the k processes are illustrated by calculating the relative proportions h_t in % of the absolute score values H_t for each of the k element at any point of time t .

$$h_t = \frac{H_t}{\sum_{i=1}^k H_{t,i}} \cdot 100\% \quad (3.19)$$

Please note that in atmospheric sciences, the NMF is also called positive matrix factorisation (PMF) and refers to the ALS algorithm by Paatero & Tapper (1994) [150], which is one of the most commonly used receptor model for source apportionment [151].

3.5.3 Principal component analysis (PCA)

Suppose a data set of m variables (e.g. m/z , chemical compounds) and n observations (e.g. samples, point in time) organised in an n -by- m data matrix M , which equals n observations in an m -dimensional space. Principal component analysis (PCA) aims to project the data for in a space of lower dimension by retaining as much information as possible, i.e. to explain as much variance as possible of M . Therefore, relations between observations as well as responsible variables can be explored.

First, variables are centred or standardised to obtain the m -by- m covariance or correlation matrix C . Subsequently, the m -by- m eigenvector matrix L and m -by- m eigenvalue matrix V of C are computed by singular value decomposition:

$$C = LS^2L^T = ZVZ^T \quad (3.20)$$

where Z is an m -by- m orthogonal matrix, S is an m -by- m diagonal matrix with the non-zero singular values on its primary diagonal. If the eigenvector in each column of L are organised in reversed order, L becomes the loadings matrix and eigenvectors the principal components (PC). PCs are orthogonal to each other, i.e. linearly uncorrelated, and defined by a linear combination of the original variables, ordered by descending amount of explained variance. From the primary diagonal

of V , containing the non-negative eigenvalues of decreasing magnitude ($v_1 \geq v_2 \geq \dots v_m \geq 0$), the explained variance of each PC can be obtained by relating each eigenvalue v to sum of eigenvalues:

$$var_i = \frac{v_i}{\sum_{i=1}^m v_i} \quad (3.21)$$

To investigate the relations between the observations n , the n -by- m score matrix S is calculated according to

$$M = SL^T \quad (3.22)$$

Often two or three PCs explain at least 60% of the total variance, thus reducing the complexity of a data sets and enable visualisation of the data in two- or three-dimensional space [152, 153].

3.5.4 Projection-on-latent-structures (PLS) regression

In contrast to PCA, which models only the variance of one matrix, PLS regression aims to find a relation to between two matrices X (predictor variables) and Y (response variable), e.g. to predict properties of a sample from an analytical measurement. The underlying models can be described as

$$X = T_k P_k^T + E \quad (3.23)$$

$$Y_{est} = T_k Q + F \quad (3.24)$$

where Y_{est} refers to the estimated dependent response variable, T represents the score matrix, P_k^T denotes the transposed loadings matrix for X , Q is the loadings matrix for Y and E and F stand for the residuals with k as the number of latent variables (PLS components).

The prediction of the response variable Y_{pred} for a measurement x_i is computed by

$$Y_{pred} = x_i b \quad (3.25)$$

where b refers to the computed vector of PLS regression coefficients by non-linear iterative partial least square algorithm (NIPALS)

$$b = W(P^T W)^{-1} Q \quad (3.26)$$

where W represents the weights of the loading matrix [154].

With PLS regression, properties Y of a sample which are difficult to determine can be derived from a PLS regression model create by simpler measurements, e.g. the prediction of cytotoxicity of river water with water-extract analysis by GC/MS [155] or the ratio of aliphatic to aromatic compounds in crude oil by Fourier-transform IR spectroscopy [156].

4 Results and discussion

4.1 Primary aerosol emissions from a marine auxiliary engine

Despite the high relevance of emissions from ship traffic for climate and human health, the number of studies is much lower than for other common anthropogenic sources, such as wood combustion or road traffic. There are several issues to overcome to analyse ship emissions directly on-board. The Faculty of Mechanical Engineering and Marine Technology of the University of Rostock owns an

80 kW marine auxiliary engine for research, which enables to examine relatively fast changes in engine conditions or fuel changes.

4.1.1 Chemical composition of carbonaceous particulate emissions

Almost each study on primary ship emissions focus on PM_{2.5}, PM_{2.5}-related quantities (OC, EC, BC) and major combustion gas emissions (CO₂, CO, NO_x), but the composition of organic emissions were poorly investigated before. On that account, a detailed molecular characterisation of OA from ships were carried out by on-line AMS and TOCA-SPI/REMPI-TOFMS analysis of filter samples taken from repeated 2 h engine cycle (ISO 8178-4 E2 including engine loads of 100%, 75%, 50% and 25%). The experiments were performed with HFO and DF in order to investigate changing emissions in the context of SECAs [157].

First, basic EFs including PM_{2.5}, OM, EC, BC and sulphate were compared to available literature data to ensure comparability of the small-scale engine with main engine of higher power output, which resulted in good agreement despite additional variances from molecular fuel composition and specific engine conditions. Switching from HFO to DF led to reduced PM_{2.5} emissions by approximately 80% from 510 mg kWh⁻¹ to 110 mg kWh⁻¹, which could be attributed to lower emissions of OC (OM) and heavy metals, such as oxides of V and Ni. Surprisingly, both soot-related emissions of EC and BC were insignificantly different between HFO and DF. However, other light-absorbing carbonaceous species, i.e. BrC emissions, accounted for approximately 20% (65 mg kWh⁻¹) of the OM emissions from HFO combustion (320 mg kWh⁻¹), but was negligible for DF use. Therefore, there is evidence that POA emissions from ships operating on HFO are a relevant source of BrC in addition to BBOA, which will be discussed in detail in a prospective manuscript [158]. Moreover, average carbon oxidation states (OS_c) were calculated according to Kroll et al. (2011) [4] based on O:C and H:C from AMS analysis and appeared between -1.6 and -1.1, which fits to molecular structures of high aromaticity found in fuels and on particles [159].

The molecular composition of OM was investigated more in detail by TOCA-SPI/REMPI-TOFMS, which heats the filter samples towards target temperatures according to the *ImproveA* protocol [138] with heating rates up to 5 °C s⁻¹. Fractions of OC1 and OC2 were combined to “thermodesorption” (OC12, 25°C – 280°C) and OC3 and OC4 to “pyrolysis” (OC34, 280°C – 580°C) due to predominant events of evaporation and decomposition, respectively.

Evolved gas analysis by SPI-TOFMS revealed that most abundant peaks belong to fatty acid methyl ester (FAME) of oleic, linoleic and palmitinic acid (m/z 296, 294 and 270), which were attributed to unburned biodiesel produced from transesterification of rapeseed oil. The biodiesel can account for up to 7%-vol and has been demonstrated to efficiently reduced soot-related emissions from diesel engines [160]. Furthermore, naphthalic anhydride and a variety of alkanes were detected in the SPI spectrum of thermodesorption, while the homologue alkylation series of phenanthrene (m/z 178) was the dominant peaks in the REMPI spectrum of OC12. In contrast, HFO thermodesorption SPI and REMPI spectra were dominated by homologue alkylation series of phenanthrene, but also by dibenzothiophene (starting from m/z 184) and chrysene (starting from m/z 228). Alkylated phenanthrenes and chrysenes are generally abundant in crude oil-based fuels due to oil precursors

from biomass, such as di- and triterpenoids [161, 162], while dibenzothiophenes were identified as most abundant sulphur-species in vacuum gas oil [163]. Both SPI and REMPI spectra of OC34 did not enable to suggest specific compounds, but to gain insights into larger molecular structure by thermal fragments as well as to discriminate between fuels by fingerprints, which can be applied in source apportionment. Two apparent differences can be found in OC34 between the fuels. First, for HFO peaks up to m/z 400 were still detectable in the REMPI spectrum despite a general shift towards smaller m/z during pyrolysis, indicating large aromatic structures present in the HFO or cracking and aromatisation of substituted cyclic structures, e.g. of asphaltenes. Second, only for HFO sulphur-containing thermal fragments were observed, such as hydrogen sulphide (m/z 34), methane thiol (m/z 48) and carbon disulphide (m/z 76), which is consistent with the fact that the majority of sulphur is located in the low-volatile fraction of HFO [96]. From the analysis of particle and fuel, similar mass spectra were obtained, indicating that unburned fuel is a major contributor to organic emissions.

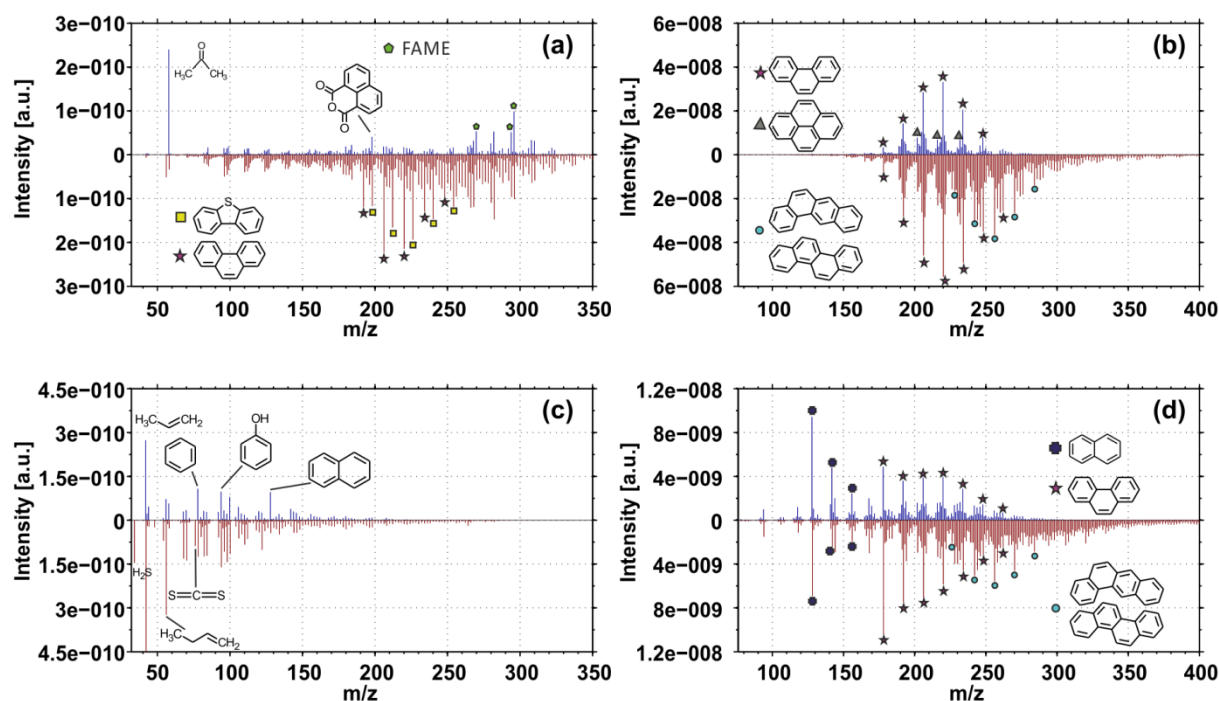


Fig. 17 SPI (left) and REMPI (right) mass spectra of thermodesorption-like OC12 ($25^{\circ}\text{C} - 280^{\circ}\text{C}$, figures a and b) and pyrolysis-like OC34 ($280^{\circ}\text{C} - 580^{\circ}\text{C}$, figures c and d) of DF particles (blue) and HFO particles (red).

4.1.2 Markers in the fraction of aromatic VOCs and IVOCs emissions from SECA-compliant and non-SECA-compliant fuels

Before this project was started, the available literature on VOC and IVOC emissions from ship was negligible. The aromatic fraction of VOCs and IVOCs from HFO and MGO combustion at constant engine loads were studied by on-line REMPI-TOFMS and combined with previously published on-line REMPI-TOFMS data with various and also dynamic engine conditions in terms of engine load and crank angle [164, 165]. Hence, a wide range of realistic emission scenarios was covered for three different HFOs and one MGO, which represent non-SECA- and SECA-compliant fuels. In order to find molecular markers, diagnostic ratios or latent variables suitable to identify ship emissions in

ambient air, further published on-line REMPI data of realistic emissions from road traffic, small non-road engines and domestic wood combustion [166-168] was also included and examined by several statistical techniques. Due to the high time resolution of the REMPI-TOFMS data, not only mean emission profiles, but also the variance of dynamic combustion processes can be taken into consideration.

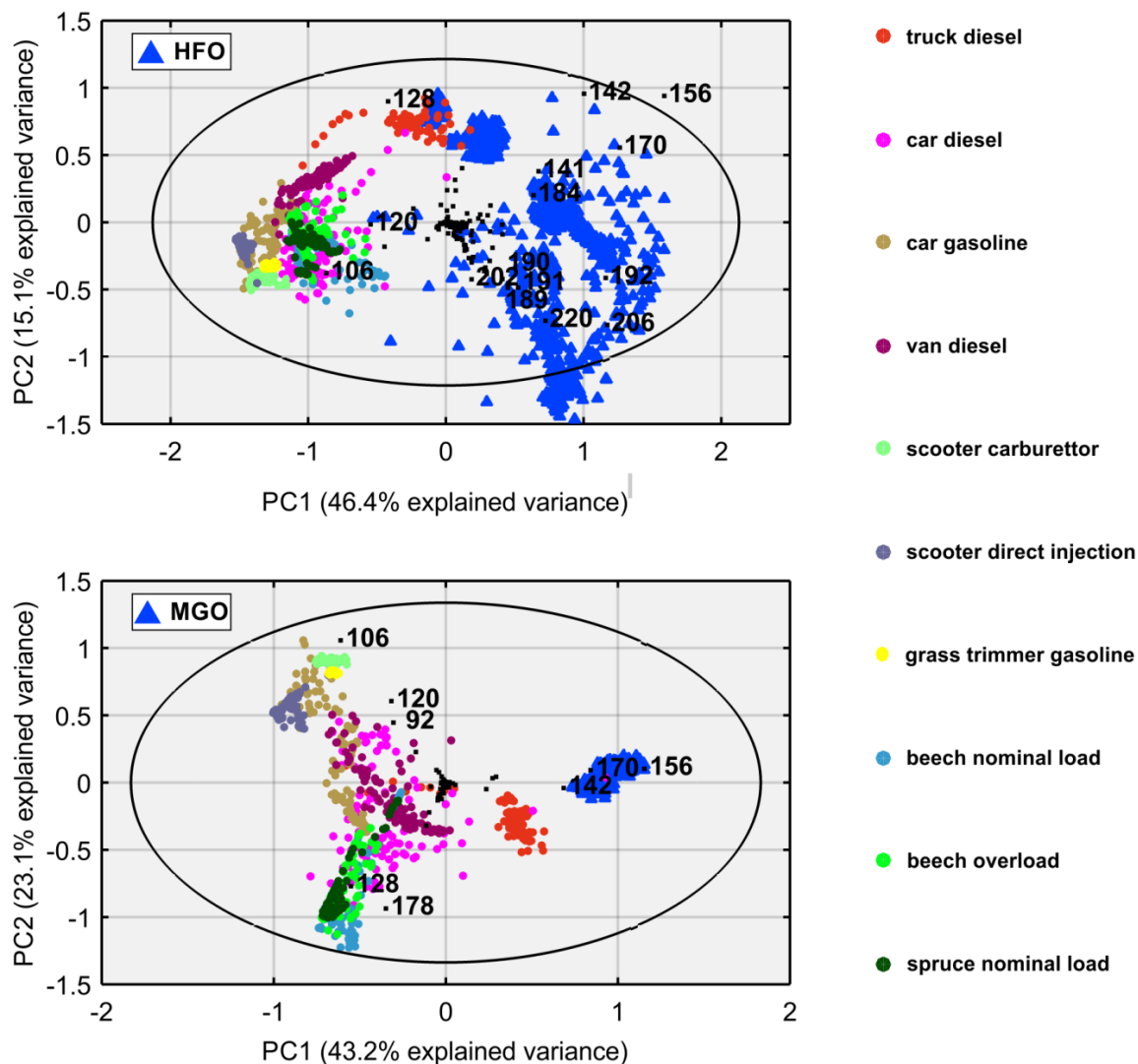


Fig. 18 PCA biplots, combining scores (samples, coloured) and loadings (m/z , black), of REMPI spectra from ship and non-ship emissions outside (top) and inside SECAs (bottom). Black ellipses denote the 95% confidence interval. For better visualisation only the most relevant m/z are included.

In PCA, ship emissions from both HFO and MGO combustion could be separated from land-based emissions by the scores of first principal component, explaining 46.4% and 43.2% of the total variance, while the second principal component explains mainly variation within the respective combustion. Alkylated phenanthrenes and especially naphthalene were responsible for the grouping of the different combustion sources and seems to be potential markers for ship emissions. Generally, high combustion temperatures inside the piston enhances the relevance of HACA formation mechanism for PAHs and derivatives, but it seems that in particular for heavy-duty engines, the fuel slip becomes more important and leads to emission patterns which are known from crude oil and its refinery products. Truck emissions appeared as most interfering emission source

with ship emissions, especially for MGO combustion, which can be explained by the fuel slip and additionally by the very similar boiling point range of MGO and DIN EN 590 diesel from the fuel station. In order to prove statistical significance, Kruskal-Wallis test with subsequent Bonferroni adjustment of the α -level was performed between HFO and MGO combustion emissions. It turned out that C₂- to C₇-naphthalenes, fluorenes, dibenzofurans and phenanthrenes were significantly enhanced in HFO combustion emissions by factors from two to eleven. Some oxy-PAHs, such as anthrone and 9H-fluoren-9-one, were also significantly increased in HFO combustion emissions, but because of further environmental sources, such as atmospheric ageing, they were not considered as markers. However, for MGO only C₃-naphthalene and C₃-phenanthrene appeared statistically significant. Moreover, the ratio of C₂- to C₁-naphthalene were found to be a simple quantity to discriminate between ambient air pollution mainly caused by ship emissions and ambient air pollution by other emission sources. Neither for HFO nor for MGO the range between the first and the fourth quintile of this ratio did not interfere with the other investigated emission sources. Thus, this ratio can be applied independently from fuel as DR inside and outside SECAs. Furthermore, both alkylated naphthalenes are similarly degraded by OH radicals in the atmosphere [38], so the ratio remains stable, which is often an issue with DR [37].

Measurements of the alkylated naphthalenes can be carried out by off-line sampling, but it is supposed that complete spectra REMPI-TOFMS can provide more reliable assessments. In addition to its low limits of detection, low interferences with non-anthropogenic emission sources are expected, which originates from its ionisation selectivity. Aromatic rings, which are necessary to fulfil the ionisation requirements, are opened and derivative by atmospheric oxidising agents. Therefore, reaction products from atmospheric oxidation of aromatic primary VOC and IVOC emissions have lower PICS or do not fulfil ionisation criteria anymore.

4.1.3 Prediction model to quantify the contribution of ships in simulated REMPI spectra of mixed anthropogenic emission sources

For a proof of concept in predicting the contribution of ships to ambient air pollution, 5% of all REMPI mass spectra of ship emissions from one fuel as well as 5% of all REMPI spectra from non-ship emissions were randomly selected and weighted averaged with a predefined weight for the ship emissions Φ_{sim} . Thus, REMPI spectra of ambient air are simulated with consecutive Φ_{sim} steps of 0.01 with 1000 repetitions, which were finally used for PLS regression. Each of the two resulting prediction model comprises of two PLS components, explain more than 97% of the total variance (R^2) and feature root mean square error (RMSE) of 0.0329 (HFO) and 0.0488 (MGO), respectively. Furthermore, R^2 and RMSE from 5-fold cross validation and external validation agreed well with the calibration function, which confirms that the model is neither over- nor underfitting the data. Following the definition of the limit of detection, lower and upper boundaries, defining the work range of the model, were derived from the point of intersection between 3-fold standard deviation at $\Phi_{sim} = 0$ and the calibration function (Fig 19).

The relevance of single variables (i.e. m/z) is determined by calculating the variable importance in projection (VIP), which considers the abundance of variable in each PLS component as well as its

contribution the overall explained variance. As a rule of thumb, squared VIPs above unity are important for the model, squared VIPs below unity less. MGO emission contribution was less precisely predicted than HFO because of higher similarity between MGO and land-based emissions, which can be attributed to a lower number of VIPs than for HFO. However, in both ship emissions C₂-naphthalene were identified to support the discrimination from land-based emissions, which emphasises its use together with the less important C₁-naphthalene in the proposed DR. Altogether, the results from three complementary statistical techniques suggest alkylated 2- and 3-ring PAHs are much more emitted by ships than land-based emissions sources and may enable reliable identification and quantification of ship emissions in source apportionment.

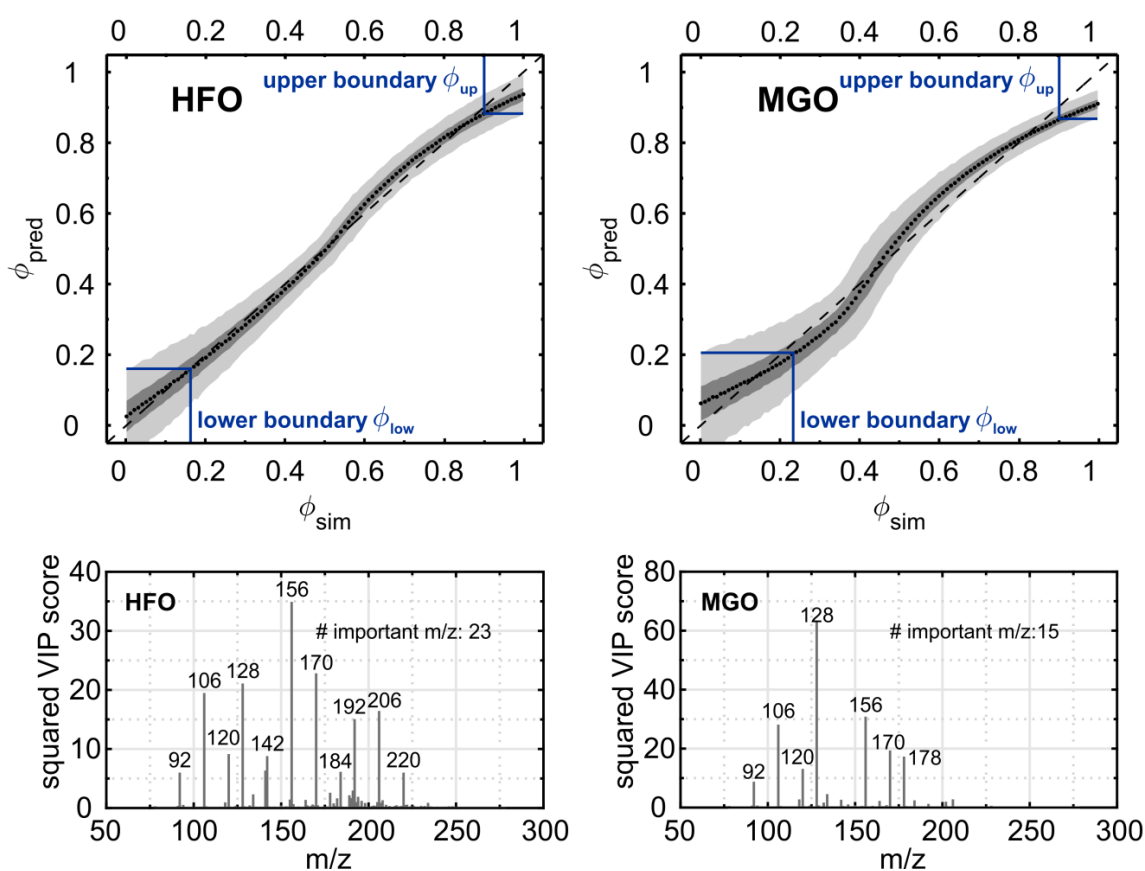


Fig. 19 Prediction model for the contribution of ship emissions Φ based on mixed combustion emission sources from a simulation. Top: PLS regression of Φ_{sim} and for Φ_{pred} from the training data sets for HFO (left) and MGO (right) with $\pm s$ (dark grey) and $\pm 3s$ (light grey) as well as related upper and lower boundaries for Φ_{sim} (blue); dashed lines illustrate the 1:1 diagonal. Bottom: Squared scores of the variable importance in projection (VIP) denoting the most relevant m/z for the PLS regression model.

4.1.4 Development of direct infusion REMPI-MS to analyse medium and heavy marine fuels from the liquid phase

Unburned fuel was identified as substantial contributor to particulate emissions from marine engines [169]. The marine fuels DF and in particular HFO have high double bond equivalents, which gives evidence for high aromaticity of the fuels [159]. REMPI-TOFMS is regarded as a valuable analytical

technique to characterise this type of fuel due to its high selectivity for aromatic compounds and generation of molecular ions, which simplifies the interpretation of mass spectra from complex mixtures [133]. However, the sample introduction is often performed by heating, e.g. by coupling thermal gravimetry (TG) to REMPI-TOFMS, which can alter the sample through decomposition [170]. On that account, the instrumental setup of Schepler et al. (2013) [171] with a direct liquid interface and quasi-simultaneous ionisation by SPI/EI was further developed to enable REMPI. The ionisation was switched from a continuously light-emitting VUV-lamp to a pulsed Nd:YAG laser (*Minilite I*, Continuum, California, USA), which required new synchronisation between light source and quadrupole. Sample introduction was realised by manual injection valve (VICI AG International, Switzerland) with an external 20 μL loop, which transfers the sample via a capillary of 25 μm inner diameter about 1 mm away from the repeller. The reduced pressure inside the ion source and heating of the repeller to 280°C support the coincident desolvation and nebulisation of the eluent (Fig. 20, left). Therefore, fuel samples are exposed to lower thermal stress, which avoids decomposition. Additionally, the accessible volatility and consequently the m/z range are increased, which enables a broader investigation of fuel composition. Apart from different DFs and HFO, crude oils of different origins were analysed to cover the entire volatility range of liquid petroleum products. Hence, the average m/z of the REMPI mass spectrum at 280°C repeller temperature could be shifted from 191 to 254 compared to the sum of TG-REMPI-TOFMS mass spectra from room temperature to 280°C of North Sea crude oil (Fig 20, right).

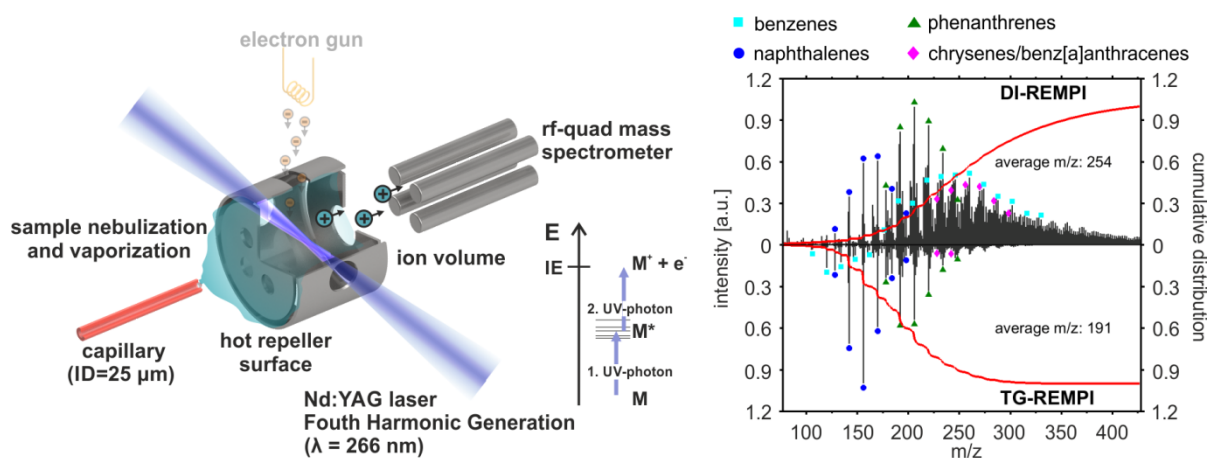


Fig. 20 Left: Instrumental setup of the direct infusion resonance-enhanced multi-photon ionisation mass spectrometry (DI-REMPI-MS) for the investigation of liquid samples under low thermal stress. The electron gun from the previous setup of Schepler et al. (2013) [171] was discarded. Right: Comparison of DI-REMPI-MS and thermal gravimetry with evolved gas analysis by REMPI-TOFMS of North Sea crude oil. DI-REMPI-MS extends the accessible m/z range compared to the sum of TG-REMPI mass spectra from room temperature to 280°C. Thus, complex heavy petroleum products, including marine fuels, can be investigated by soft REMPI-MS.

4.2 Secondary emissions from a marine auxiliary engine

The SOA formation from the primary marine auxiliary engine emissions were studied by ageing in a mobile smog chamber with a volume of 12 m^3 [172]. As pointed out in section 1.4.2., emissions from diesel engine may feature low ratios of VOCs to NO_x , which hampers SOA formation. Hence, diesel cars with relatively high NO_x emissions contribute negligibly to ambient SOA [173], whereas low

NO_x-emitting combustion aerosol sources, such as wood burning or spark-ignition engines, cover high SOA formation potential [173-176]. Additionally, ships emissions have also been characterised as high emitter of PM, but relatively low concentrations of VOCs, and combine the two introduced unfavourable conditions. Unfortunately, the increase of OA mass during ageing was lower than wall losses determined by continuous BC measurements. Hence, SOA formation potential might be low and aged-POA exhibits larger relevance. However, the majority of ship emissions are released in international waters and are transported over long distances, which is associated with higher exposure to atmospheric oxidising agents, until they reach mainland or inhabited areas. Therefore, more artificial ageing by PAM flow reactors seems to be justified. Very recently, Simonen et al. (2017) [177] demonstrated increasing PM mass and shifts in PM mass distribution over aerodynamic diameters on a conference poster for HFO and DF, but the chemical speciation and role of organic aerosol constituents is still pending.

4.3 Primary emissions from two modern small-scale wood combustion appliances

The following section deals with primary and secondary emissions from a modern masonry heater (MMH) and a pellet boiler (PB), which are both equipped with state-of-the-art combustion technology by means of air staging. So far, these appliances are representative for residential heating with wood fuels in Scandinavia, but can be supposed to replace conventional wood stoves, pellet burners and boilers industrialised countries in the future. Furthermore, changing emission patterns of complex composition in logwood combustion is still an analytical challenging for instrumentation and data analysis.

The experiments with the MMH comprise of six consecutive logwood batches of 2.5 kg (beech, birch and spruce wood), which were burned for 35 min, and an additional char-burning phase of 30 min for a total experimental duration of 4 h. Integrated emission data of the PB were obtained from 4 h sampling of constant operation at nominal load with commercial softwood pellets. Additionally, emissions from the starting phase, birch bark pellets and the effect of reduced secondary air supply were investigated.

4.3.1 Time-resolved analysis of volatile emissions

Wood stoves are usually operated by ignition of small amounts of wood and subsequent batchwise refilling with logs. Since temperature inside the combustion chamber steadily increases, new introduced batches lead to different quantitative emissions. However, even within a batch the logwood passes different combustion stadia leading to different emission patterns, which can be simply described the composition of three carbon-containing main combustion gases CO, CO₂ and VOCs (measured as OGC), but also by particle composition [168]. However, the changing composition of VOCs over different combustion stadia has not been described. On that account, a similar approach to Elsasser et al. (2013) [168] by means of NMF was applied on SPI mass spectra for every 4 h experiment with the MMH, leading to three identified combustion stadia from the normalised NMF scores, referred to “ignition”, “stable combustion” and “ember” (Fig 21).

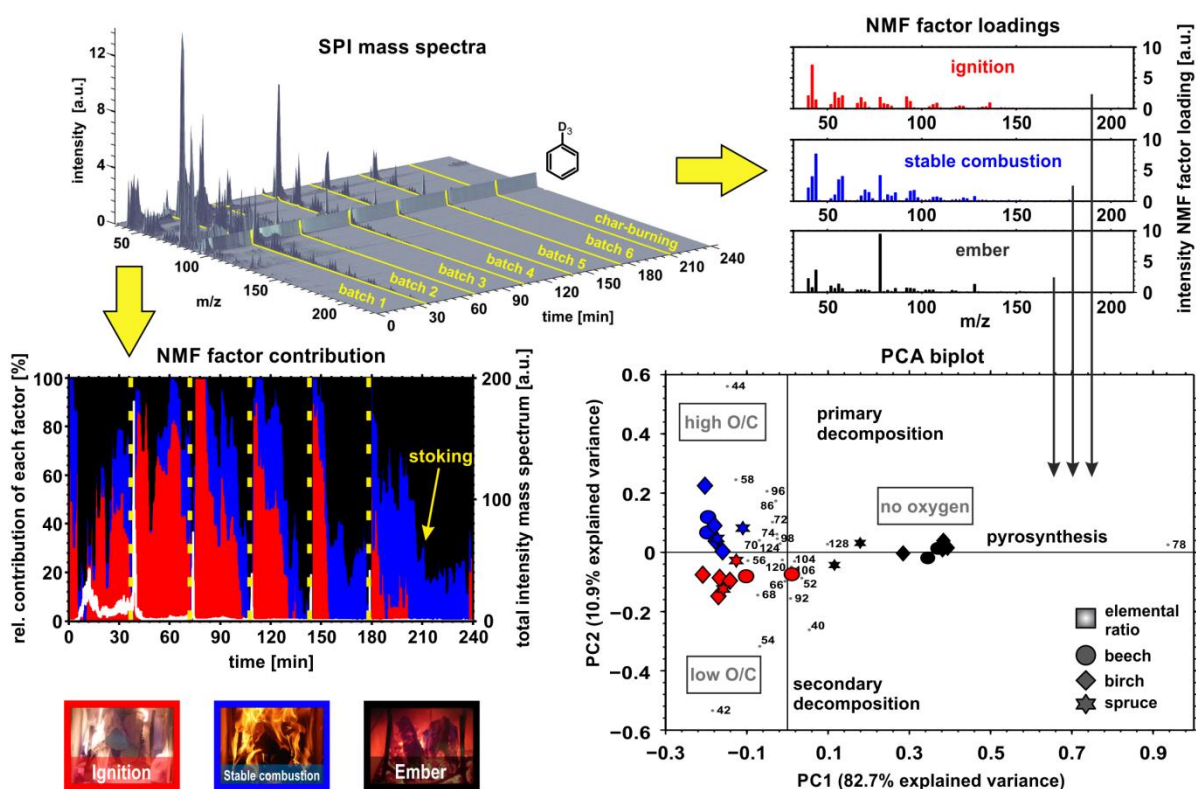


Fig. 21 NMF results (relative factor contribution and factor loadings) of SPI mass spectra from one logwood combustion experiment and prove of consistency for all combustion experiments by PCA of NMF factor loadings.

The temporary order of the phases are clearly visible as well as the decreasing contribution of “ignition” and increasing contribution of “ember” because at higher temperatures inside the combustion chamber, the wood turns faster into charcoal. The NMF loadings contain representative patterns for the three combustion stadia. To include all combustion experiments in the evaluation of the combustion stadia, NMF loadings were normalised and examined by PCA. The PCA scores illustrate similar compositions of the combustion stadia from different wood fuels. Usually it is assumed that during ignition, monomers of the wood biopolymers are released because of low temperature pyrolysis. However, the NMF loading “ignition” contains moderately unsaturated hydrocarbons (e.g. propene, butadiene and cyclopentadiene) and alkenyl-substituted benzenes (e.g. styrene) from secondary decomposition, whereas early stage decomposition products with oxygen-containing functionalities appear in NMF loadings of “stable combustion”. Those compounds include anhydrous sugars, furan derivatives and carbonyls from carbohydrate decomposition as well as substituted phenols from lignin. This can be explained by a shortly false NMF factor assignment during the first two minutes in which “ignition” and “stable combustion” are switched, predominantly associated with burning of the kindlings, but return into the correct assignment after ignition of the entire first batch. This phenomenon occurs only at the first ignition because the MMH generates sufficient heat that new batches do not pass low, but already pyrolysis at higher temperatures. This observation is attributed as a feature of the combustion technology and property of the MMH. When burning wood turns into glowing embers, the emission spectrum shifts towards higher polyunsaturated compounds formed by pyrosynthesis, such as benzene and vinylacetylene, which agrees well with results from charcoal burning [178].

Regarding the six consecutive batches of logwood in the MMH, it was found that the majority of the organic emissions, represented by the signal intensities of SPI mass spectra, appeared during the first two batches and accounted for at least 50% of the total 4h emissions. This result was further statistically supported by single Grubbs and double Grubbs outlier test at a significance level of 5%. In case the null hypothesis of the single Grubbs outlier test was not rejected, the double Grubbs outlier test was performed, which is able to detect two outliers simultaneously. Except birch wood which also showed significantly enhanced intensities for the second and third batch, the majority of even numbered m/z were significantly higher than in the subsequent batches.

In contrast to logwood stove, PBs are usually operated at constant load because they do not refer to room space heating appliances, but heating by warm water supply. Nevertheless, the time-resolution of the SPI-TOFMS can be exploited to decrease limits of detection by averaging or to examine rarer appearing events, such as ignition or unfavourable combustion conditions, or the effect of low-quality fuels. During ignition, highest volatile emissions could be observed, which comprise of typical wood combustion products from low-temperature pyrolysis. However, during stable combustion very low intensities were detected solely for unsaturated hydrocarbons, such as benzene and propene, and acetaldehyde. A reduction in secondary air caused dynamic and substantially increased emissions of benzene and 2- to 4-ring PAHs, which was used in PAM flow reactor study to mimic pellet boilers of older generation. Also the feed of low-quality birch bark pellets led to higher benzene and PAH emissions, which was linked to higher aromaticity of the wood fuel, but to higher carbonyl emissions as well.

4.3.2 Emission factors (EFs) and PAH toxicity equivalents (PAH-TEQ) from 4 h combustion experiments

Emission factors (EF) were related to the heating value of the wood fuels according to the Finnish Standard Association method SFS 5624. Generally, the MMH of this study emitted more than one order of magnitude lower OGC and 50% lower particles than conventional wood stoves without air staging technology, which is attributed to a reduction in organic matter. However, emissions of EC were not affected. Regarding the molecular composition of the emissions, primary decomposition products and thus wood combustion markers were more reduced than products from secondary reactions and pyrosynthesis, which is discussed in previous section. Major differences in EFs between the wood types were only observed for primary decomposition products for lignin pyrolysis, which enables to distinguish between hard- and softwood combustion, as well as evaporating resinic acids and phytosterols. Despite slightly different experimental designs and combustion conditions, the results of key quantities, such as OGC, OC, EC and CO, were comparable with previously published studies of the same MMH [122]. Moreover, emissions from a MMH by with the same combustion technology but different manufacturer appeared in the same order of magnitude. Hence, it can be concluded that the emission characteristics are not only a feature of the investigated MMH, but a general feature of logwood stoves with air staging technology. Regarding the PB, carbonaceous emissions, including OM and EC, were even one additional order of magnitude lower than the high efficient logwood stoves when operated under stable nominal load.

Therefore, organic compounds typically linked to wood combustion appeared below the limit of quantification. However, some evidence was found that the quality of the pellets is inversely correlated with several volatile emissions.

As health effects of the emissions are one of the main motivations for this study, the mutagenic potential of the particle emissions were estimated by the concept of PAH toxicity equivalents. Each PAH-EF is multiplied with a compound-specific factor which describes the mutagenic potential relative to benzo[a]pyrene. From Fig 22, it can be observed that MMH and PB with air staging not only emit lower amounts of PAHs, but also lead to particle emissions of lower mutagenic potential compared to conventional wood combustion appliances [8]. However, despite lower mutagenic potential of the particulate PAHs, an overall reduction in toxicity cannot be concluded because especially phenolic compounds are regarded to be responsible for the generally lower toxicity of wood combustion emissions than the summed toxicity of each single constituent suggests.

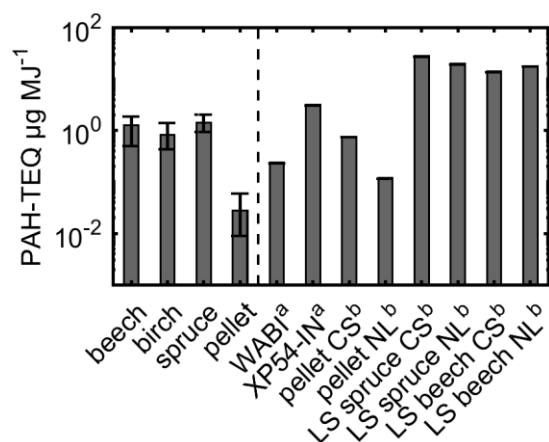


Fig. 22 Toxicity equivalent (TEQ) of particle-bound PAHs related to heating value of the different wood fuels; error bars represent minimum and maximum EFs. Results appear in the same order of magnitude as other modern masonry heaters from Tschamber et al. (2016)^a [7], but significantly lower than conventional wood stoves and pellet boilers published by Orasche et al. (2012)^b [8].

4.3.3 Effect of slow ignition of logwood on EFs and emission patterns

Although it was taken great care of reproducible experiments, logwood combustion exhibits large emission variability and a hardly controllable progress after ignition. By chance, two combustion experiments turned into temporary smouldering after ignition of the first batch, indicated by an intermediate drop in the usual bell-shaped curve of the flue gas temperature. This combustion event of was even noticeable in the integrated 4 h EFs. Approximately 70% of the total OGC was release during the first batch of spruce log combustion with 2-fold to 5-fold increased EFs for single VOCs compared to regular spruce log combustion. In particular, EFs of primary decomposition products, such as coniferyl aldehyde or levoglucosan, were elevated by one order of magnitude. However, also differences were found between smouldering of spruce and birch logs. The analysis of particle from birch log combustion revealed a shift towards larger PAHs than the regular birch experiments, but no significantly increased EFs of primary decomposition products. Despite the agreement of spruce wood smouldering emissions with current knowledge from literature, the reasons for the observation of this birch wood experiment are speculative. Nevertheless, it has been generally observed that birch wood ignites much faster than spruce, perhaps because of the macrostructure of the birch [179] or essential oils in the birch bark which might accelerates the expansion of the flames and raise the temperature of the combustion chamber. Further investigations are necessary to clarify ignition properties of different wood species.

Apart from the polymeric components, wood contains phytosterols and resin acids, which are specifically emitted by certain wood species and allow statements about the predominantly used firewood in aerosol research of ambient air. Many of those molecules belong to the fraction of LVOCs, but contain functional groups, such as hydroxyl and carboxylic functions, which are prone for decomposition upon thermal stress. During smouldering, the combustion temperature remains relative low, so phytosterols and resin acids evaporate and condensate on existing particle during dilution and cooling in the atmosphere. In contrast, proper ignition increases the heat transfer to the logwood that phytosterols and resin acids eliminate small molecules, such as CO₂, H₂ or H₂O, or become partly oxidised, such as 7-oxodehydroabietic acid. Regarding EFs, smouldering not only shifts the distribution of these wood constituents and thermal alteration products, but is also able to increase their emissions up to two orders of magnitude.

4.3.4 Implications for source apportionment of modern wood combustion appliances

The three presented studies about primary wood combustion emissions of appliances with modern combustion technology point out changes in widely accepted emissions profiles for wood combustion. Higher combustion efficiency is associated with lower emissions of wood-related primary decomposition products, but constant emissions for general combustion products, such as PAHs. Consequently, frequently used diagnostic ratios of wood combustion emissions, which include primary decomposition products such as phenolic species and anhydrous sugars, may become invalid in the future when conventional wood stoves are subsequently replaced. This aspect holds especially for automatically appliances, such as PBs, for which those molecular markers could hardly be detected. Therefore, the risk of identification wood combustion as different emission in source apportionment studies can be expected to increase through incorrect PMF factor interpretations. However, even more crucial would be the effect in chemical mass balances (CMB) to quantify source contributions, whose results strongly depends on the accuracy of the emission profile inputs.

4.3.5 Statistical concepts from wood combustion for process control: application on coffee roasting

The combination of NMF and further statistical analysis of NMF loadings and scores was applied to on-line monitoring of coffee roasting, which is also known to pass different roasting phases. Components of the roasting off-gas evolved from evaporation of bean constituents (e.g. caffeine), caramelisation, Maillard and Strecker reactions [180]. Research on on-line and real-time monitoring of coffee roasting is demanded because industrially roasted coffee should be produced in time-effective manner, i.e. short roast times, but acceptable and reproducible taste. Real-time prediction of the roast degree using proton-transfer reaction (PTR) mass spectrometry and principal component regression was already achieved [181], but prediction of taste has been only demonstrated for off-line analysis [182]. On that account, the dynamic changes of the molecular composition of two coffee cultivars (Arabica, Robusta) from Mexico and Vietnam were investigated at three different roasting profiles and four different photoionisation wavelengths (SPI: 118 nm; REMPI: 227 nm, 248 nm and 266 nm). Similar to the burning phases of logwood (section 4.3.1.),

roasting off-gas components have different temporal evolutions, which were grouped into four roasting phases “evaporation”, “early roast”, “late roast” and “overroast”. For each photoionisation wavelength, similar molecular patterns were observed for each roasting phase and proven to be consistent between repeated roast experiments by PCA. Moreover, five pairs of m/z were selected based on Fisher ratio to derive linear classifier function from linear discriminant analysis (LDA).

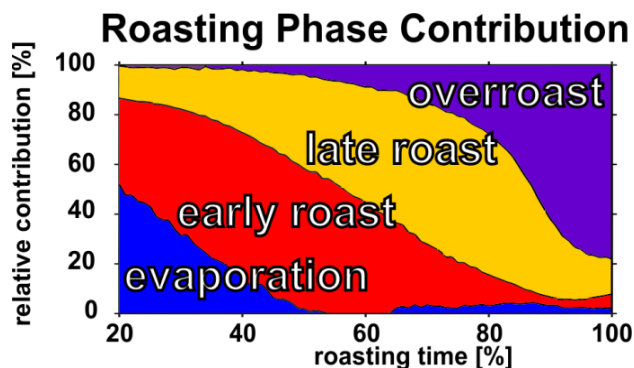


Fig. 23 Application of NMF on SPI mass spectra of coffee roasting off-gas to identify four roasting phases.

Therefore, transitions of roasting phases can be detected in a real-time measurement if the intensity threshold given by the classifier function is exceeded. Despite different ionisation selectivity, all photoionisation wavelengths exhibited best performance in predicting NMF phase limits between later roasting phases “early roast” to “late roast” and “late roast” to “overroast” because of low intensities and peak number during “evaporation”.

4.4 Secondary emissions from modern small-scale wood combustion appliances

4.4.1 Ageing of primary emissions from logwood combustion in a smog chamber

New particle formation through atmospheric (photo)oxidation of organic vapours were found to be substantial for logwood combustion and open biomass burning [175, 183, 184]. However, similar to the characterisation of emissions from new combustion technology there is still a demand for estimating SOA formation potential, which can finally lead to additional OA emissions by a factor of 2.5 after 2 days of OH exposure [176]. Primary emissions from a MMH fuelled with one batch of spruce logwood were aged under dark, UV or dark with subsequent UV conditions in ILMARI smog chamber of 29 m³ to cover oxidising agent exposure at different daytimes. Moreover, fast and slow ignition of the logwoods was carried out in order to achieve different ratios of VOCs to NO_x.

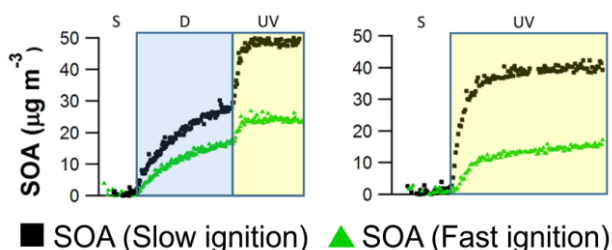


Fig. 24 SOA formation from spruce logwood combustion after slow and fast ignition in a smog chamber. First, the smog chamber was filled and stabilised (S) followed by ozone addition (“dark ageing”, D) and subsequent UV ageing (UV, left) or prompt UV ageing (right).

In all ageing experiments, the initial OA mass, measured by SP-AMS was enhanced by 60% to 165% after oxidising agent exposure equivalent to approximately 12 h. Higher VOC emissions from slow ignition were directly related to higher SOA formation. Compared to old stove, the absolute SOA formation was one order of magnitude lower (old: 880 mg kg⁻¹), but appeared with 91 to 237 mg kg⁻¹ in the same range as a conventional stove (100 mg kg⁻¹) [175]. However, it must be

noted that in Heringa et al. (2011) [175] the equivalent ageing time was only 5 h and SOA-EFs are related to flaming phases. Hence, lower primary emissions are also associated with lower SOA formation.

Both dark and UV ageing led to substantial SOA formation and aged-POA within few hours, while less than 25% of the initial POA mass remained unoxidised. For the first time, UV ageing was carried out subsequent to dark ageing, which additionally increased OA mass by almost 100% (Fig 24). However, the composition of the formed SOA is fundamentally different due to different concentrations of atmospheric oxidising agents. By applying PMF on the SP-AMS spectra, three SOA factors could be obtained which represent ageing products for each of the considered oxidising agents. Additionally, two factor of POA were obtained, which either contain primary species reacting with all oxidising agents (double bond containing species, BBOA) or only with OH and NO₃ radicals (saturated compounds, HOA). During dark ageing, O₃ and NO₃ oxidise the aerosol, leading to SOA and aged-POA with lower average carbon oxidation state than from ageing with OH radicals [185] and substantial formation of organonitrates, which were derived from a high ratio of NO⁺ to NO₂⁺ in the SP-AMS spectrum. ON formation was previously observed in ambient air studies [186, 187], but can now be linked to ageing of wood combustion emissions.

4.4.2 Ageing of primary emissions from pellet combustion in a PAM flow reactor

Few experiments with PB emissions in a smog chamber revealed that no SOA was formed, which was later confirmed in a more comprehensive study by Kari et al. (2017) [188] and also agrees with previously published SOA yields from a pellet burner [175]. On that account, a PAM flow reactor which is capable to expose the combustion aerosol to higher OH concentration was used, but also led to only insignificant increase in OA mass for the PB operating under optimised conditions (OPT). Nevertheless, oxygen-to-carbon ratios (O:C) were distinctly enhanced, indicating relevance of heterogeneous oxidation reactions and the formation of aged-POA. However, the equivalent concentration of carbonate carbon to OC and EC contributes to peaks at m/z 44 (CO₂⁺) and m/z 30 (CO⁺), which may bias the result of OM and explain O:C as well as average carbon oxidation states [4] outside the range of typical values observed in ambient air. To simulate PB of older technology, the secondary

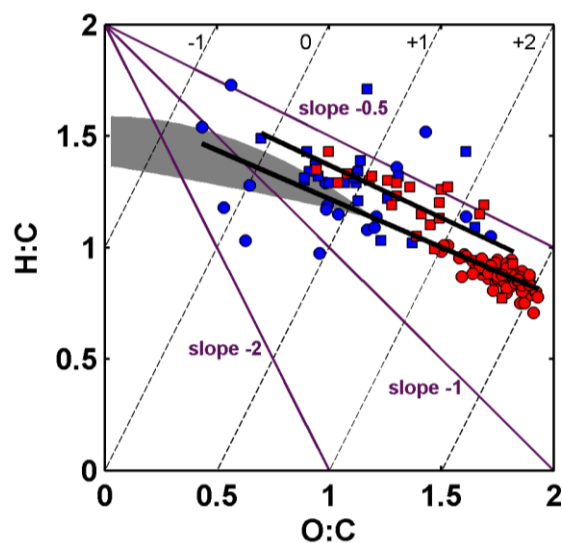


Fig. 25 Van Krevelen diagram of aged (red) and non-aged OA (blue) from optimized combustion conditions (OPT, circles) and reduced secondary air supply (RSA, squares). Solid purple lines belong to slopes indicating main functionalisation of OA [2], where the black lines represent slopes from non-aged to aged OA (-0.44 ± 0.07 for OPT and -0.47 ± 0.10 for RSA). The grey area refers to the triangular space of f_{44} vs. f_{43} in which ambient OA was found to be usually located [3], converted into the H:C vs. O:C dimension. Dashed lines are average carbon oxidation states (\overline{OS}_C) [4].

air supply was reduced by approximately 30% (reduced secondary air, RSA). Hence, organic emissions increased, especially volatile and intermediate-volatile aromatic hydrocarbons, which are considered as potent precursors for SOA formation [189]. In contrast to the PB at full secondary air supply, OA mass was doubled associated with increased relative amounts of the fragment ions $C_2H_3O^+$ (m/z 43), CO_2^+ (m/z 44) and $C_2H_4O_2^+$ (m/z 60), which belong to typical SOA compound classes of non-acid oxygenates, carboxylic acids and long-chain carboxylic acids.

The obtained increases of OA mass were converted in to SOA-EFs and compared with the single precursor approach by Bruns et al. (2016) [189]. For OPT, experimental SOA-EFs covered 30% of SOA-EFs obtained from single precursors, while for RSA it was even only 10%. Slopes close to 0.5 in the Van-Krevelen diagram indicate that C-C-bond cleavages occurred during ageing, leading to reaction products of higher volatility than the primarily emitted precursors, which may explain the large discrepancies between the different approaches. Altogether, the overall formation of SOA was low for both OPT and RSA compared to SOA formation from logwood stoves and expected to be negligible with ongoing advances in combustion technology.

5 Summary and outlook

Although the vast majority of aerosol originates from natural sources, combustion aerosols play a key role for climate and air pollution. In particular, emissions from ship traffic and wood combustion gained increasing public attention during the last decade and were investigated within the framework of the DACH-project WOOSHI (“WOOD combustion and SHIpping”). One focus of this study was put on the identification of marker substances by chemometric approaches, which allows the detection and quantification of emission sources by receptor models, such as positive matrix factorisation and chemical mass balance.

In 2015, the fuel sulphur content (FSC) of marine fuels was restricted to 0.1% in coastal areas of Europe and North America (sulphur emission control area), which forces the ship owners to switch from heavy fuel oil (HFO) with an average FSC of 2.7% to marine gas oil (MGO) or diesel fuel (DF). In particular the composition of the organic emissions from both HFO and MGO/DF is unknown, which was examined by advanced mass spectrometric techniques. In accordance with the high contribution of unburned fuel to the total emissions, mass spectra of particulate organic matter revealed the dominance of homologue series of several compound classes, such as alkylated PAHs, alkylated heterocycles and alkanes. A shift to organic compounds of higher volatility when going from HFO to DF was also observed as well as a general reduction in organic emissions could be observed with DF, but emissions of soot particles measured as elemental carbon (EC) remained stable. Furthermore, evidence was found that ships are a substantial emitter of brown carbon. Consequences for direct effects on climate by affecting radiative forcing will be discussed in a future publication. Since markers for ship emissions are based on HFO emissions, complementary multivariate statistical analyses were performed with emission profiles of aromatic (intermediate-)volatile organic compounds from ships, road traffic and residential heating in a meta-analysis. Alkylated PAHs were found to discriminate well between land-based and ship emissions

with high statistical significance, independently from the used marine fuel, while the ratio of C₂- to C₁-naphthalene as an easy-to-use metric allows a first estimation of high ship impact on air pollution. In an ageing experiment with a mobile smog chamber, no significant increase in organic aerosol mass was detected, thus further investigations involving potential aerosol mass flow reactors are recommended.

Contrary to ships, primary wood combustion emissions are comparably well investigated, but have changed with ongoing advances in combustion technology, such as secondary air supply by air staging or automatically-fired pellet boilers. Appliances with such new combustion technology burn efficiently while reducing organic emissions. Especially the release of primary decomposition products from carbohydrates and lignin is decreased. Hence, simple approaches based on ratios of phenolic species to organic carbon (OC) or OC to EC for identifying the fraction of wood combustion in ambient air are heavily biased, in particular for pellet boilers. Inorganic PM constituents or latent variables from multivariate statistical analyses containing several organic PM constituents may provide more reliable results. Additionally, burning conditions in terms of proper ignition and burning stadia were found to considerably affect the emission profile and results from PMF or CMB.

Besides reduction in primary emissions, the potential of secondary organic aerosol (SOA) formation, investigated with smog chamber and flow reactor, also declines with advances in combustion technology. However, it still exhibits a substantial increase of additional organic aerosol for the modern logwood stove by gas-to-particle conversion and heterogeneous oxidation. Simulation of nighttime atmospheric processing suggests a substantial contribution of logwood combustion SOA to ambient organonitrate concentrations. For the pellet boiler emissions, the SOA formation was negligible even at high exposures of OH radicals although increases in average carbon oxidation state indicated heterogeneous oxidation.

Altogether, this thesis explored the chemical composition of the rarely investigated but relevant emissions by ship, considered advances in wood combustion technology and gave valuable implications for the identification and quantification of wood combustion and ship traffic in source apportionment. The results emphasise the necessary connection between primary and secondary emissions as well as combustion, atmospheric, biological and mathematical science to understand complex effects and consequences from changes of the atmospheric composition on the total environment.

6 References

- [1] I. Riipinen, J.R. Pierce, T. Yli-Juuti, T. Nieminen, S. Häkkinen, M. Ehn, H. Junninen, K. Lehtipalo, T. Petäjä, J. Slowik, R. Chang, N.C. Shantz, J. Abbatt, W.R. Leitch, V.M. Kerminen, D.R. Worsnop, S.N. Pandis, N.M. Donahue, M. Kulmala, Organic condensation: A vital link connecting aerosol formation to cloud condensation nuclei (CCN) concentrations, *Atmospheric Chemistry and Physics*, 11 (2011) 3865-3878.
- [2] C.L. Heald, J.H. Kroll, J.L. Jimenez, K.S. Docherty, P.F. Decarlo, A.C. Aiken, Q. Chen, S.T. Martin, D.K. Farmer, P. Artaxo, A simplified description of the evolution of organic aerosol composition in the atmosphere, *Geophysical Research Letters*, 37 (2010).
- [3] N.L. Ng, M.R. Canagaratna, Q. Zhang, J.L. Jimenez, J. Tian, I.M. Ulbrich, J.H. Kroll, K.S. Docherty, P.S. Chhabra, R. Bahreini, S.M. Murphy, J.H. Seinfeld, L. Hildebrandt, N.M. Donahue, P.F. Decarlo, V.A. Lanz, A.S.H. Prévôt, E. Dinar, Y. Rudich, D.R. Worsnop, Organic aerosol components observed in Northern Hemispheric datasets from Aerosol Mass Spectrometry, *Atmospheric Chemistry and Physics*, 10 (2010) 4625-4641.
- [4] J.H. Kroll, N.M. Donahue, J.L. Jimenez, S.H. Kessler, M.R. Canagaratna, K.R. Wilson, K.E. Altieri, L.R. Mazzoleni, A.S. Wozniak, H. Bluhm, E.R. Mysak, J.D. Smith, C.E. Kolb, D.R. Worsnop, Carbon oxidation state as a metric for describing the chemistry of atmospheric organic aerosol, *Nature Chemistry*, 3 (2011) 133-139.
- [5] NASA Earth Observatory, Ship Tracks Off The Californian Coast, in: P. Przyborski (Ed.) *Visible Earth - A catalog of NASA images and animations of our home planet*, NASA Goddard Space Flight Center, 2017.
- [6] J. Orasche, J. Schnelle-Kreis, G. Abbaszade, R. Zimmermann, Technical Note: In-situ derivatization thermal desorption GC-TOFMS for direct analysis of particle-bound non-polar and polar organic species, *Atmospheric Chemistry and Physics*, 11 (2011) 8977-8993.
- [7] V. Tschamber, G. Trouvé, G. Leyssens, C. Le-Dreff-Lorimier, J.L. Jaffrezo, P. Genevray, D. Dewaele, F. Cazier, S. Labbé, S. Postel, Domestic Wood Heating Appliances with Environmental High Performance: Chemical Composition of Emission and Correlations between Emission Factors and Operating Conditions, *Energy and Fuels*, 30 (2016) 7241-7255.
- [8] J. Orasche, T. Seidel, H. Hartmann, J. Schnelle-Kreis, J.C. Chow, H. Ruppert, R. Zimmermann, Comparison of emissions from wood combustion. part 1: Emission factors and characteristics from different small-scale residential heating appliances considering particulate matter and polycyclic aromatic hydrocarbon (PAH)-related toxicological potential of particle-bound organic species, *Energy and Fuels*, 26 (2012) 6695-6704.
- [9] U. Pöschl, Aerosol particle analysis: Challenges and progress, *Analytical and Bioanalytical Chemistry*, 375 (2003) 30-32.

- [10] R. Zhang, C. Liu, G. Zhou, J. Sun, N. Liu, P.C. Hsu, H. Wang, Y. Qiu, J. Zhao, T. Wu, W. Zhao, Y. Cui, Morphology and property investigation of primary particulate matter particles from different sources, *Nano Research*, (2017) 1-11.
- [11] S. Fuzzi, U. Baltensperger, K. Carslaw, S. Decesari, H. Denier Van Der Gon, M.C. Facchini, D. Fowler, I. Koren, B. Langford, U. Lohmann, E. Nemitz, S. Pandis, I. Riipinen, Y. Rudich, M. Schaap, J.G. Slowik, D.V. Spracklen, E. Vignati, M. Wild, M. Williams, S. Gilardoni, Particulate matter, air quality and climate: Lessons learned and future needs, *Atmospheric Chemistry and Physics*, 15 (2015) 8217-8299.
- [12] J.H. Seinfeld, S.N. Pandis, *Atmospheric Chemistry and Physics: From Air Pollution to Climate Change*, Second Edition ed., John Wiley & Sons, Inc., Hoboken, New Jersey, 2006.
- [13] F. Raes, R. Van Dingenen, E. Vignati, J. Wilson, J.P. Putaud, J.H. Seinfeld, P. Adams, Formation and cycling of aerosols in the global troposphere, *Atmospheric Environment*, 34 (2000) 4215-4240.
- [14] J. Williams, M. De Reus, R. Krejci, H. Fischer, J. Ström, Application of the variability-size relationship to atmospheric aerosol studies: Estimating aerosol lifetimes and ages, *Atmospheric Chemistry and Physics*, 2 (2002) 133-145.
- [15] C.N. Hewitt, A.V. Jackson, *Atmospheric Science for Environmental Scientists*, John Wiley & Sons, Chicester, 2009.
- [16] D. Xu, B. Ge, Z. Wang, Y. Sun, Y. Chen, D. Ji, T. Yang, Z. Ma, N. Cheng, J. Hao, X. Yao, Below-cloud wet scavenging of soluble inorganic ions by rain in Beijing during the summer of 2014, *Environmental Pollution*, 230 (2017) 963-973.
- [17] X.Y. Ni, H. Huang, W.P. Du, Relevance analysis and short-term prediction of PM_{2.5} concentrations in Beijing based on multi-source data, *Atmospheric Environment*, 150 (2017) 146-161.
- [18] R.J. Huang, Y. Zhang, C. Bozzetti, K.F. Ho, J.J. Cao, Y. Han, K.R. Daellenbach, J.G. Slowik, S.M. Platt, F. Canonaco, P. Zotter, R. Wolf, S.M. Pieber, E.A. Brunns, M. Crippa, G. Ciarelli, A. Piazzalunga, M. Schwikowski, G. Abbazade, J. Schnelle-Kreis, R. Zimmermann, Z. An, S. Szidat, U. Baltensperger, I. El Haddad, A.S.H. Prévôt, High secondary aerosol contribution to particulate pollution during haze events in China, *Nature*, 514 (2015) 218-222.
- [19] Q. Zhang, J.L. Jimenez, M.R. Canagaratna, J.D. Allan, H. Coe, I. Ulbrich, M.R. Alfarra, A. Takami, A.M. Middlebrook, Y.L. Sun, K. Dzepina, E. Dunlea, K. Docherty, P.F. DeCarlo, D. Salcedo, T. Onasch, J.T. Jayne, T. Miyoshi, A. Shimono, S. Hatakeyama, N. Takegawa, Y. Kondo, J. Schneider, F. Drewnick, S. Borrmann, S. Weimer, K. Demerjian, P. Williams, K. Bower, R. Bahreini, L. Cottrell, R.J. Griffin, J. Rautiainen, J.Y. Sun, Y.M. Zhang, D.R. Worsnop, Ubiquity and dominance of oxygenated species in organic aerosols in anthropogenically-influenced Northern Hemisphere midlatitudes, *Geophysical Research Letters*, 34 (2007).

- [20] J.C. Chow, D.H. Lowenthal, L.W.A. Chen, X. Wang, J.G. Watson, Mass reconstruction methods for PM_{2.5}: a review, *Air Quality, Atmosphere and Health*, 8 (2015) 243-263.
- [21] M.O. Andreae, A. Gelencsér, Black carbon or brown carbon? the nature of light-absorbing carbonaceous aerosols, *Atmospheric Chemistry and Physics*, 6 (2006) 3131-3148.
- [22] C. Pio, M. Cerqueira, R.M. Harrison, T. Nunes, F. Mirante, C. Alves, C. Oliveira, A. Sanchez de la Campa, B. Artíñano, M. Matos, OC/EC ratio observations in Europe: Re-thinking the approach for apportionment between primary and secondary organic carbon, *Atmospheric Environment*, 45 (2011) 6121-6132.
- [23] A. Ångström, Techniques of Determining the Turbidity of the Atmosphere, *Tellus*, (1961).
- [24] T.W. Kirchstetter, T.L. Thatcher, Contribution of organic carbon to wood smoke particulate matter absorption of solar radiation, *Atmospheric Chemistry and Physics*, 12 (2012) 6067-6072.
- [25] K.M. Updyke, T.B. Nguyen, S.A. Nizkorodov, Formation of brown carbon via reactions of ammonia with secondary organic aerosols from biogenic and anthropogenic precursors, *Atmospheric Environment*, 63 (2012) 22-31.
- [26] J.L. Jimenez, M.R. Canagaratna, N.M. Donahue, A.S.H. Prevot, Q. Zhang, J.H. Kroll, P.F. DeCarlo, J.D. Allan, H. Coe, N.L. Ng, A.C. Aiken, K.S. Docherty, I.M. Ulbrich, A.P. Grieshop, A.L. Robinson, J. Duplissy, J.D. Smith, K.R. Wilson, V.A. Lanz, C. Hueglin, Y.L. Sun, J. Tian, A. Laaksonen, T. Raatikainen, J. Rautiainen, P. Vaattovaara, M. Ehn, M. Kulmala, J.M. Tomlinson, D.R. Collins, M.J. Cubison, E.J. Dunlea, J.A. Huffman, T.B. Onasch, M.R. Alfarra, P.I. Williams, K. Bower, Y. Kondo, J. Schneider, F. Drewnick, S. Borrmann, S. Weimer, K. Demerjian, D. Salcedo, L. Cottrell, R. Griffin, A. Takami, T. Miyoshi, S. Hatakeyama, A. Shimono, J.Y. Sun, Y.M. Zhang, K. Dzepina, J.R. Kimmel, D. Sueper, J.T. Jayne, S.C. Herndon, A.M. Trimborn, L.R. Williams, E.C. Wood, A.M. Middlebrook, C.E. Kolb, U. Baltensperger, D.R. Worsnop, Evolution of organic aerosols in the atmosphere, *Science*, 326 (2009) 1525-1529.
- [27] N.M. Donahue, A.L. Robinson, C.O. Stanier, S.N. Pandis, Coupled partitioning, dilution, and chemical aging of semivolatile organics, *Environmental Science and Technology*, 40 (2006) 2635-2643.
- [28] N.M. Donahue, S.A. Epstein, S.N. Pandis, A.L. Robinson, A two-dimensional volatility basis set: 1. organic-aerosol mixing thermodynamics, *Atmospheric Chemistry and Physics*, 11 (2012) 3303-3318.
- [29] N.M. Donahue, J.H. Kroll, S.N. Pandis, A.L. Robinson, A two-dimensional volatility basis set - Part 2: Diagnostics of organic-aerosol evolution, *Atmospheric Chemistry and Physics*, 12 (2012) 615-634.
- [30] B.R.T. Simoneit, Biomass burning - A review of organic tracers for smoke from incomplete combustion, *Applied Geochemistry*, 17 (2002) 129-162.

- [31] D.R. Oros, B.R.T. Simoneit, Identification and emission factors of molecular tracers in organic aerosols from biomass burning Part 1. Temperate climate conifers, *Applied Geochemistry*, 16 (2001) 1513-1544.
- [32] D.R. Oros, B.R.T. Simoneit, Identification and emission factors of molecular tracers in organic aerosols from biomass burning Part 2. Deciduous trees, *Applied Geochemistry*, 16 (2001) 1545-1565.
- [33] G.R. Cass, Organic molecular tracers for particulate air pollution sources, *TrAC - Trends in Analytical Chemistry*, 17 (1998) 356-366.
- [34] W.F. Rogge, L.M. Hildemann, M.A. Mazurek, G.R. Cass, B.R.T. Simoneit, Sources of fine organic aerosol. 2. Nuncatalyst and catalyst-equipped automobiles and heavy-duty diesel trucks, *Environmental Science and Technology*, 27 (1993) 636-651.
- [35] B. Nozière, M. Kalberer, M. Claeys, J. Allan, B. D'Anna, S. Decesari, E. Finessi, M. Glasius, I. Grgić, J.F. Hamilton, T. Hoffmann, Y. Iinuma, M. Jaoui, A. Kahnt, C.J. Kampf, I. Kourtchev, W. Maenhaut, N. Marsden, S. Saarikoski, J. Schnelle-Kreis, J.D. Surratt, S. Szidat, R. Szmigielski, A. Wisthaler, The Molecular Identification of Organic Compounds in the Atmosphere: State of the Art and Challenges, *Chemical Reviews*, 115 (2015) 3919-3983.
- [36] M. Tobiszewski, J. Namieśnik, PAH diagnostic ratios for the identification of pollution emission sources, *Environmental Pollution*, 162 (2012) 110-119.
- [37] E. Galarnau, Source specificity and atmospheric processing of airborne PAHs: Implications for source apportionment, *Atmospheric Environment*, 42 (2008) 8139-8149.
- [38] I.J. Keyte, R.M. Harrison, G. Lammel, Chemical reactivity and long-range transport potential of polycyclic aromatic hydrocarbons-a review, *Chemical Society Reviews*, 42 (2013) 9333-9391.
- [39] M.M. Coggon, P.R. Veres, B. Yuan, A. Koss, C. Warneke, J.B. Gilman, B.M. Lerner, J. Peischl, K.C. Aikin, C.E. Stockwell, L.E. Hatch, T.B. Ryerson, J.M. Roberts, R.J. Yokelson, J.A. de Gouw, Emissions of nitrogen-containing organic compounds from the burning of herbaceous and arboraceous biomass: Fuel composition dependence and the variability of commonly used nitrile tracers, *Geophysical Research Letters*, 43 (2016) 9903-9912.
- [40] J.G. Watson, J.C. Chow, E.M. Fujita, Review of volatile organic compound source apportionment by chemical mass balance, *Atmospheric Environment*, 35 (2001) 1567-1584.
- [41] A. Bonnicksen, D. Newbold, *A Practical Approach to Motor Vehicle Engineering and Maintenance*, second ed., Routledge, 2013.
- [42] M.M. Rhead, S.A. Hardy, The sources of polycyclic aromatic compounds in diesel engine emissions, *Fuel*, 82 (2003) 385-393.
- [43] M. Frenklach, Reaction mechanism of soot formation in flames, *Physical Chemistry Chemical Physics*, 4 (2002) 2028-2037.

- [44] J.P. Carroll, J.M. Finnan, F. Biedermann, T. Brunner, I. Obernberger, Air staging to reduce emissions from energy crop combustion in small scale applications, *Fuel*, 155 (2015) 37-43.
- [45] J. Jandačka, J. Mičieta, M. Holubčík, R. Nosek, Experimental Determination of Bed Temperatures during Wood Pellet Combustion, *Energy and Fuels*, 31 (2017) 2919-2926.
- [46] B.R.T. Simoneit, J.J. Schauer, C.G. Nolte, D.R. Oros, V.O. Elias, M.P. Fraser, W.F. Rogge, G.R. Cass, Levoglucosan, a tracer for cellulose in biomass burning and atmospheric particles, *Atmospheric Environment*, 33 (1999) 173-182.
- [47] E.B. Ledesma, N.D. Marsh, A.K. Sandrowitz, M.J. Wornat, Global kinetic rate parameters for the formation of polycyclic aromatic hydrocarbons from the pyrolysis of catechol, a model compound representative of solid fuel moieties, *Energy and Fuels*, 16 (2002) 1331-1336.
- [48] D.K. Shen, S. Gu, The mechanism for thermal decomposition of cellulose and its main products, *Bioresource Technology*, 100 (2009) 6496-6504.
- [49] M. Nowakowska, O. Herbinet, A. Dufour, P.A. Glaude, Detailed kinetic study of anisole pyrolysis and oxidation to understand tar formation during biomass combustion and gasification, *Combustion and Flame*, 161 (2014) 1474-1488.
- [50] R. Atkinson, Atmospheric chemistry of VOCs and NO(x), *Atmospheric Environment*, 34 (2000) 2063-2101.
- [51] J.H. Kroll, J.H. Seinfeld, Chemistry of secondary organic aerosol: Formation and evolution of low-volatility organics in the atmosphere, *Atmospheric Environment*, 42 (2008) 3593-3624.
- [52] H.J. Chacon-Madrid, N.M. Donahue, Fragmentation vs. functionalization: chemical aging and organic aerosol formation, *Atmospheric Chemistry and Physics*, 11 (2011) 10553-10563.
- [53] D.H. Ehhalt, Photooxidation of trace gases in the troposphere, *Physical Chemistry Chemical Physics*, 1 (1999) 5401-5408.
- [54] J.J. Bufalini, T.A. Walter, M.M. Butalini, OZONE FORMATION POTENTIAL OF ORGANIC COMPOUNDS, *Environmental Science and Technology*, 10 (1976) 908-912.
- [55] R. Criegee, Die Ozonolyse, *Chemie in Unserer Zeit*, 7 (1973) 75-83.
- [56] R. Atkinson, W.P.L. Carter, Kinetics and mechanisms of the gas-phase reactions of ozone with organic compounds under atmospheric conditions, *Chemical Reviews*, 84 (1984) 437-470.
- [57] X. Zhang, R.H. Schwantes, M.M. Coggon, C.L. Loza, K.A. Schilling, R.C. Flagan, J.H. Seinfeld, Role of ozone in SOA formation from alkane photooxidation, *Atmospheric Chemistry and Physics*, 14 (2014) 1733-1753.
- [58] Y. Wang, Q.Q. Zhang, K. He, Q. Zhang, L. Chai, Sulfate-nitrate-ammonium aerosols over China: Response to 2000-2015 emission changes of sulfur dioxide, nitrogen oxides, and ammonia, *Atmospheric Chemistry and Physics*, 13 (2013) 2635-2652.

- [59] J. Ringuet, A. Albinet, E. Leoz-Garziandia, H. Budzinski, E. Villenave, Reactivity of polycyclic aromatic compounds (PAHs, NPAHs and OPAHs) adsorbed on natural aerosol particles exposed to atmospheric oxidants, *Atmospheric Environment*, 61 (2012) 15-22.
- [60] J.H. Kroll, C.Y. Lim, S.H. Kessler, K.R. Wilson, Heterogeneous Oxidation of Atmospheric Organic Aerosol: Kinetics of Changes to the Amount and Oxidation State of Particle-Phase Organic Carbon, *Journal of Physical Chemistry A*, 119 (2015) 10767-10783.
- [61] C.J. Hennigan, M.A. Miracolo, G.J. Engelhart, A.A. May, A.A. Presto, T. Lee, A.P. Sullivan, G.R. McMeeking, H. Coe, C.E. Wold, W.M. Hao, J.B. Gilman, W.C. Kuster, J. De Gouw, B.A. Schichtel, J.L. Collett Jr, S.M. Kreidenweis, A.L. Robinson, Chemical and physical transformations of organic aerosol from the photo-oxidation of open biomass burning emissions in an environmental chamber, *Atmospheric Chemistry and Physics*, 11 (2011) 7669-7686.
- [62] N.L. Ng, M.R. Canagaratna, J.L. Jimenez, P.S. Chhabra, J.H. Seinfeld, D.R. Worsnop, Changes in organic aerosol composition with aging inferred from aerosol mass spectra, *Atmospheric Chemistry and Physics*, 11 (2011) 6465-6474.
- [63] D.K. Farmer, A. Matsunaga, K.S. Docherty, J.D. Surratt, J.H. Seinfeld, P.J. Ziemann, J.L. Jimenez, Response of an aerosol mass spectrometer to organonitrates and organosulfates and implications for atmospheric chemistry, *Proceedings of the National Academy of Sciences of the United States of America*, 107 (2010) 6670-6675.
- [64] A. Laskin, J. Laskin, S.A. Nizkorodov, Chemistry of Atmospheric Brown Carbon, *Chemical Reviews*, 115 (2015) 4335-4382.
- [65] W. Trivittayanurak, P.J. Adams, Does the POA-SOA split matter for global CCN formation?, *Atmospheric Chemistry and Physics*, 14 (2014) 995-1010.
- [66] E. Kang, M.J. Root, D.W. Toohey, W.H. Brune, Introducing the concept of Potential Aerosol Mass (PAM), *Atmospheric Chemistry and Physics*, 7 (2007) 5727-5744.
- [67] E. Kang, D.W. Toohey, W.H. Brune, Dependence of SOA oxidation on organic aerosol mass concentration and OH exposure: Experimental PAM chamber studies, *Atmospheric Chemistry and Physics*, 11 (2011) 1837-1852.
- [68] A. Keller, H. Bartscher, A continuous photo-oxidation flow reactor for a defined measurement of the SOA formation potential of wood burning emissions, *Journal of Aerosol Science*, 49 (2012) 9-20.
- [69] E.A. Brunns, I. El Haddad, A. Keller, F. Klein, N.K. Kumar, S.M. Pieber, J.C. Corbin, J.G. Slowik, W.H. Brune, U. Baltensperger, A.S.H. Prévôt, Inter-comparison of laboratory smog chamber and flow reactor systems on organic aerosol yield and composition, *Atmospheric Measurement Techniques*, 8 (2015) 2315-2332.
- [70] M. Hallquist, J.C. Wenger, U. Baltensperger, Y. Rudich, D. Simpson, M. Claeys, J. Dommen, N.M. Donahue, C. George, A.H. Goldstein, J.F. Hamilton, H. Herrmann, T. Hoffmann, Y. Iinuma, M. Jang, M.E. Jenkin, J.L. Jimenez, A. Kiendler-Scharr, W. Maenhaut, G. McFiggans, T.F. Mentel, A.

Monod, A.S.H. Prévôt, J.H. Seinfeld, J.D. Surratt, R. Szmigielski, J. Wildt, The formation, properties and impact of secondary organic aerosol: Current and emerging issues, *Atmospheric Chemistry and Physics*, 9 (2009) 5155-5236.

[71] U.S. EPA, Global Emissions by Gas based on: Contribution of Working Group III to the Fifth Assessment Report of the Intergovernmental Panel on Climate Change (IPCC 2014), in: *Global Greenhouse Gas Emission Data*, 2017.

[72] C.T. Crowe, J.D. Schwarzkopf, M. Sommerfeld, Y. Tsuji, *Multiphase Flows with Droplets and Particles*, CRC Press, Boca Raton, FL, USA, 1999.

[73] M.O. Andreae, The dark side of aerosols, *Nature*, 409 (2001) 671-672.

[74] T.C. Bond, S.J. Doherty, D.W. Fahey, P.M. Forster, T. Berntsen, B.J. Deangelo, M.G. Flanner, S. Ghan, B. Kärcher, D. Koch, S. Kinne, Y. Kondo, P.K. Quinn, M.C. Sarofim, M.G. Schultz, M. Schulz, C. Venkataraman, H. Zhang, S. Zhang, N. Bellouin, S.K. Guttikunda, P.K. Hopke, M.Z. Jacobson, J.W. Kaiser, Z. Klimont, U. Lohmann, J.P. Schwarz, D. Shindell, T. Storelvmo, S.G. Warren, C.S. Zender, Bounding the role of black carbon in the climate system: A scientific assessment, *Journal of Geophysical Research Atmospheres*, 118 (2013) 5380-5552.

[75] R. Bahadur, P.S. Praveen, Y. Xu, V. Ramanathan, Solar absorption by elemental and brown carbon determined from spectral observations, *Proceedings of the National Academy of Sciences of the United States of America*, 109 (2012) 17366-17371.

[76] P. Ceppi, F. Briant, M.D. Zelinka, D.L. Hartmann, Cloud feedback mechanisms and their representation in global climate models, *Wiley Interdisciplinary Reviews: Climate Change*, 8 (2017).

[77] O. Boucher, D. Randall, P. Artaxo, C. Bretherton, G. Feingold, P.M. Forster, V.-M. Kerminen, Y. Kondo, H. Liao, U. Lohmann, P. Rasch, S.K. Satheesh, S. Sherwood, B. Stevens, X.Y. Zhang, *Clouds and Aerosols*, in: T.F. Stocker, D. Qin, G.-K. Plattner, M. Tignor, S.K. Allen, J. Boschung, A. Nauels, Y. Xia, V. Bex and P.M. Midgale (Ed.) *Climate Change 2013: The Physical Science Basis. Contribution of Working Group I to the Fifth Assessment Report of the Intergovernmental Panel on Climate Change*, Cambridge, UK, and New York, NY, USA, 2013.

[78] J.E. Hart, Invited Commentary: Epidemiologic Studies of the Impact of Air Pollution on Lung Cancer, *American Journal of Epidemiology*, 179 (2014) 452-454.

[79] S. Socco, R.C. Bovee, M.B. Palczewski, J.R. Hickok, D.D. Thomas, Epigenetics: The third pillar of nitric oxide signaling, *Pharmacological Research*, 121 (2017) 52-58.

[80] S.N. Pandis, K. Skylakou, K. Florou, E. Kostenidou, C. Kaltsonoudis, E. Hasa, A.A. Presto, Urban particulate matter pollution: A tale of five cities, *Faraday Discussions*, 189 (2016) 277-290.

[81] H. Guo, S.H. Kota, S.K. Sahu, J. Hu, Q. Ying, A. Gao, H. Zhang, Source apportionment of PM_{2.5} in North India using source-oriented air quality models, *Environmental Pollution*, 231 (2017) 426-436.

- [82] R.T. Burnett, C. Arden Pope Iii, M. Ezzati, C. Olives, S.S. Lim, S. Mehta, H.H. Shin, G. Singh, B. Hubbell, M. Brauer, H. Ross Anderson, K.R. Smith, J.R. Balmes, N.G. Bruce, H. Kan, F. Laden, A. Prüss-Ustün, M.C. Turner, S.M. Gapstur, W.R. Diver, A. Cohen, An integrated risk function for estimating the global burden of disease attributable to ambient fine particulate matter exposure, *Environmental Health Perspectives*, 122 (2014) 397-403.
- [83] M.L. Bell, D.L. Davis, Reassessment of the lethal London fog of 1952: Novel indicators of acute and chronic consequences of acute exposure to air pollution, *Environmental Health Perspectives*, 109 (2001) 389-394.
- [84] F. Laden, L.M. Neas, D.W. Dockery, J. Schwartz, Association of fine particulate matter from different sources with daily mortality in six U.S. cities, *Environmental Health Perspectives*, 108 (2000) 941-947.
- [85] CAFE, Loss in life expectancy attributable to exposure to fine particulate matter - 2000 in: Clean Air for Europe (CAFE), European Union (EU), 2011.
- [86] R. Schmidt, H. Ryan, A. Hoetzel, Carbon monoxide - toxicity of low-dose application, *Current Pharmaceutical Biotechnology*, 13 (2012) 837-850.
- [87] A.C. Aiken, P.F. Decarlo, J.H. Kroll, D.R. Worsnop, J.A. Huffman, K.S. Docherty, I.M. Ulbrich, C. Mohr, J.R. Kimmel, D. Sueper, Y. Sun, Q. Zhang, A. Trimborn, M. Northway, P.J. Ziemann, M.R. Canagaratna, T.B. Onasch, M.R. Alfarra, A.S.H. Prevot, J. Dommen, J. Duplissy, A. Metzger, U. Baltensperger, J.L. Jimenez, O/C and OM/OC ratios of primary, secondary, and ambient organic aerosols with high-resolution time-of-flight aerosol mass spectrometry, *Environmental Science and Technology*, 42 (2008) 4478-4485.
- [88] E.A. Kowal, U. Seneviratne, S. Wickramaratne, K.E. Doherty, X. Cao, N. Tretyakova, M.P. Stone, Structures of exocyclic R,R - And S,S - N6, N 6-(2,3-dihydroxybutan-1,4-diyl)-2'-deoxyadenosine adducts induced by 1,2,3,4-diepoxybutane, *Chemical Research in Toxicology*, 27 (2014) 805-817.
- [89] J. Whysner, M.V. Reddy, P.M. Ross, M. Mohan, E.A. Lax, Genotoxicity of benzene and its metabolites, *Mutation Research - Reviews in Mutation Research*, 566 (2004) 99-130.
- [90] J. Heyder, Deposition of inhaled particles in the human respiratory tract and consequences for regional targeting in respiratory drug delivery, *Proc Am Thorac Soc*, 1 (2004) 315-320.
- [91] O. Uski, P.I. Jalava, M.S. Happonen, T. Torvela, J. Leskinen, J. Mäki-Paakkanen, J. Tissari, O. Sippula, H. Lamberg, J. Jokiniemi, M.R. Hirvonen, Effect of fuel zinc content on toxicological responses of particulate matter from pellet combustion in vitro, *Science of the Total Environment*, 511 (2015) 331-340.
- [92] L.D. Claxton, The history, genotoxicity, and carcinogenicity of carbon-based fuels and their emissions. Part 3: Diesel and gasoline, *Mutation Research - Reviews in Mutation Research*, 763 (2015) 30-85.

- [93] J.J. Corbett, J.J. Winebrake, E.H. Green, P. Kasibhatla, V. Eyring, A. Lauer, Mortality from ship emissions: A global assessment, *Environmental Science and Technology*, 41 (2007) 8512-8518.
- [94] L. Tian, K.F. Ho, P.K.K. Louie, H. Qiu, V.C. Pun, H. Kan, I.T.S. Yu, T.W. Wong, Shipping emissions associated with increased cardiovascular hospitalizations, *Atmospheric Environment*, 74 (2013) 320-325.
- [95] Z. Wan, M. Zhu, S. Chen, D. Sperling, Pollution: Three steps to a green shipping industry, *Nature*, 530 (2016) 275-277.
- [96] P.Y. Hsieh, K.R. Abel, T.J. Bruno, Analysis of marine diesel fuel with the advanced distillation curve method, *Energy and Fuels*, 27 (2013) 804-810.
- [97] O. Popovicheva, E. Kireeva, N. Shonija, N. Zubareva, N. Persiantseva, V. Tishkova, B. Demirdjian, J. Moldanová, V. Mogilnikov, Ship particulate pollutants: Characterization in terms of environmental implication, *Journal of Environmental Monitoring*, 11 (2009) 2077-2086.
- [98] H. Agrawal, Q.G.J. Malloy, W.A. Welch, J. Wayne Miller, D.R. Cocker lii, In-use gaseous and particulate matter emissions from a modern ocean going container vessel, *Atmospheric Environment*, 42 (2008) 5504-5510.
- [99] J. Moldanová, E. Fridell, O. Popovicheva, B. Demirdjian, V. Tishkova, A. Faccinotto, C. Focsa, Characterisation of particulate matter and gaseous emissions from a large ship diesel engine, *Atmospheric Environment*, 43 (2009) 2632-2641.
- [100] V. Jayaram, H. Agrawal, W.A. Welch, J.W. Miller, D.R. Cocker III, Real-time gaseous, PM and ultrafine particle emissions from a modern marine engine operating on biodiesel, *Environmental Science and Technology*, 45 (2011) 2286-2292.
- [101] D.A. Cooper, Exhaust emissions from high speed passenger ferries, *Atmospheric Environment*, 35 (2001) 4189-4200.
- [102] D.A. Cooper, Exhaust emissions from ships at berth, *Atmospheric Environment*, 37 (2003) 3817-3830.
- [103] S. Murphy, H. Agrawal, A. Sorooshian, L.T. Padró, H. Gates, S. Hersey, W.A. Welch, H. Jung, J.W. Miller, D.R. Cocker lii, A. Nenes, H.H. Jonsson, R.C. Flagan, J.H. Seinfeld, Comprehensive simultaneous shipboard and airborne characterization of exhaust from a modern container ship at sea, *Environmental Science and Technology*, 43 (2009) 4626-4640.
- [104] D.A. Lack, C.D. Cappa, J. Langridge, R. Bahreini, G. Buffaloe, C. Brock, K. Cerully, D. Coffman, K. Hayden, J. Holloway, B. Lerner, P. Massoli, S.M. Li, R. McLaren, A.M. Middlebrook, R. Moore, A. Nenes, I. Nuaaman, T.B. Onasch, J. Peischl, A. Perring, P.K. Quinn, T. Ryerson, J.P. Schwartz, R. Spackman, S.C. Wofsy, D. Worsnop, B. Xiang, E. Williams, Impact of fuel quality regulation and speed reductions on shipping emissions: Implications for climate and air quality, *Environmental Science and Technology*, 45 (2011) 9052-9060.

- [105] R.A. Kotchenruther, The effects of marine vessel fuel sulfur regulations on ambient PM_{2.5} along the west coast of the U.S, *Atmospheric Environment*, 103 (2015) 121-128.
- [106] S. Oeder, T. Kanashova, O. Sippula, S.C. Sapcariu, T. Streibel, J.M. Arteaga-Salas, J. Passig, M. Dilger, H.-R. Paur, C. Schlager, S. Mülhopt, S. Diabaté, C. Weiss, B. Stengel, R. Rabe, H. Harndorf, T. Torvela, J.K. Jokiniemi, M.-R. Hirvonen, C. Schmidt-Weber, C. Traidl-Hoffmann, K.A. BéruBé, A.J. Wlodarczyk, B. Michalke, T. Krebs, A.S.H. Prévôt, M. Kelbg, J. Tiggesbäumker, E. Karg, G. Jakobi, S. Scholtes, J. Schnelle-Kreis, J. Lintelmann, G. Matuschek, M. Sklorz, S. Klingbeil, J. Orasche, P. Richthammer, L. Müller, M. Elsasser, A.A. Reda, T.M. Gröger, B. Weggler, H. Czech, C.P. Rüger, G. Abbaszade, C. Radischat, K. Hiller, J.T.M. Buters, G. Dittmar, R. Zimmermann, Particulate Matter from Both Heavy Fuel Oil and Diesel Fuel Shipping Emissions Show Strong Biological Effects on Human Lung Cells at Realistic and Comparable In Vitro Exposure Conditions, *PLOS ONE*, 10 (2015) 1932-6203.
- [107] B. Long, J.L. Bao, D.G. Truhlar, Reaction of SO₂ with OH in the atmosphere, *Physical Chemistry Chemical Physics*, 19 (2017) 8091-8100.
- [108] P.V. Hobbs, T.J. Garrett, R.J. Ferek, S.R. Strader, D.A. Hegg, G.M. Frick, W.A. Hoppel, R.F. Gasparovic, L.M. Russell, D.W. Johnson, C. O'Dowd, P.A. Durkee, K.E. Nielsen, G. Innis, Emissions from ships with respect to their effects on clouds, *Journal of the Atmospheric Sciences*, 57 (2000) 2570-2590.
- [109] V. Eyring, I.S.A. Isaksen, T. Berntsen, W.J. Collins, J.J. Corbett, O. Endresen, R.G. Grainger, J. Moldanová, H. Schlager, D.S. Stevenson, Transport impacts on atmosphere and climate: Shipping, *Atmospheric Environment*, 44 (2010) 4735-4771.
- [110] J. Fuglestvedt, T. Berntsen, G. Myhre, K. Rypdal, R.B. Skeie, Climate forcing from the transport sectors, *Proceedings of the National Academy of Sciences of the United States of America*, 105 (2008) 454-458.
- [111] M.F. Heringa, P.F. DeCarlo, R. Chirico, A. Lauber, A. Doberer, J. Good, T. Nussbaumer, A. Keller, H. Burtscher, A. Richard, B. Miljevic, A.S.H. Prévôt, U. Baltensperger, Time-resolved characterization of primary emissions from residential wood combustion appliances, *Environmental Science and Technology*, 46 (2012) 11418-11425.
- [112] C. Schmidl, M. Luisser, E. Padouvas, L. Lasselsberger, M. Rzaca, C. Ramirez-Santa Cruz, M. Handler, G. Peng, H. Bauer, H. Puxbaum, Particulate and gaseous emissions from manually and automatically fired small scale combustion systems, *Atmospheric Environment*, 45 (2011) 7443-7454.
- [113] C. Brandt, R. Kunde, B. Dobmeier, J. Schnelle-Kreis, J. Orasche, G. Schmoeckel, J. Diemer, R. Zimmermann, M. Gaderer, Ambient PM₁₀ concentrations from wood combustion - Emission modeling and dispersion calculation for the city area of Augsburg, Germany, *Atmospheric Environment*, 45 (2011) 3466-3474.

- [114] G.W. Fuller, J. Sciare, M. Lutz, S. Moukhtar, S. Wagener, New Directions: Time to tackle urban wood burning?, *Atmospheric Environment*, 68 (2013) 295-296.
- [115] K. Gaeggeler, A.S.H. Prévôt, J. Dommen, G. Legreid, S. Reimann, U. Baltensperger, Residential wood burning in an Alpine valley as a source for oxygenated volatile organic compounds, hydrocarbons and organic acids, *Atmospheric Environment*, 42 (2008) 8278-8287.
- [116] P.I. Jalava, M.S. Happo, J. Kelz, T. Brunner, P. Hakulinen, J. Mäki-Paakkanen, A. Hukkanen, J. Jokiniemi, I. Obernberger, M.R. Hirvonen, In vitro toxicological characterization of particulate emissions from residential biomass heating systems based on old and new technologies, *Atmospheric Environment*, 50 (2012) 24-35.
- [117] M. Sehlstedt, R. Dove, C. Boman, J. Pagels, E. Swietlicki, J. Löndahl, R. Westerholm, J. Bosson, S. Barath, A.F. Behndig, J. Pourazar, T. Sandström, I.S. Mudway, A. Blomberg, Antioxidant airway responses following experimental exposure to wood smoke in man, *Particle and Fibre Toxicology*, 7 (2010).
- [118] L.P. Naeher, M. Brauer, M. Lipsett, J.T. Zelikoff, C.D. Simpson, J.Q. Koenig, K.R. Smith, Woodsmoke health effects: A review, *Inhalation Toxicology*, 19 (2007) 67-106.
- [119] A.K. Bølling, A.I. Totlandsdal, G. Sallsten, A. Braun, R. Westerholm, C. Bergvall, J. Boman, H.J. Dahlman, M. Sehlstedt, F. Cassee, T. Sandstrom, P.E. Schwarze, J.I. Herseth, Wood smoke particles from different combustion phases induce similar pro-inflammatory effects in a co-culture of monocyte and pneumocyte cell lines, *Particle and Fibre Toxicology*, 9 (2012).
- [120] T. Nussbaumer, Combustion and Co-combustion of Biomass: Fundamentals, Technologies, and Primary Measures for Emission Reduction, *Energy and Fuels*, 17 (2003) 1510-1521.
- [121] H. Khodaei, F. Guzzomi, D. Patiño, B. Rashidian, G.H. Yeoh, Air staging strategies in biomass combustion-gaseous and particulate emission reduction potentials, *Fuel Processing Technology*, 157 (2017) 29-41.
- [122] K. Nuutinen, J. Jokiniemi, O. Sippula, H. Lamberg, J. Sutinen, P. Horttanainen, J. Tissari, Effect of air staging on fine particle, dust and gaseous emissions from masonry heaters, *Biomass and Bioenergy*, 67 (2014) 167-178.
- [123] H. Lamberg, O. Sippula, J. Tissari, J. Jokiniemi, Effects of air staging and load on fine-particle and gaseous emissions from a small-scale pellet boiler, *Energy and Fuels*, 25 (2011) 4952-4960.
- [124] J. Lyyränen, J. Jokiniemi, E.I. Kauppinen, U. Backman, H. Vesala, Comparison of Different Dilution Methods for Measuring Diesel Particle Emissions, *Aerosol Science and Technology*, 38 (2004) 12-23.
- [125] J.H. Gross, *Mass Spectrometry - A Textbook*, second ed., Springer-Verlag Berlin-Heidelberg, 2011.
- [126] T.D. Märk, Fundamental aspects of electron impact ionization, *International Journal of Mass Spectrometry and Ion Physics*, 45 (1982) 125-145.

- [127] R.C. Powell, *Physics of Solid-State Laser Materials*, first ed., Springer-Verlag, 1998.
- [128] D.A. Skoog, J.J. Leary, *Instrumentelle Analytik: Grundlagen - Geräte - Anwendungen*, fourth ed., Springer-Verlag, 1996.
- [129] N.P. Lockyer, J.C. Vickerman, Single photon ionisation mass spectrometry using laser-generated vacuum ultraviolet photons, *Laser Chemistry*, 17 (1997) 139-159.
- [130] D.J. Butcher, Vacuum ultraviolet radiation for single-photoionization mass spectrometry: A review, *Microchemical Journal*, 62 (1999) 354-362.
- [131] L. Hanley, R. Zimmermann, Light and molecular ions: The emergence of vacuum UV single-photon ionization in MS, *Analytical Chemistry*, 81 (2009) 4174-4182.
- [132] T. Adam, R. Zimmermann, Determination of single photon ionization cross sections for quantitative analysis of complex organic mixtures, *Analytical and Bioanalytical Chemistry*, 389 (2007) 1941-1951.
- [133] U. Boesl, Laser mass spectrometry for environmental and industrial chemical trace analysis, *Journal of Mass Spectrometry*, 35 (2000) 289-304.
- [134] W.C. Wiley, I.H. McLaren, Time-of-Flight Mass Spectrometer with Improved Resolution, *Review of Scientific Instruments*, 26 (1955) 1150-1157.
- [135] B.A. Mamyrin, V.I. Karataev, D.V. Shmikk, V.A. Zagulin, The mass-reflectron, a new nonmagnetic time-of-flight mass spectrometer with high resolution, *Soviet physics JETP*, 64 (1973) 82-89.
- [136] H. Czech, O. Sippula, M. Kortelainen, J. Tissari, C. Radischat, J. Passig, T. Streibel, J. Jokiniemi, R. Zimmermann, On-line analysis of organic emissions from residential wood combustion with single-photon ionisation time-of-flight mass spectrometry (SPI-TOFMS), *Fuel*, 177 (2016) 334-342.
- [137] T. Streibel, F. Mühlberger, R. Geißler, M. Saraji-Bozorgzad, T. Adam, R. Zimmermann, Influence of sulphur addition on emissions of polycyclic aromatic hydrocarbons during biomass combustion, *Proceedings of the Combustion Institute*, 35 (2015) 1771-1777.
- [138] J.C. Chow, J.G. Watson, L.W.A. Chen, M.C.O. Chang, N.F. Robinson, D. Trimble, S. Kohl, The IMPROVE_A temperature protocol for thermal/optical carbon analysis: Maintaining consistency with a long-term database, *Journal of the Air and Waste Management Association*, 57 (2007) 1014-1023.
- [139] J. Grabowsky, T. Streibel, M. Sklorz, J.C. Chow, J.G. Watson, A. Mamakos, R. Zimmermann, Hyphenation of a carbon analyzer to photo-ionization mass spectrometry to unravel the organic composition of particulate matter on a molecular level, *Analytical and Bioanalytical Chemistry*, 401 (2011) 3153-3164.
- [140] J. Diab, T. Streibel, F. Cavalli, S.C. Lee, H. Saathoff, A. Mamakos, J.C. Chow, L.W.A. Chen, J.G. Watson, O. Sippula, R. Zimmermann, Hyphenation of a EC / OC thermal-optical carbon analyzer to photo-ionization time-of-flight mass spectrometry: An off-line aerosol mass spectrometric

approach for characterization of primary and secondary particulate matter, *Atmospheric Measurement Techniques*, 8 (2015) 3337-3353.

[141] J.T. Jayne, D.C. Leard, X. Zhang, P. Davidovits, K.A. Smith, C.E. Kolb, D.R. Worsnop, Development of an aerosol mass spectrometer for size and composition analysis of submicron particles, *Aerosol Science and Technology*, 33 (2000) 49-70.

[142] M.R. Canagaratna, J.T. Jayne, J.L. Jimenez, J.D. Allan, M.R. Alfarra, Q. Zhang, T.B. Onasch, F. Drewnick, H. Coe, A. Middlebrook, A. Delia, L.R. Williams, A.M. Trimborn, M.J. Northway, P.F. DeCarlo, C.E. Kolb, P. Davidovits, D.R. Worsnop, Chemical and microphysical characterization of ambient aerosols with the aerodyne aerosol mass spectrometer, *Mass Spectrometry Reviews*, 26 (2007) 185-222.

[143] M.R. Canagaratna, J.L. Jimenez, J.H. Kroll, Q. Chen, S.H. Kessler, P. Massoli, L. Hildebrandt Ruiz, E. Fortner, L.R. Williams, K.R. Wilson, J.D. Surratt, N.M. Donahue, J.T. Jayne, D.R. Worsnop, Elemental ratio measurements of organic compounds using aerosol mass spectrometry: characterization, improved calibration, and implications, *Atmospheric Chemistry and Physics*, 15 (2015) 253-272.

[144] T.B. Onasch, A. Trimborn, E.C. Fortner, J.T. Jayne, G.L. Kok, L.R. Williams, P. Davidovits, D.R. Worsnop, Soot particle aerosol mass spectrometer: Development, validation, and initial application, *Aerosol Science and Technology*, 46 (2012) 804-817.

[145] H. Abdi, The Bonferroni and Šidák Corrections for Multiple Comparisons, in: N. Salkind (Ed.) *Encyclopedia of Measurement and Statistics*, Sage Publications, Thousand Oaks, CA, 2007, pp. 103-107.

[146] E. Schmider, M. Ziegler, E. Danay, L. Beyer, M. Bühner, Is It Really Robust?: Reinvestigating the robustness of ANOVA against violations of the normal distribution assumption, *Methodology*, 6 (2010) 147-151.

[147] W.H. Kruskal, W.A. Wallis, Use of Ranks in One-Criterion Variance Analysis, *Journal of the American Statistical Association*, 47 (1952) 583-621.

[148] M.W. Berry, M. Browne, A.N. Langville, V.P. Pauca, R.J. Plemmons, Algorithms and applications for approximate nonnegative matrix factorization, *Computational Statistics and Data Analysis*, 52 (2007) 155-173.

[149] D.D. Lee, H.S. Seung, Learning the parts of objects by non-negative matrix factorization, *Nature*, 401 (1999) 788-791.

[150] P. Paatero, U. Tapper, Positive matrix factorization: a non-negative factor model with optimal utilization of error estimates of data values, *Environmetrics*, 5 (1994) 111-126.

[151] A.M. Taiwo, R.M. Harrison, Z. Shi, A review of receptor modelling of industrially emitted particulate matter, *Atmospheric Environment*, 97 (2014) 109-120.

[152] I.T. Jolliff, *Principal Component Analysis*, Second Edition, Springer Verlag, New York, 2002.

- [153] D. Ballabio, A MATLAB toolbox for Principal Component Analysis and unsupervised exploration of data structure, *Chemometrics and Intelligent Laboratory Systems*, 149 (2015) 1-9.
- [154] S. Wold, M. Sjöström, L. Eriksson, PLS-regression: A basic tool of chemometrics, *Chemometrics and Intelligent Laboratory Systems*, 58 (2001) 109-130.
- [155] D. Tian, W. Zheng, G. He, Y. Zheng, M.E. Andersen, H. Tan, W. Qu, Predicting cytotoxicity of complex mixtures in high cancer incidence regions of the Huai River Basin based on GC-MS spectrum with partial least squares regression, *Environmental Research*, 137 (2015) 391-397.
- [156] O. Abbas, C. Rebufa, N. Dupuy, A. Permanyer, J. Kister, PLS regression on spectroscopic data for the prediction of crude oil quality: API gravity and aliphatic/aromatic ratio, *Fuel*, 98 (2012) 5-14.
- [157] H. Czech, J. Schnelle-Kreis, T. Streibel, R. Zimmermann, New directions: Beyond sulphur, vanadium and nickel - About source apportionment of ship emissions in emission control areas, *Atmospheric Environment*, 163 (2017) 190-191.
- [158] J.C. Corbin, S.M. Pieber, H. Czech, M. Zanatta, G. Jakobi, D. Massabó, J. Orasche, I. El Haddad, A.A. Mensah, B. Stengel, L. Drinovec, G. Močnik, R. Zimmermann, A.S.H. Prévôt, M. Gysel, Black and brown carbon emitted by a ship engine operating on distillate and residual fuels, *Journal of Geophysical Research D: Atmospheres*, (manuscript in preparation).
- [159] C.P. Rüger, M. Sklorz, T. Schwemer, R. Zimmermann, Characterisation of ship diesel primary particulate matter at the molecular level by means of ultra-high-resolution mass spectrometry coupled to laser desorption ionisation - Comparison of feed fuel, filter extracts and direct particle measurements, *Analytical and Bioanalytical Chemistry*, 407 (2015) 5923-5937.
- [160] J.K. Mwangi, W.J. Lee, Y.C. Chang, C.Y. Chen, L.C. Wang, An overview: Energy saving and pollution reduction by using green fuel blends in diesel engines, *Applied Energy*, 159 (2015) 214-236.
- [161] W. Püttmann, H. Villar, Occurrence and geochemical significance of 1,2,5,6-tetramethylnaphthalene, *Geochimica et Cosmochimica Acta*, 51 (1987) 3023-3029.
- [162] B.R.T. Simoneit, J.O. Grimalt, T.G. Wang, R.E. Cox, P.G. Hatcher, A. Nissenbaum, Cyclic terpenoids of contemporary resinous plant detritus and of fossil woods, ambers and coals, *Organic Geochemistry*, 10 (1986) 877-889.
- [163] H. Behbehani, M.K. Andari, Determination of organic sulfur compound types in vacuum gas oils using GC-FID-SCD method, *Petroleum Science and Technology*, 18 (2000) 51-61.
- [164] C. Radischat, O. Sippula, B. Stengel, S. Klingbeil, M. Sklorz, R. Rabe, T. Streibel, H. Harndorf, R. Zimmermann, Real-time analysis of organic compounds in ship engine aerosol emissions using resonance-enhanced multiphoton ionisation and proton transfer mass spectrometry *Aerosols and Health, Analytical and Bioanalytical Chemistry*, 407 (2015) 5939-5951.

- [165] T. Streibel, J. Schnelle-Kreis, H. Czech, H. Harndorf, G. Jakobi, J. Jokiniemi, E. Karg, J. Lintelmann, G. Matuschek, B. Michalke, L. Müller, J. Orasche, J. Passig, C. Radischat, R. Rabe, A. Reda, C. Rüger, T. Schwemer, O. Sippula, B. Stengel, M. Sklorz, T. Torvela, B. Weggler, R. Zimmermann, Aerosol emissions of a ship diesel engine operated with diesel fuel or heavy fuel oil, *Environmental Science and Pollution Research*, 24 (2017) 10976-10991.
- [166] T.W. Adam, R. Chirico, M. Clairotte, M. Elsasser, U. Manfredi, G. Martini, M. Sklorz, T. Streibel, M.F. Heringa, P.F. Decarlo, U. Baltensperger, G. De Santi, A. Krasenbrink, R. Zimmermann, A.S.H. Prevot, C. Astorga, Application of modern online instrumentation for chemical analysis of gas and particulate phases of exhaust at the european commission heavy-duty vehicle emission laboratory, *Analytical Chemistry*, 83 (2011) 67-76.
- [167] T.W. Adam, M. Clairotte, T. Streibel, M. Elsasser, A. Pommeres, U. Manfredi, M. Carriero, G. Martini, M. Sklorz, A. Krasenbrink, C. Astorga, R. Zimmermann, Real-time analysis of aromatics in combustion engine exhaust by resonance-enhanced multiphoton ionisation time-of-flight mass spectrometry (REMPI-TOF-MS): A robust tool for chassis dynamometer testing, *Analytical and Bioanalytical Chemistry*, 404 (2012) 273-276.
- [168] M. Elsasser, C. Busch, J. Orasche, C. Schön, H. Hartmann, J. Schnelle-Kreis, R. Zimmermann, Dynamic changes of the aerosol composition and concentration during different burning phases of wood combustion, *Energy and Fuels*, 27 (2013) 4959-4968.
- [169] O. Sippula, B. Stengel, M. Sklorz, T. Streibel, R. Rabe, J. Orasche, J. Lintelmann, B. Michalke, G. Abbaszade, C. Radischat, T. Gröger, J. Schnelle-Kreis, H. Harndorf, R. Zimmermann, Particle emissions from a marine engine: Chemical composition and aromatic emission profiles under various operating conditions, *Environmental Science and Technology*, 48 (2014) 11721-11729.
- [170] R. Geissler, M.R. Saraji-Bozorgzad, T. Gröger, A. Fendt, T. Streibel, M. Sklorz, B.M. Krooss, K. Fuhrer, M. Gonin, E. Kaisersberger, T. Denner, R. Zimmermann, Single photon ionization orthogonal acceleration time-of-flight mass spectrometry and resonance enhanced multiphoton ionization time-of-flight mass spectrometry for evolved gas analysis in thermogravimetry: Comparative analysis of crude oils, *Analytical Chemistry*, 81 (2009) 6038-6048.
- [171] C. Schepler, M. Sklorz, J. Passig, G. Famigliani, A. Cappiello, R. Zimmermann, Flow injection of liquid samples to a mass spectrometer with ionization under vacuum conditions: A combined ion source for single-photon and electron impact ionization, *Analytical and Bioanalytical Chemistry*, 405 (2013) 6953-6957.
- [172] S.M. Platt, I. El Haddad, A.A. Zardini, M. Clairotte, C. Astorga, R. Wolf, J.G. Slowik, B. Temime-Roussel, N. Marchand, I. Ježek, L. Drinovec, G. Močnik, O. Möhler, R. Richter, P. Barnet, F. Bianchi, U. Baltensperger, A.S.H. Prévôt, Secondary organic aerosol formation from gasoline vehicle emissions in a new mobile environmental reaction chamber, *Atmospheric Chemistry and Physics*, 13 (2013) 9141-9158.

- [173] R. Bahreini, A.M. Middlebrook, J.A. De Gouw, C. Warneke, M. Trainer, C.A. Brock, H. Stark, S.S. Brown, W.P. Dube, J.B. Gilman, K. Hall, J.S. Holloway, W.C. Kuster, A.E. Perring, A.S.H. Prevot, J.P. Schwarz, J.R. Spackman, S. Szidat, N.L. Wagner, R.J. Weber, P. Zotter, D.D. Parrish, Gasoline emissions dominate over diesel in formation of secondary organic aerosol mass, *Geophysical Research Letters*, 39 (2012).
- [174] S.M. Platt, I.E. Haddad, S.M. Pieber, R.J. Huang, A.A. Zardini, M. Clairotte, R. Suarez-Bertoa, P. Barmet, L. Pfaffenberger, R. Wolf, J.G. Slowik, S.J. Fuller, M. Kalberer, R. Chirico, J. Dommen, C. Astorga, R. Zimmermann, N. Marchand, S. Hellebust, B. Temime-Roussel, U. Baltensperger, A.S.H. Prévôt, Two-stroke scooters are a dominant source of air pollution in many cities, *Nature Communications*, 5 (2014).
- [175] M.F. Heringa, P.F. DeCarlo, R. Chirico, T. Tritscher, J. Dommen, E. Weingartner, R. Richter, G. Wehrle, A.S.H. Prévôt, U. Baltensperger, Investigations of primary and secondary particulate matter of different wood combustion appliances with a high-resolution time-of-flight aerosol mass spectrometer, *Atmospheric Chemistry and Physics*, 11 (2011) 5945-5957.
- [176] A.M. Ortega, D.A. Day, M.J. Cubison, W.H. Brune, D. Bon, J.A. De Gouw, J.L. Jimenez, Secondary organic aerosol formation and primary organic aerosol oxidation from biomass-burning smoke in a flow reactor during FLAME-3, *Atmospheric Chemistry and Physics*, 13 (2013) 11551-11571.
- [177] P. Simonen, E. Saukko, L. Ntziachristos, K. Lehtoranta, H. Timonen, F. Mylläri, T. Rönkkö, P. Karjalainen, J. Keskinen, M. Dal Maso, Secondary aerosol formation from shipping emissions, in: *European Aerosol Conference (EAC)*, Zürich, Switzerland, 2017.
- [178] M. Olsson, G. Petersson, Benzene emitted from glowing charcoal, *Science of the Total Environment*, 303 (2003) 215-220.
- [179] A.M. Grishin, A.S. Yakimov, Mathematical modeling of the wood ignition process, *Thermophysics and Aeromechanics*, 20 (2013) 463-475.
- [180] I. Flament, Y. Bessière-Thomas, *Coffee Flavor Chemistry*, John Wiley & Sons, Ltd, Chichester, UK, 2002.
- [181] F. Wieland, A.N. Gloess, M. Keller, A. Wetzel, S. Schenker, C. Yeretjian, Online monitoring of coffee roasting by proton transfer reaction time-of-flight mass spectrometry (PTR-ToF-MS): Towards a real-time process control for a consistent roast profile, *Analytical and Bioanalytical Chemistry*, 402 (2012) 2531-2543.
- [182] J.S. Ribeiro, F. Augusto, T.J.G. Salva, M.M.C. Ferreira, Prediction models for Arabica coffee beverage quality based on aroma analyses and chemometrics, *Talanta*, 101 (2012) 253-260.
- [183] A.P. Grieshop, J.M. Logue, N.M. Donahue, A.L. Robinson, Laboratory investigation of photochemical oxidation of organic aerosol from wood fires 1: Measurement and simulation of organic aerosol evolution, *Atmospheric Chemistry and Physics*, 9 (2009) 1263-1277.

- [184] A.P. Grieshop, N.M. Donahue, A.L. Robinson, Laboratory investigation of photochemical oxidation of organic aerosol from wood fires 2: Analysis of aerosol mass spectrometer data, *Atmospheric Chemistry and Physics*, 9 (2009) 2227-2240.
- [185] P.S. Chhabra, R.C. Flagan, J.H. Seinfeld, Elemental analysis of chamber organic aerosol using an aerodyne high-resolution aerosol mass spectrometer, *Atmospheric Chemistry and Physics*, 10 (2010) 4111-4131.
- [186] A.W. Rollins, E.C. Browne, K.E. Min, S.E. Pusede, P.J. Wooldridge, D.R. Gentner, A.H. Goldstein, S. Liu, D.A. Day, L.M. Russell, R.C. Cohen, Evidence for NO_x control over nighttime SOA formation, *Science*, 337 (2012) 1210-1212.
- [187] A. Kiendler-Scharr, A.A. Mensah, E. Friese, D. Topping, E. Nemitz, A.S.H. Prévôt, M. Äjälä, J. Allan, F. Canonaco, M. Canagaratna, S. Carbone, M. Crippa, M. Dall'Osto, D.A. Day, P. De Carlo, C.F. Di Marco, H. Elbern, A. Eriksson, E. Freney, L. Hao, H. Herrmann, L. Hildebrandt, R. Hillamo, J.L. Jimenez, A. Laaksonen, G. McFiggans, C. Mohr, C. O'Dowd, R. Otjes, J. Ovadnevaite, S.N. Pandis, L. Poulain, P. Schlag, K. Sellegri, E. Swietlicki, P. Tiitta, A. Vermeulen, A. Wahner, D. Worsnop, H.C. Wu, Ubiquity of organic nitrates from nighttime chemistry in the European submicron aerosol, *Geophysical Research Letters*, 43 (2016) 7735-7744.
- [188] E. Kari, L. Hao, P. Yli-Pirilä, A. Leskinen, M. Kortelainen, J. Grigonyte, D.R. Worsnop, J. Jokiniemi, O. Sippula, C.L. Faiola, A. Virtanen, Effect of Pellet Boiler Exhaust on Secondary Organic Aerosol Formation from α -Pinene, *Environmental Science and Technology*, 51 (2017) 1423-1432.
- [189] E.A. Bruns, I. El Haddad, J.G. Slowik, D. Kilic, F. Klein, U. Baltensperger, A.S.H. Prévôt, Identification of significant precursor gases of secondary organic aerosols from residential wood combustion, *Scientific Reports*, 6 (2016) 27881.